Republic of Iraq
Ministry of Higher Education
and Scientific Research
Al-Nahrain University
College of Science
Department of Chemistry

Photocatalysis of Azo Compounds on Doped Titanium dioxide

A Thesis

Submitted to the College of Science / Al-Nahrain University as a partial fulfillment of the requirements for the Degree of Master of Science in Chemistry

By

Hussein Mohammed Hadi

B.Sc. Chemistry / College Science / Karbala University

Supervised by

Dr. Hilal S. Wahab

(Prof.)

June 2015 **Shaaban 1436**

بسم الله الرحمن الرحيم

إِنَّا مَكَّنَّا لَهُ فِي الْأَرْضِ وَآتَيْنَاهُ مِن كُلِّ شَيْءٍ سَبَبًا ﴿٨٤﴾

صدق الله العظيم

سورة الكهف

Acknowledgements

I thank God for the great and countless graces. It is the greatest blessing that gave me this opportunity to write this thesis, which is a result of a research project in physical chemistry over three years to contribute to enrich my knowledge in a specialized field and helped me to learn a lot about myself.

First of all, I earnestly like to thank and express my profound appreciation to my supervisor Prof. Dr. Hilal S. Wahab who has coordinated and administered with interest the improvement of this work.

Many thanks and deep gratitude goes to the Iraqi Ministry of Higher Education and Scientific Research / Research and Development Directorate for awarding me the financially supported research fellowship for three months.

Special thanks to Prof. Dr. Igor. F. Perepichka, co-director of my work during research scholarship period in the United Kingdom / School of Chemistry / Bangor University.

My thanks also go to Dr. David D. Hughes and Mr. Shrikanth Kommana / School of Chemistry / Bangor University, Dr. Simon Curling / Biocomposites Centre/ School of Chemistry / Bangor University, Dr. Jeffrey Kettle and Dr. Yanhua Hong / School of Electronic Engineering/ Bangor University and Dr. Ridha Al-Bayati / Chemistry Department / College of Science / Al- Mustansiriya University.

My sincere thanks go also to Mr. Salama AlDouri and Ms. Noor AlZubaidi for their sustained assistance during my stay at Bangor.

My thanks and gratefulness to my research colleagues, Ahmed. A. Hussein, Atheer Fadhel and Ali Najah.

Special appreciation to Al-Nahrain University and all members of the department of chemistry in College of Science for their help during my implementation of this research work.

Finally, very special thanks to my family, parents and brothers because they are always the best hope in my life.

Table of Contents

List of Figures

List of Images

List of Tables

List of Schemes

List of Abbreviations

Ads	Adsorbed species on a surface
AOP	Advanced Oxidation Process
BET	Brunauer, Emmett and Teller
C_o	Initial concentration
Ct	Concentration at any time
CB	Conduction band
CR	Congo red
DBPs	Disinfection byproducts
e^-	Electron formed upon illumination of a semiconductor
Ea	Activation energy
EDX	Energy Dispersive X-ray spectroscopy
Eg	Band gap energy
EPR	Electron Paramagnetic Resonance
ESR	Electron Spin Resonance
HOMO	Highest occupied molecular orbital
hν	Incident photon energy
FTIR	Fourier transforms infrared spectrometry
K_{ads}	Equilibrium adsorption constant
k	Kinetic constant
k_{app}	Apparent rate constant
L-H	Langmuir–Hinshelwood
LUMO	Lowest unoccupied molecular orbital
MO	Methyl orange
NFDW	Nano filtered deionized water
nm	nanometer
NOM	Natural organic matter
O^-_2	Superoxide ion radical
OH^-	Hydroxyl radical
PL	Photoluminescence
ppm	Parts per million
T	Temperature (Kelvin)
TOF-SIMS	Time of Flight Secondary Ion Mass Spectroscopy
US	Ultrasound

UV	ultraviolet
VB	Valence band
VIS	Visible component of light
SC	Semiconductor
SEM	Scanning electron microscopy
TEM	Transmission electron microscope
UV-VIS	UV-Vis diffuse reflectance spectroscopy
Wt. %	Weight percent
XRD	X-ray diffraction
A_1g B_1g	Mulliken symbols
Φoverall	Overall quantum yield
λ	Wavelength

Summary

The photodegradation and degradation of two azo group containing dyes namely; methyl orange (MO) as mono azo model and congo red (CR) as di azo model moieties, have been investigated, throughout this thesis, in aqueous medium. Three different nitrogen content (2.5%, 5% and 7%) laboratory synthesized doped anatase TiO_2 nano particles (N-TiO_2) have been employed as a photocatayst utilizing visible light illumination. The N-TiO_2 photocatalysts have been characterized employing several spectroscopic and electronic tools encompassing. Scanning Electron Microscope (SEM) which presented smooth and ordered surfaces, Enegry Dispersive X-ray spectrometer (EDXS) and Time of Flight Mass Spectrometer (TOF-MS) which focused on the composition of various nitrogen doped TiO_2 photocatalys, X-ray Diffractometer (XRD) which presented via the pattern a neat anatase allotrope without rutile diffraction peaks with particle sizes in the nano range 52.4 nm, Diffused integrated sphere UV-VIS spectrophotometer (DU-UV-VIS) which determined the band gap energies at visible region of the electromagnetic spectrum where Eg of 2.5 % N-TiO_2 was 3.02 eV (410nm) compared with 3.26 eV (380nm) of anatase TiO_2, Photoluminescence (PLS) spectrometry for the recording of $e^- - h^+$ recombination spectra which corroborated that 2.5% N-TiO_2 photocatalyst contained the least recombination rate and finally Brunauer–Emmett–Teller (BET) measurements which confirmed the mesoporosity of all the prepared N-TiO_2 nano catalysts with surface area of 48.412 m^2/g of 2.5% N-TiO_2.

The effects of some experimental variables for the photodegradation of the two azo dyes have been investigated including,

initial solution pH, initial dye concentration, N-TiO_2 loading amount, visible light intensity and role of some oxidants.

At optimum operational conditions for MO including pH = 2.5, 50 mg/l N-TiO_2 loading, and 3.05 x 10^{-5}mol/l (10 mg/l) methyl orange, the value of the apparent rate constant, k_{app} , obtained has been 0.085 min^{-1} (0.00141 sec^{-1}) and the half life of the process, accordingly is equal to 0.133 hours. Whereas, for CR dye implying pH = 2.5, 40 mg/l N-TiO_2 loading, and 2.15 x 10^{-5} mol/l (15 mg/l) , the value of the apparent rate constant, k_{app} , obtained has been 0.034 min^{-1} (0.000305 sec^{-1}) and the half life of the process, accordingly is equal to 0.34 hours.

The kinetic studies for the photobleaching of MO and CR have revealed that the process follows the pseudo first order pattern regardless of reaction conditions. Moreover, the computed apparent quantum yields for the photodecolorization process have been 0.077 and 0.0135 for MO and CR, respectively.

The rate and yield results of the Photo oxidation process show that both dyes are influenced massively by the addition of hydrogen peroxide and other oxidants like persulfate, chlorate, bromate and iodate. The main process activation thermodynamic parameters namely, Gibbs energy, enthalpy and entropy were also deduced following the computation of photolysis activation energy employing the well known Arrhenius relation.

The mechanistic study employing GC-MS, NMR, FTIR and HPLC techniques has revealed the probable pathways for the formation of various degradation intermediates and mineralization products.

Chapter one

INTRODUCTION AND LITERATURE REVIEW

1. Introduction

1.1 Advanced oxidation processes for water remediation

Water is the most fundamental substance for all life on earth and a valuable asset for human development. Dependable access to clean and reasonable water is viewed as a standout amongst the most fundamental compassionate objectives, and remains a major global challenge for the 21st century [1]. Current water supply faces enormous challenges, both old and new. Over worldwide, about 780 million people need access to enhanced drinking water sources. It is pressing to implement basic water treatment in the influenced areas (chiefly in developing countries) where water and wastewater infrastructure often does not exist. In both developing and industrialized countries, human activities play a great role in a massive water scarcity by contaminating natural water sources [1].

The waste products generated from the textiles, chemicals, mining and metallurgical industries are mainly responsible for contaminating the water. This contaminated water contains non-biodegradable effluents, such as heavy metal ions (arsenic, zinc, copper, nickel, mercury, cadmium, lead and chromium…. etc.) and organic materials that are carcinogenic to human beings and harmful to the environment [2].

There are many traditional treatment methods such as biological treatment, air stripping, using of activated carbon and non photochemical oxidation that are used to removal of resistance organic compounds.
But these processes are not destroyed; they only transfer the contaminants from one phase to another [3].

Alternatively advanced oxidation processes (AOT) are considered as one of the critical utilizations of photochemical process that depending on hydroxyl radical formation using excitation sources [4]. The oxidation

potential values of different oxidants are listed in Table 1.1 and show that the $^{\bullet}OH$ are very powerful oxidants. The $^{\bullet}OH$ can subsequently, when adequate contact time is available, leading organic compounds to complete degradation to CO_2 and H_2O and mineral acids [5].

Table 1-1: Standard electrochemical reduction potentials of common oxidants [5].

Oxidant	Half-cell reaction oxidation	Potential (V)
$^{\bullet}OH$ (hydroxyl radical)	$^{\bullet}OH + H^+ + e^- \rightarrow H_2O$	2.80
O_3 (ozone)	$O_3\ (g) + H^+ + 2\ e^- \rightarrow O_2(g) + H_2O$	2.07
H_2O_2(hydrogen peroxide)	$H_2O_2 + 2H^+ + 2\ e^- \rightarrow 2H_2O$	1.77
HOCl (hypochlorous acid)	$2HOCl + 2H^+ + 2\ e^- \rightarrow Cl_2 + 2H_2O$	1.49
Cl_2 (chlorine)	$Cl_2\ (g) + 2e- \rightarrow 2Cl$	-1.36

These radicals can oxidize natural organic matter (NOM) and disinfection byproducts (DBPs) precursors by elimination of hydrogen atoms or addition of electrophilic agent to their unsaturated bonds [6].

There are two types of AOPs when the free radical precursor is dissolved in water and the reaction takes place in aqueous phase is called homogeneous photoreaction but when the precursor of free radical is solid and the interaction between organic compounds and free radical in solid-water interface this type is called heterogeneous photoreaction. For example CH_3OH (as simple pollutant model) is degradated to CO_2 and H_2O via cascade reaction in presence of hydroxyl radical (Figure 1-1) [7].

Numerous systems are qualified under this wide meaning of AOP. Most of these systems use an interaction of strong oxidants, e.g. O_3 and H_2O_2,

catalysts, e.g. transition metal ions or photocatalyst, and excitation source, e.g. ultraviolet (UV), ultrasonication or electron beam. Table 1-2 lists typical AOP systems [8].

Table 1-2: List of typical AOP systems

Non-photochemical	Photochemical
O_3/ ^{-}OH	H_2O_2/UV
O_3/H_2O_2	O_3/UV
O_3/ ultrasonication	O_3/H_2O_2/UV
O_3 / granulated activated carbon	H_2O_2/Fe^{2+} (photo-Fenton)
Fe^{2+}/H_2O_2 (Fenton system)	UV/TiO_2
electro-Fenton	H_2O_2/TiO_2/UV
electron beam irradiation	O_2/TiO_2/UV
ultrasound	UV/ ultrasonication
H_2O_2/ ultrasonication	
O_3/ catalyst	

The key advantages of these processes are destructive nature and on-site degradation of contaminants leading to mineralization.

Disadvantages of AOPs involve addition of inorganic oxidants, illumination source requirement, control pH, presence of some species that decrease the efficiency of process like carbonate which considered $^{\bullet}OH$ consuming and nitrate that adsorb UV light rather than catalyst and need for removal of secondary contaminants in some cases [7].

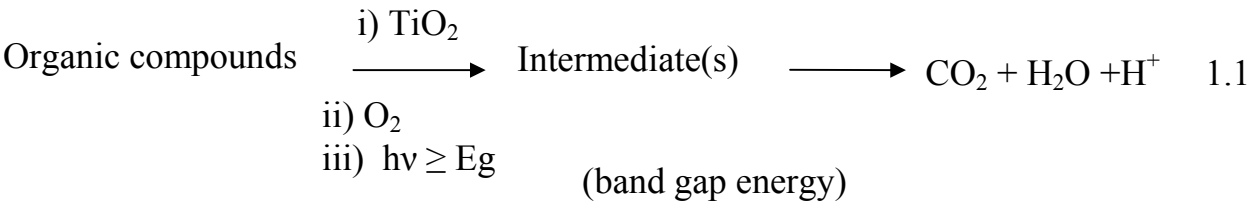
Organic compounds
i) TiO_2
ii) O_2
iii) $h\nu \geq Eg$
(band gap energy)
Intermediate(s)
$CO_2 + H_2O + H^+$

1.1

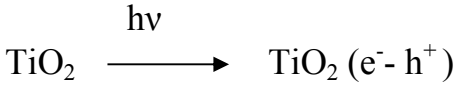
$h\nu$
TiO_2
$TiO_2\ (e^- - h^+)$

1.2

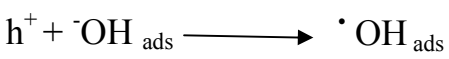
$h^+ + {}^-OH_{ads}$
$^{\bullet}OH_{ads}$

1.3

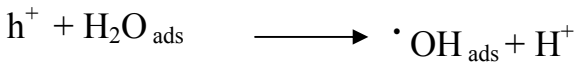
$h^+ + H_2O_{ads}$
$^{\bullet}OH_{ads} + H^+$

1.4

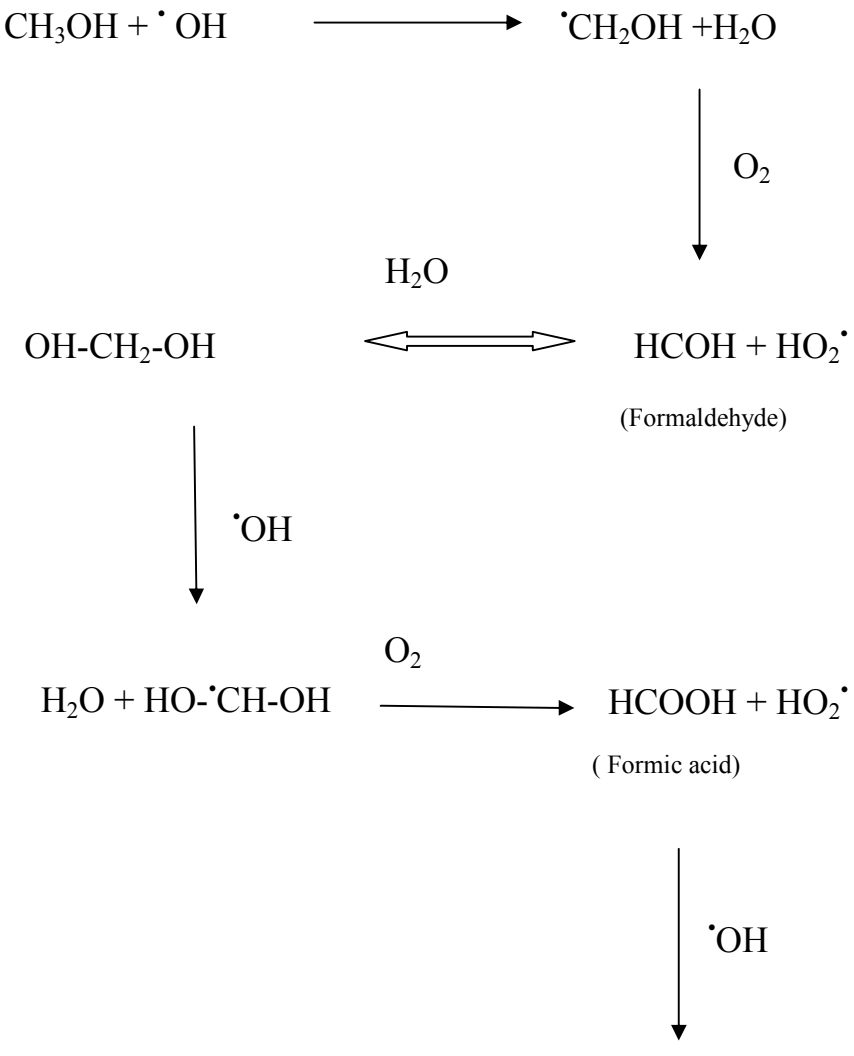
$CH_3OH + {}^{\bullet}OH$
$^{\bullet}CH_2OH + H_2O$
O_2
H_2O
$OH\text{-}CH_2\text{-}OH$
$HCOH + HO_2^{\bullet}$
(Formaldehyde)
$^{\bullet}OH$
O_2
$H_2O + HO\text{-}^{\bullet}CH\text{-}OH$
$HCOOH + HO_2^{\bullet}$
(Formic acid)
$^{\bullet}OH$

$CO_2 + H_2O$ ←——— $^{\bullet}COOH$ 1.5

Figure 1-1: Methanol as an example for mineralization by AOP

1.2 Heterogeneous photocatalysis process

Water purification, water splitting and isotopic exchange are classified as heterogeneous photocatalysis systems [9].

Semiconductors are characterized by having electronic band structure in which the highest occupied band (the valence band) and lowest unoccupied energy band (the conductance band) with energy gaps between them (Eg).

When light strikes the surface of semiconductor with energy equal to or greater than energy gap, the electron is excited from (VB) to (CB) leaving behind hole with positive charge. The recombination of e^- - h^+ pair takes in few nanoseconds and the energy emits as light or heat, but in presence of suitable scavenger the photo charge carriers are trapped and reduction-oxidation (redo) reactions can be started (Figure 1-2) [10].

The most important features of this process making it applicable to the treatment of contaminated aqueous effluents are [11]:

- The process does not need extreme conditions.
- Complete degradation of target materials into CO_2, H_2O and small inorganic species.
- The oxygen necessary for free radical formation can be acquired from atmosphere.
- The catalyst is photoactive, chemical inert, non-toxic, can be recycle and it can be modified to improvement its properties.
- Sun can be used as excitation source.

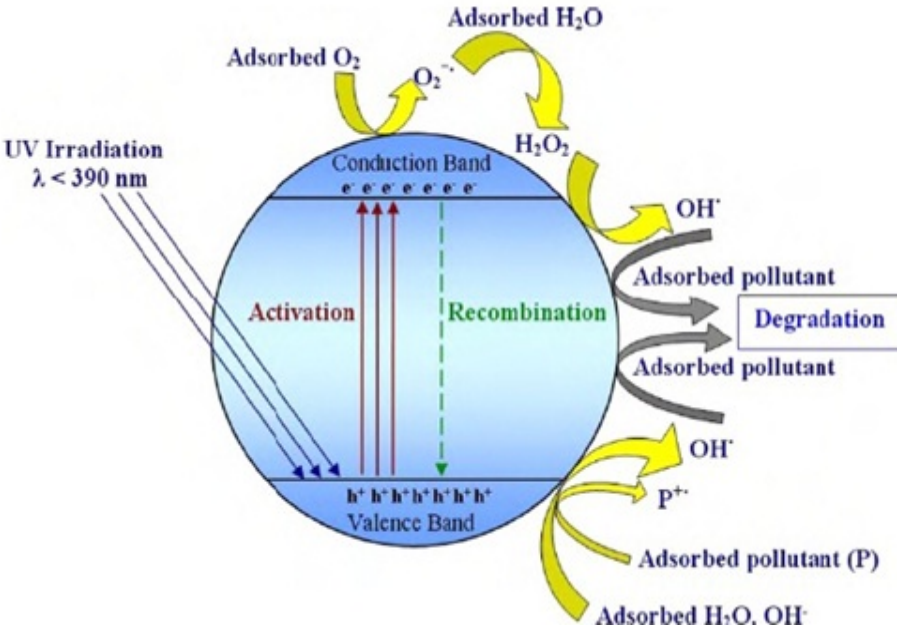

Figure 1-2: General mechanism of the photocatalysis on TiO_2 nanomaterials , reprinted and modified from ref. [12]

Many elementary mechanistic processes have been described in the photocatalytic degradation of organic compounds over one of the very common [9, 13]. The proposed mechanism is depicted as follow:

1. Formation of e^- - h^+ pair by absorption of photons

$$(TiO_2) + h\nu \rightarrow e^-_{CB} + h^+_{VB} \qquad 1.6$$

2. Production of superoxide anion

$$(O_2)_{ads} + e^-_{CB} \rightarrow O_2^{\cdot -} \qquad 1.7$$

3. reaction of ^-OH groups with hole to give $^{\cdot}OH$ radical

$$(H_2O \Leftrightarrow H^+ + {}^-OH)_{ads} + h^+_{VB} \rightarrow H^+ + {}^{\cdot}OH \qquad 1.8$$

4. Hydroperoxyl radical formation

$$O_2^{\cdot -} + H^+ \rightarrow HO_2^{\cdot} \qquad 1.9$$

5. Transformation of hydroperoxyl to hydrogenperoxide and oxygen

$$2HO_2^{\bullet -} \rightarrow H_2O_2 + O_2 \quad 1.10$$

6. Reduction of hydrogen peroxide by electron

$$H_2O_2 + e^- \rightarrow {}^{\bullet}OH + {}^{-}OH \quad 1.11$$

7. Oxidation of the organic compound by highly reactive $^{\bullet}OH$

$$R + {}^{\bullet}OH \rightarrow R^{\bullet} + H_2O \quad 1.12$$

8. decomposition of organic compound by reaction with hole

$$R + h^+ \rightarrow R^{+\bullet} \rightarrow \text{degradation products} \quad 1.13$$

1.3 Azo dyes

Generally, dye structures contain two principal parts. The first one is called chromophores which are unsaturated covalent groups responsible for appearance of color while the second is saturated covalent group and called (auxochrome) which enables the dye to dissolve in water and produces a bathochromic shift [14].

Dyes have great significance in our lives. But unfortunately 12% of these dyes are wasted during the coloring process and enters water resource [15].The effect of these dyes on the environment is a great concern because of the potentially cancer-causing and allergenic properties of these materials especially when dyes suffer from anaerobic discolorations [16]. In addition, these dyes can prevent both sunlight penetration and dissolved oxygen, which are essential for aquatic life. Advanced oxidation technologies are the most widely used approach that is employed for dye destruction process [17]. On the other hand, the dyes are classified depending on their color, structure, principle uses and chromophores groups [18].

Azo-dyes are characterized by nitrogen to nitrogen double bonds (–N=N–) that are usually attached to two radicals of which at least one but usually both are aromatic groups (benzene or naphthalene rings). The presence of sulphonic acid groups in azo dyes improve their water solubility, and the azo chromophoric ones gives resistance to the dyes against biological treatment [19- 20].

Monoazo, diazo and triazo are various types of azo dyes based on the number of azo group in the dyes [18, 21-24], as they are illustrated in Figure 1-3.

Few azo dyes can be degraded by homogeneous system because of large number of azo dyes are usually resistant to UV light and their solubility decreases when molecular weight increases. A complete degradation is not achieved due to the very low quantum yield of these systems [23, 25-26]. Therefore H_2O_2, O_3, Fenton's reagent, and titanium dioxide are often added to generate highly reactive radicals for azo dyes removal [12, 27].

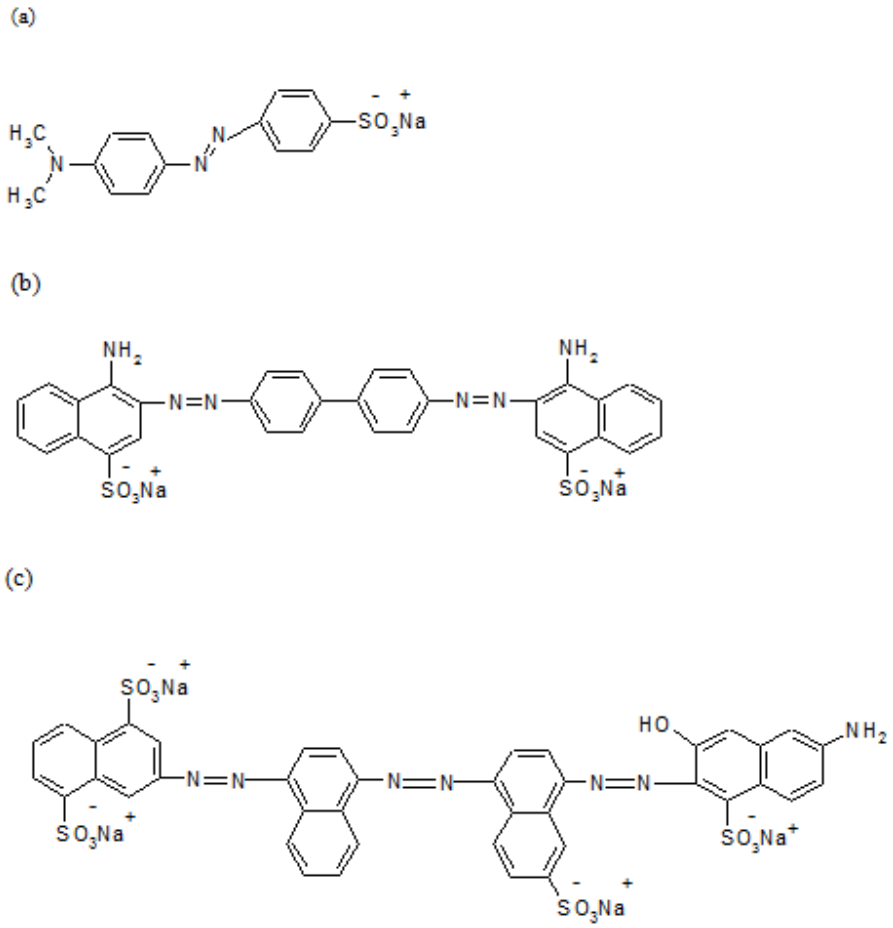

Figure 1-3: The molecular structures of (a) Methyl Orange; (b) Congo red; (c) Direct Blue 71

1.4 Surface modification

According to flash photolysis measurements, the lifetimes of e^- and h^+ are only few nanoseconds. In order to inhibit the recombination process and enhance redox reaction, the charge carriers must be trapped within about 20 picoseconds (ps) [28]. On the other hand, the efficiency of photocatalytic process is evaluated through many factors including the resistance of the semiconductor to photo corrosion, the nature of the end products and the excitation wavelength [29]. For example, small band-gap semiconductors such as CdS (2.4 eV) [30], ZnO (3.37 eV) [31] are active under illumination

by solar light but they usually suffer from photocorrosion induced by self decomopsition [32-33].

$$CdS + 2h^{+} \longrightarrow Cd^{2+} + S \qquad 1.14$$

$$ZnO + 2h^{+} \longrightarrow ZnO^{2+} + 1/2\ O_2 \qquad 1.15$$

These unfavorable reactions lead to lowered photoactivity and produce toxic metal ions (e.g., Cd^{+2}) into solution. Beside of that, anatase TiO_2 is photoactive, but its band gap energy is relatively large (Eg = 3.2 eV). it is only active under UV light therefore UV source is needed and further, as it is known that the ultraviolet light is ionizing and consequently, can cause damage to the human body leading to cancer [9, 14, 34].

Coupling of TiO_2 with other semiconductors (composite), adsorption of dye on the surface of titania (sensitization) and formation of oxygen vacancies can be shifted the excitation wavelength to the longer wavelength (red shift) [35-36].

Physical adsorption of dyes on surface of titanium dioxide via weak Van der Waals forces is considered successful method to expand the response of TiO_2 into visible light spectrum [37]. In this case the excitation process takes place at the surface of dye rather than the surface of semiconductor where the electron is promoted from the highest occupied molecular orbital (HOMO) to the lowest unoccupied molecular orbital (LUMO) of a dye to transfer directly to conduction band of TiO_2 [38]. Using of sensitized TiO_2 gives good results under solar light [39]. Various types of dyes such as commercial dye sensitizers and natural dye sensitizers have been used to

sensitize TiO_2 particles to visible light (Figure 1-4) [40-41]. The scheme of dye-sensitization of TiO_2 is illustrated in Figure 1-5.

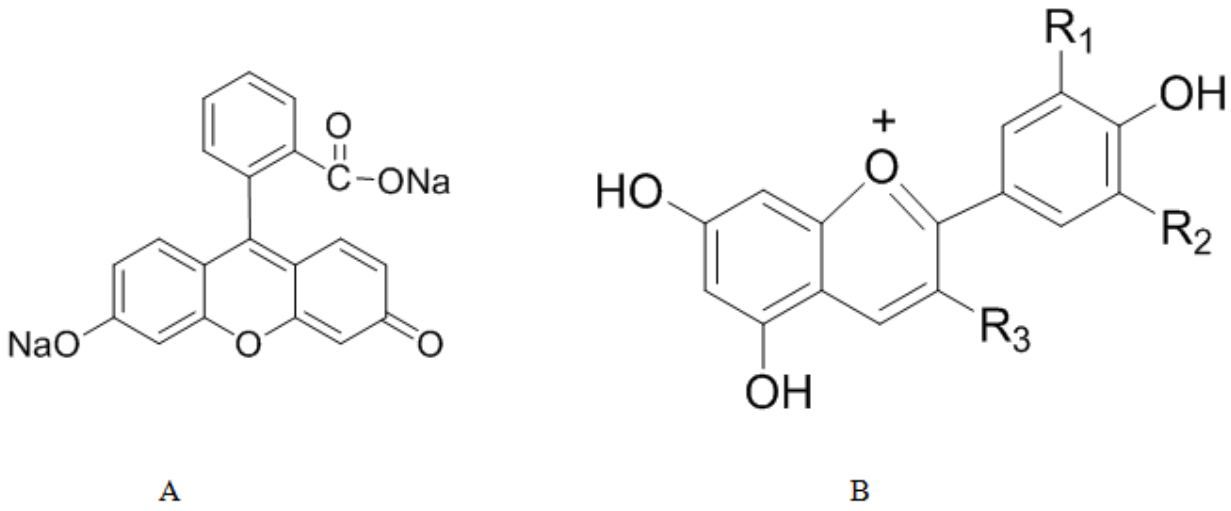

Figure 1-4: Chemical structures of natural dye (A) Fluorescein Sodium and commercial dye (B) Anthocyanin

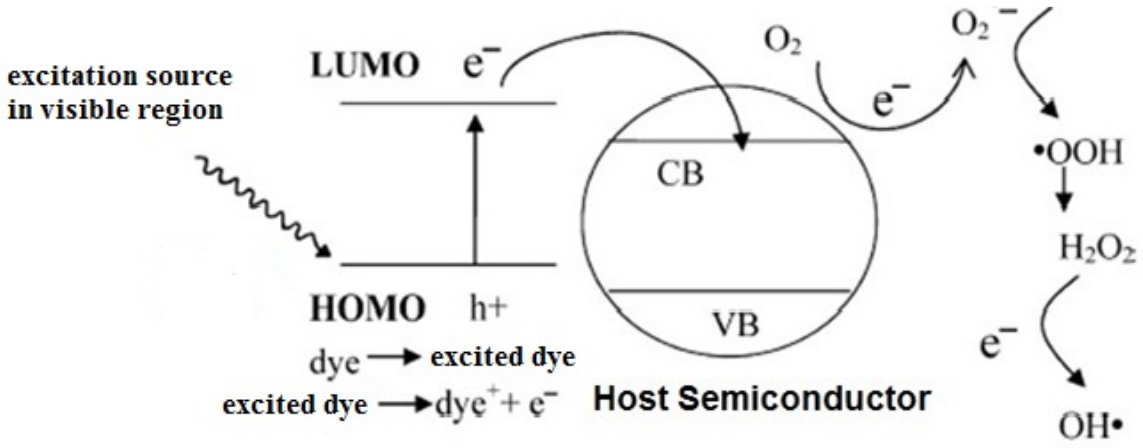

Figure 1-5: Visible light activation of a wide band gap semiconductor by dye sensitization, adapted from [36]

Coupling or composite is another way to suppress the e^--h^+ recombination process. This method involves combination between large band gap semiconductor and narrow band gap semiconductor that can absorb visible light (Figure 1-6) [42- 43]. Both semiconductors should be

photostable, the CB energy of large band gap semiconductor should be more than that of water oxidation to spilt water into H_2 and O_2 and more electronegative than CB of low band gap semiconductor in order to be able to trap electron from CB of low band gap semiconductor [44].

TiO_2 has been coupled with low band gap semiconductors such as Bi_2S_3/ TiO_2, CdS/TiO_2 [45]. Through electron spin resonance (ESR) studies, the observed signal is attributed to Ti^{+3} which confirms electron transfer from low band gap semiconductor to TiO_2 [46].

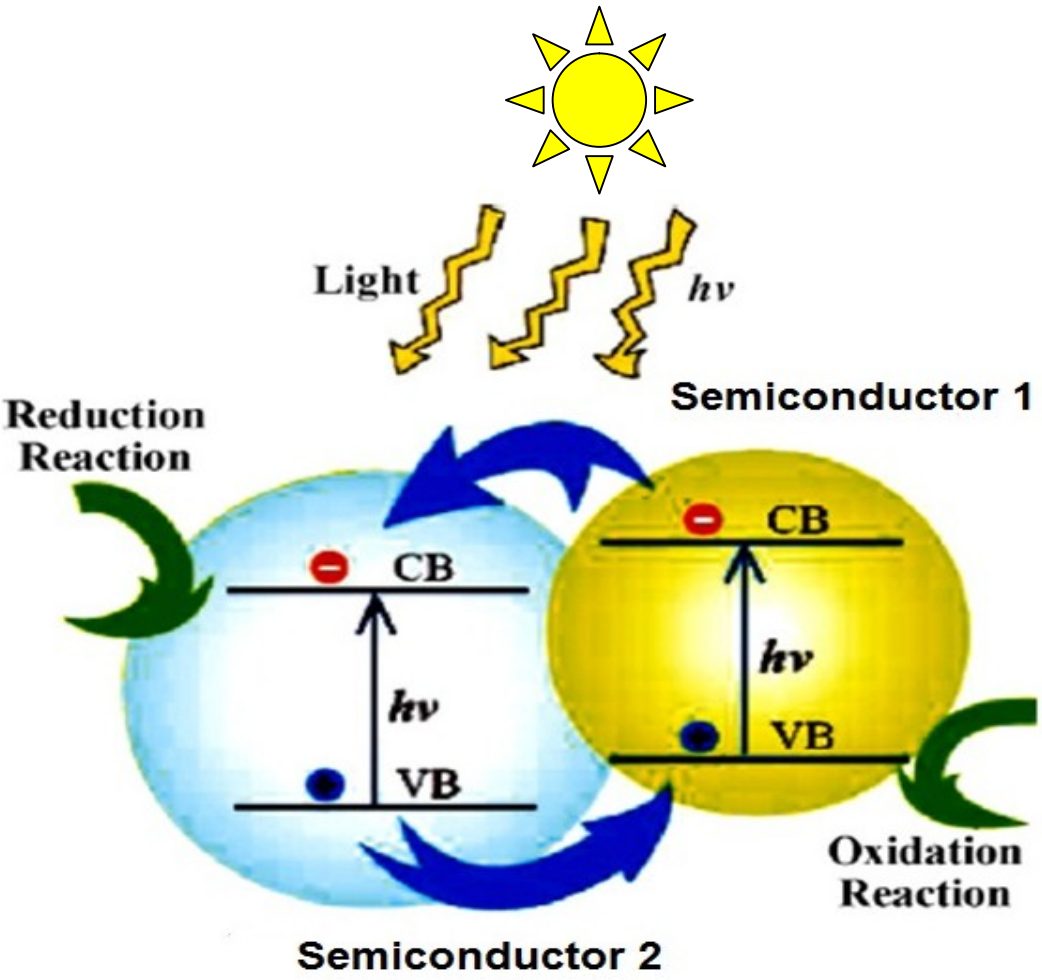

Figure 1-6: Schematic illustration of charge transfer in a coupled semiconductor system, adapted from [46]

Doping or deposition of Both, metal and non-metal like N and S [47] are effective way to increase spectral response of TiO_2 into visible light region through creating electronic states under CB of TiO_2 leading to lowering of its band gap energy [42, 48]. Among non-metals, N-doped TiO_2 is the most effective in narrowing the band gap [42]. Noble metals, including Pt [49] and Au [50], have been reported to be very active for development of TiO_2 photocatalysis. In this type of systems, the photoinduced electrons are transferred from CB to metal particles deposited on the surface of TiO_2, while photogenerated VB holes stay on the TiO_2 because of fact that the Fermi energy of these metals are lower than that of TiO_2 [51]. These activities enormously inhibit the electron-hole recombination, resulting in enhance separation and efficient photocatalytic reactions [51].

Impurity states $M^{(n+1)+}$ and $M^{(n-1)+}$ that responsible of absorption of visible light are generated as result of incorporation of metal ion into the lattice of TiO_2 as indicated in equations 1.16 and 1.17 where M and M^{n+} represent metal and metal ion dopant, respectively. Besides, the e^- transfer between M^{n+} and TiO_2 can suppress the recombination process, equations 1.18 and 1.19 [44, 51]. The energy level of the CB of TiO_2 should be more negative than that of $M^{n+}/M^{(n-1)+}$, while the energy level of the VB edge of TiO_2 should be more positive than that of $M^{n+}/M^{(n+1)+}$ [5].

$$M^{n+} + h\nu \rightarrow M^{(n+1)+} + e^-_{CB} \qquad 1.16$$

$$M^{n+} + h\nu \rightarrow M^{(n-1)+} + h^+_{VB} \qquad 1.17$$

$$\text{Electron trap : } M^{n+} + e^-_{CB} \rightarrow M^{(n-1)+} \qquad 1.18$$

$$\text{Hole trap : } M^{n+} + h_{VB}{}^+ \rightarrow M^{(n+1)+} \qquad 1.19$$

Thus modification of semiconductor by different strategies result in important advantages [28, 52-55] as follows:

1- Recombination process is retarded by enhancing the charge carrier separation and therefore increasing the activity of the photocatalytic process.
2- Shifting the excitation wavelength to visible light region.
3- Quantum yield and rates of photocatalytic reaction are increased.
4- Modification of catalyst surface increases surface reactivity.
5- Trapping of electron and/ or hole makes the photocatalysis process smooth.

1.4.1 Nitrogen doped-TiO_2 (N-TiO_2)

One of the problematic features of anatase usage in water purification application is its large band gap energy that needs ultra violet radiation to be excited and one of the active tools to overcome this limitation is doping with different types of transition metal, and /or doping with nonmetals to increase the visible light absorption and to retard the recombination of photoinduced charge carries [56-57]. To get efficient TiO_2 in visible light region, Asahi et al. [58], showed several terms, dopants should create intra band gap or electronic states into the bandgap of TiO_2 that absorb visible light, to make sure the doped TiO_2 is active in water splitting process, the energy of CB and the electronic states that belong to dopants should be equal or higher than water oxidation level (1.23 V) and in order to separate e^- - h^+ pair there must be effective overlap between mid band gap of impurity states and the band gap of TiO_2. In spite of the widespread of cationic metal doped TiO_2, there are many problems including the cost of metal doped TiO_2 synthesis procedure, thermal instability, localized d state in the deep band gap of TiO_2 that belong to metal dopant which behave as recombination center of charge carriers [59-60].

Many reports showed that nitrogen is the best option among the doping types like the transition metals and nonmetals due to its small

ionization energy, comparable atomic size and atomic radius with oxygen, formation of meta stable center, thermal stability, low recombination centers and can absorb visible light. Nitrogen is introduced into the lattice of titanium dioxide by several ways such as ion implantation, magnetron coating, titanium nitride oxidation and sol–gel [61-62].

Many physical and chemical properties is changed during the doping of nitrogen into TiO_2 but the significant changed property is the photocatalytic activity toward visible light spectrum. Deposition of titania with urea is the best procedure to form N doped TiO_2 compared with heating of TiO_2 with molecular nitrogen gas or ammonia at high temperature which is reduced the active sites on the surface of TiO_2 [63-64,]. It is worth mentioning that the mechanism of nitrogen incorporation is still unknown [65].

There are many assumptions to explain the mechanism of photocatalytic activity of N-TiO_2. One of them suggest oxygen is replaced by interstitial nitrogen via formation of Ti-O-N and then interaction between nitrogen and O^-_2 to form $(NO)_3^-$ that induce oxygen vacancy formation [66]. In the case of interstitial nitrogen doped titania, 2p orbital of nitrogen overlaps with 2p orbital of oxygen to give π* localized states under the conduction band of TiO_2 which lower the band gap energy of approximately 0.73 eV [67]. The other explanation suggests formation of one oxygen vacancy when two nitrogen atoms introduced substitutionally into lattice of TiO_2 [68]. 2p orbital of substitutional nitrogen that located above VB is not hybridized withy 2p orbital of oxygen and is responsible of visible light absorption and reduce band gap energy about 0.14 eV [69]. High concentration of nitrogen precursor during preparation of N-TiO_2 leads to interstitial nitrogen and vice versa [67]. Substitutional and interstitial

nitrogen doped TiO_2 model and reduction of band gap energy are showed in Figures 1-7 and 1-8 respectively.

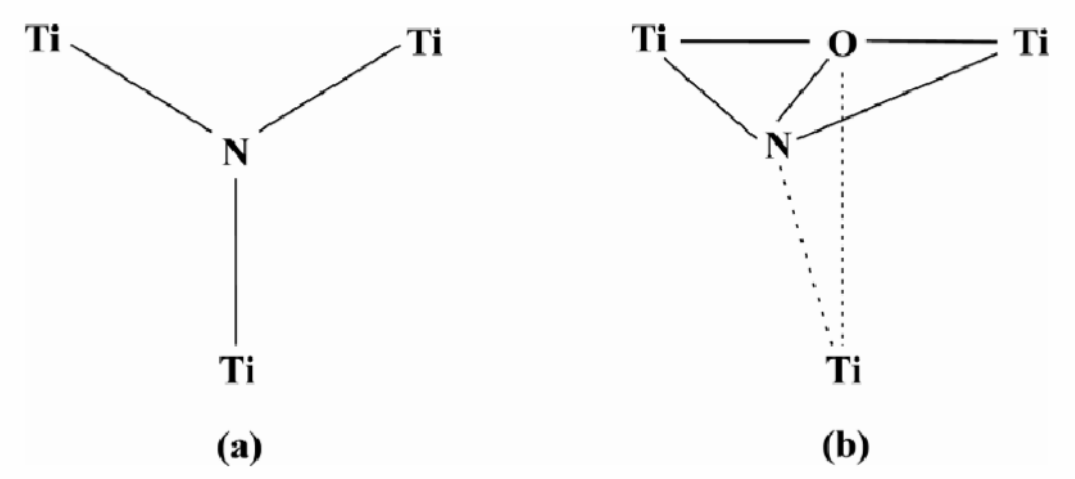

Figure 1-7: Substitutional (a) and interstitial (b) location of N in TiO_2 lattice lattice, reprinted [59]

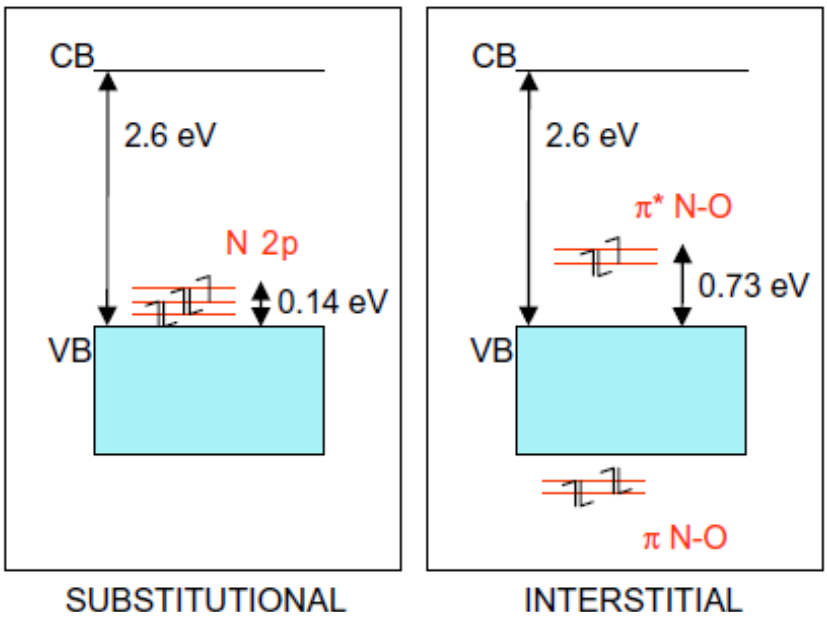

Figure 1-8: Electronic structure computed for substitutional and interstitial models, reprinted from ref. [68]

According to reported data [70-72], the band gap narrowing due to doping process results in large number of electrons and holes under illumination and in absence of suitable scavenger it is possible to reduce Ti^{+4} to Ti^{+3} and to generate 3d orbital under CB edge which subsequently contributes to decrease the band gap energy, beside of nitrogen impurity role as shown in Figure 1-9.

Serpone and co-worker [73-74] noted that there is what is known as color center that forms during nitrogen incorporation that reacts with oxygen vacancy to decrease band edge energy.

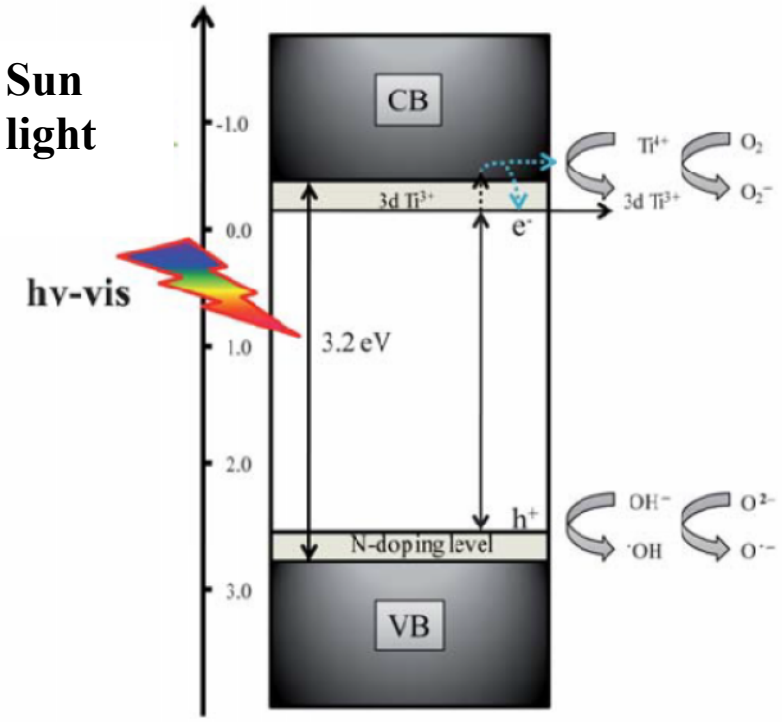

Figure 1-9: A possible mechanism of photocatalytic reactions of $O^{\bullet -}$ radical and the schematic band structure of N-doped TiO_2 under visible light irradiation, adapted from [70].

1.5 Sol-gel method

Sol-gel is simple and easy method to prepare three-dimensional metal oxide network and does not require complicated equipment [75-76]. Sol–gel processing allows to control of formats and shape of oxides [77]. Beside of that, it enables to incorporate impurities into network of semiconductor leading to the formation of materials with unique properties for different applications [78].

By hydrolysis of metal alkoxide into three dimensional network, sol is formed where often used such as Ti(IV) or Nb(V) because they are very reactive towards hydrolysis [75,79]. Controlling of the reaction rate through variation of some parameters like temperatre, acidic medium, alkoxide nature and addition of some chemicals can prevent the dispersed sol particles from agglomeration and solubility [80]. The hydrolysis, condensation and general reaction are summarized in the following equations [79].

$$M\text{-}OH + HO\text{-}M \longrightarrow M\text{-}O\text{-}M + H_2O \qquad 1.20$$

By modifying the reactivity of the precursors, sequential formation of sols and gels are allowed [75,79].

$$\text{Hydrolysis: } -MOR + H_2O \longrightarrow -MOH + ROH \qquad 1.21$$

Thus, it is possible to control subsequent condensation reactions according to equations (1.20) or (1.22), preventing the primary particles from further condensation (in an ideal case, a sol is formed):

$$\text{Condensation: } -MOH + ROM- \longrightarrow -MOM- + ROH \qquad 1.22$$

Self-assemblies between metal alkoxide molecules are resulted from interactions between them via hydrogen bonds; van der Waals forces network [81-82]. Unfortunately, the sol-gel processing requires long time, using high temperature for the crystallization and removal of organic part

and most metal precursor is sensitive to moisture [83-84]. Doped TiO_2 can be prepared by sol gel [63] according to the chart which is shown in Scheme 1-1 [85].

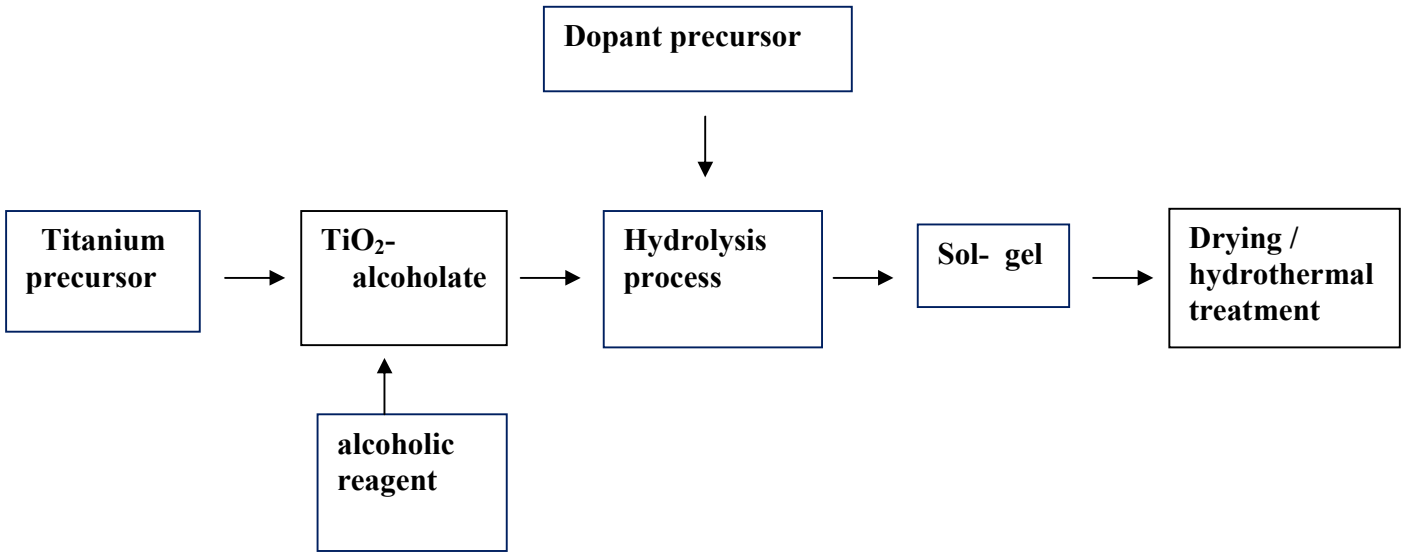

Scheme 1-1: Process flow chart for the preparation of doped TiO_2-based photocatalysts by sol–gel method, adapted from [85]

1.6 The role and mechanism of added oxidants

The presence of oxidant in photocatalytic suspension plays important role in enhancement of photocatalytic efficiency [86]. This feature is the result of several roles performed by the oxidant which can be summarized as follows [20,87] :

1- It acts as scavenger of electron and holes and hence prevents recombination process.

2- Generation of oxidizing agents and increasing their concentration especially $^{\cdot}OH$ leading to increase of reaction rate because of ability of these reactive species to degrade organic substrate.

3- Increasing of quantum yield.

Oxygen is the most commonly used in photocatalytic system which able to produce superoxide anion directly and then generate hydroxyl radical according to the following equations [88].

$(O_2)_{ads} + TiO_2(e^-) \rightarrow TiO_2 + O_2^{\bullet -}$ 1.23

$O_2^{\bullet -} + 2H_2O \rightarrow 2H_2O_2$ 1.24

$H_2O_2 \rightarrow 2^{\bullet}OH$ 1.25

The main and direct source to produce hydroxyl radical in adequate amount is hydrogen peroxide (H_2O_2). In addition, hydrogen peroxide can be trapped conduction band electron to contribute in inhibition of electron-hole recombination as following [89-90].

$H_2O_2 + O_2^- \rightarrow {}^{\bullet}OH \quad + {}^-OH + O_2^{\bullet}$ 1.26

$H_2O_2 + h\nu \rightarrow 2^{\bullet}OH$ 1.27

$H_2O_2 + e^- \rightarrow OH^- + {}^{\bullet}OH$ 1.28

Persulfate ($S_2O_8^{2-}$) is another free radical precursor which has many advantages including high solubility, thermal stability, non expensive, it is easy stored and its higher potential (E_o= 2.01 V) [91-92]. Persulfate can be formed $SO_4^{\bullet -}$ by reaction with electron or exposure to direct photolysis equations (1.29) and (1.30).

$e_{aq}^- + S_2O_8^{2-} \rightarrow SO_4^{\bullet -} + SO_4^{2-}$ 1.29

$S_2O_8^{2-} + h\nu \rightarrow SO_4^{\bullet -} + SO_4^{\bullet -}$ 1.30

Inorganic oxidants that have three oxygen atoms and central halogen atom are called oxyhalogen oxidants. Halogen atom has high electronegativity,

therefore they are capable to trap electron and give different radicals, despite chlorate is not very active compared with bromate and iodate [93]. Their activity could be understood through the following reactions:

$$IO_4^- + h^+ \rightarrow IO_3^{\bullet} + O^{\bullet -} \quad 1.31$$

$$O^{\bullet -} + H^+ \rightarrow {}^{\bullet}OH \quad 1.32$$

$${}^{\bullet}OH + IO_4^- \rightarrow {}^{-}OH + IO_4^{\bullet} \quad 1.33$$

$$BrO^{-3} + 6e^-_{CB} + 6H^+ \rightarrow Br^- + 3H_2O \quad 1.34$$

$$ClO_3 + 6e^-_{CB} + 6H^+ \rightarrow 3H_2O + Cl^- \quad 1.35$$

1.7 Literature Review

Wide range contaminants in wastewater is degraded and removed using advanced oxidation process that rely largely on the use of titanium dioxide as catalyst [2,4]. One of the most dangerous pollutants is what is known as azo dyes. Many researchers have worked to remove these compounds by using UV or VIS light with pure or modified TiO_2 [116, 142]. Employment of N doped TiO_2 in photocatalysis process showed a great activity under visible light [58]. Sol-gel method is successful way to prepare N-TiO_2 by coprecipetation of urea and precursor of titanium dioxide that followed by thermal treatment [63, 67, 70].

Several experimental parameters like amount of catalyst, concentration of dye, pH, temperature and light intensity are studied to accomplish the optimum conditions. Authors [56, 177] noted when pH decreased the degradation percent of dye increased. Furthermore, as the dye initial concentration increases the rate of photocatalytic reaction becomes low [22, 27]. Daneshvar et al. [123] reported that the number of reached photons

reduced when adding high catalyst amount that has negative effect on the degradation percent of dyes. A major goal of the modification of TiO_2 is to extend the adsorption threshold wavelength from UV to the visible light range in order to utilize solar light since the latter is one of the cleanest and cheapest forms of energy [31, 121]. Different analytical techniques such as high performance liquid chromatography (HPLC), gas chromatography–mass spectrometry (GC–MS), ^1H NMR, diffuse reflectance UV-VIS and FTIR [174-176] were utilized to find out the intermediates of organic compounds degradation.

1.8 Scope of the project

Azo group containing compounds are potential organic pollutants which are usually characterized by the presence of one or more azo group bound to aromatic rings and their release into the environment is intuitively of great concern. Accordingly, the main purpose of this project is to build up an optimum photocatalytic slurry reactor system based on the visible illumination of three different contents (2.5%, 5% and 7%) of N-doped TiO_2 nanoparticles, which presumably improve the photocatalytic activity by nitrogen impregnated TiO_2 nanostructure, aiming consequently to remove the model dye pollutants (MO and CR) from aqueous media and further to explore the mechanistic pathways of the photocatalytic degradation process.

This set up will absolutely allow exploration of the impacts of several operational parameters on the rate and photoedegradation quantum yield of nominated azo dyes. Among those parameters namely; initial concentration of mono azo group (MO) and di azo group (CR) dyes, N- doped TiO_2 dosage with variable nitrogen content, visible light source intensity, initial pH of photocatalysis media, illumination time and different added oxidants have

been intended to be extensively investigated. Moreover, the characterization of the synthesized three level nano anatase N-TiO_2 photocatalysts has been another objective of this project encompassing structural (XRD, EDX,TOF-MS and FTIR), morphological (SEM and BET) and optical (UV/VIS reflection, PL and Raman) techniques. The kinetic, thermodynamic and plausible photodegradation mechanism studies have also been one of the objectives of this research work.

This chapter includes all the experimental activities done involving synthesis of catalyst, characterization devices and procedures, parameters effect, experimental instruments and chemical materials utilized all through this work.

2.1 Chemicals

2.1.1 Solid Chemicals

Material	purity	Source
$FeSO_4.7H_2O$	99%	Riedel-Dehaen
$H_2C_2O_4.2H_2O$	99.6%	HW
$KBrO_3$	99.8%	Merck
$KClO_3$	99%	Fluka
KIO_3		Prolapo
$KMnO_4$	99%	BDH
Methyl Orange	99%	Fisher Chemical
$NaBH_4$	99%	Aldrich
$(NH_4)_2\ SO_4.FeSO_4.6H_2O$	99.5%	BDH
TiO_2	99.7%	Aldrich

Sodium acetate	98%	Riedel-Dehaen
Congo red	99.8%	Fisher Chemical
Urea	99.5%	Fluka
1,10-phenanthroline	97%	BDH

2.1.2 Liquid Chemicals

Material	purity	Source
acetone	99%	Analyt
Ethanol	97%	Fluka
HNO_3	69.5%	Medex
H_2O_2	50% wt/wt	Scharlau
H_2SO_4	98%	Himedih
Iso-propoxide	99.8%	Riedel-Dehaen
Ti-isopropoxide	97%	Aldrich

DMSO-D6	99.8%	Apollo Scientific

2.2 Procedures

2.2.1 Preparation of N-doped TiO_2 catalyst by sol gel method

1- Ten grams of urea was dissolved in 200 milliliter nano filtered deionized water (NFDW) with stirring.

2- Ten milliliters of titanium isopropoxide was added dropwise at room temperature, with rate of 2 milliliter/minutes, onto the above solution with vigorous stirring, meanwhile, a few extra milliliters of isopropanol was added.

3- The solution was stirred further for 2 hrs after completion of titanium isopropoxide and isopropanol additions to achieve complete hydrolysis.

4- Solution was left for 20 hrs in dark for aging.

5- Solution was filtered by Buchner (solution was neglected), the precipitation was dried at 60 °C for 2 hrs.

6- The solid filtrate was calcined for 4 hrs at 400 °C to remove organic part.

7- A yellow product of N-TiO2 appeared after calcination, which assigned as 2.5% N-TiO_2

Note: Two other N- doped TiO_2 were prepared following similar procedure that stated above. The only difference was addition of 20.8g and 30g urea to 200 milliliter NFDW in the first step, which assigned as 5% and 7% N-TiO_2, respectively.

2.2.2 Preparation of $K_3[Fe(C_2O_4)_3]$. 3H2O

1- Approximately 5g of $Fe(NH_4)_2(SO_4)_2.6H_2O$ was weighed in a 125 milliliter Erlenmeyer flask and dissolved in 20 milliliter hot NFDW and finally 1 milliliter of 3M H_2SO_4 was added.

2- 2.5g of oxalic acid ($H_2C_2O_4$) was dissolved in 25 milliliter of NFDW, afterwards, this solution was added to the above solution, mentioned in step 1, and heated to boiling while stirring constantly to prevent bumping.

3- The Erlenmeyer flask was removed from the heat source and allowed the yellow precipitate of FeC_2O_4 to settle for 10 minutes.

4- The supernatant liquid was decanted (poured the liquid away from the solid) and the precipitate was washed using 15 milliliter of hot NFDW. The mixture was swirled and filtered.

5- Ten milliliters of hot NFDW that contains 3.5g of $K_2C_2O_4$ was added to the precipitate, then was stirred and heated to 40°C. While the temperature was at 40°C, immediately, 8 milliliter of H_2O_2 was added dropwise and stirred continuously. Periodically the temperature of the solution was checked and made sure that it was at least 40°C (but not >50°C) during the addition of H_2O_2. (Some brown Fe $(OH)_3$ may precipitate at this time).

6- The resulting solution was heated to boiling. 20 milliliter of $H_2C_2O_4$ was added (prepared by dissolving 1g in 30 milliliter of NFDW). It was stirred continuously and the last 10 milliliter of $H_2C_2O_4$ was added dropwise, while maintaining the temperature near boiling. The solution was turned clear green.

7- Twenty milliliters of ethanol was added to solution of neglected precipitate (when crystals were formed, it was dissolved by heating in water bath).

8- The solution was left in dark about 24 hrs.

9- The solution was filtered under vacuum and washed with 10 milliliter of 1:1 ethanol / NFDW solution.

10- Finally, the precipitate was washed using 10 milliliter of acetone.

2.2.3 Measurement of light intensity using actinometrical method

The intensity measurement of the incident light was carried out with a potassium ferrioxalate actinometer as described by Hatchard and Parker [94] and examined extensively through a previous work in our laboratory [95]. This method is usually used to determine the number of quanta entering the reaction vessel and consequently, the apparent quantum yields for the photocatalytic reaction will be estimated. The actinometer solution (6×10^{-3} mol/L) was prepared by dissolving 2.947g of $K_3Fe(C_2O_4)_3.3H_2O$ in 800 milliliter of NFDW.

One hundred milliliter of 1N H_2SO_4 was added and the whole solution was diluted to one liter with NFDW.

The method used for the determination of light intensity involves irradiation of actinometer solution for known period time (1 hour).

A calibration curve for Fe^{+2} was drawn using the following solutions:

1- 4×10^{-4} mol.L^{-1} of $FeSO_4$ in 0.1 N H_2SO_4.
2- 0.1% w/v phenanthroline monohydrate in water.
3- Buffer solution was prepared by mixing 600 milliliter of 1N sodium acetate and 360 milliliter of 1N H_2SO_4 then diluted to one liter.

Different concentrations of Fe^{+2} solutions were prepared by further dilution of solution (1) above in 25 milliliter volumetric flask. Then after, the followings are added to each flask;

a- Two milliliter phenanthroline solution.
b- Five milliliter of buffer solution.
c- Different volumes of 0.1N H_2SO_4 solution were used to make equivalent to 10 milliliter 0.1 N H_2SO_4 and finally dilute the whole solution to 25 milliliter with NFDW.

The volumetric flask was covered with aluminum foil and kept in the dark for 30 minutes. Then the optical densities at wavelength of 510 nm were measured.

A blank solution was used as reference which contained all the liquids except the ferrous ion solution.

Plot the optical density versus ferrous ion concentration, Figure 2-1. The slope of the straight line gives the extinction coefficient (absorptivity) of $FeSO_4$ solution.

In order to determine the light intensity, 100 milliliter of actinometer solution was irradiated in the irradiation cell. Post illumination, one milliliter of the irradiated solution was transferred into 25 milliliter volumetric flask, two milliliter of phenanthroline solution and 0.5 milliliter of buffer solution were added to the flask, and then it was diluted to 25 milliliter using NFDW. A Blank solution was prepared by mixing one milliliter of unirradiated potassium ferrioxalate solution with other components. The optical density was measured.

The incident light intensity was calculated as follows:

$I_o = A \times V_1 \times 10^{-3} \times V_3 / Q_y \times € \times V_2 \times t$

Where:

I_o = photo flow (incident light intensity)

A= optical density (absorbance) at 510 nm

V_1 = initial volume (50 milliliter)

V_3 = final volume (25 milliliter)

Q_y = quantum yield at 365 nm which equals to 1.21 [58]

€=extinction coefficient = slope of calibration curve (1.112×10^4 L mol^{-1} cm^{-1})

V_2 = volume taken from irradiated solution (1 milliliter).

t = irradiation time in seconds

The apparent quantum yield is calculated using the following expression :

ϕ_{app} = rate of reaction / rate of absorbed photons (I_o)

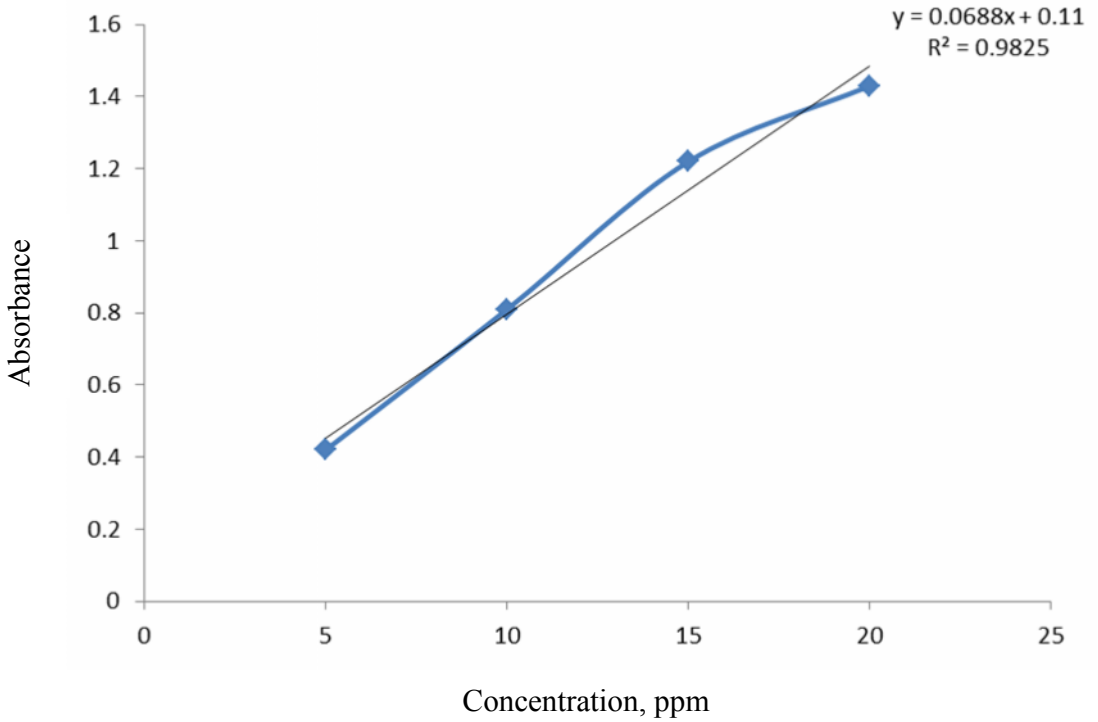

Figure 2-1: Calibration curve for Fe^{+2}

$Y_2 - Y_1 = 0.8 - 0.4 = 0.4$

$X_2 - X_1 = 18 - 9 = 9$ ppm / 278000 = 0.00003237 mol/L

Slope = 0.4 / 0.00003237 = 1.235×10^4 L mol^{-1} cm^{-1}

2.2.4 Preparation of azo dyes solution

2.2.4.1 Preparation of methyl orange solution

1- A stock solution of methyl orange of 10 ppm was prepared by dissolving 0.01g of MO dye into 1 liter NFDW.

2- Different concentrations (2, 4, 6, and 8 ppm) of methyl orange were prepared from stock solution by a series of dilution in order to prepare the calibration curve.

3-The calibration curve was drawn by measuring absorbance at 465 nm for all prepared methyl orange solutions mentioned previously in steps 1 and 2, as shown in Figure 2-2.

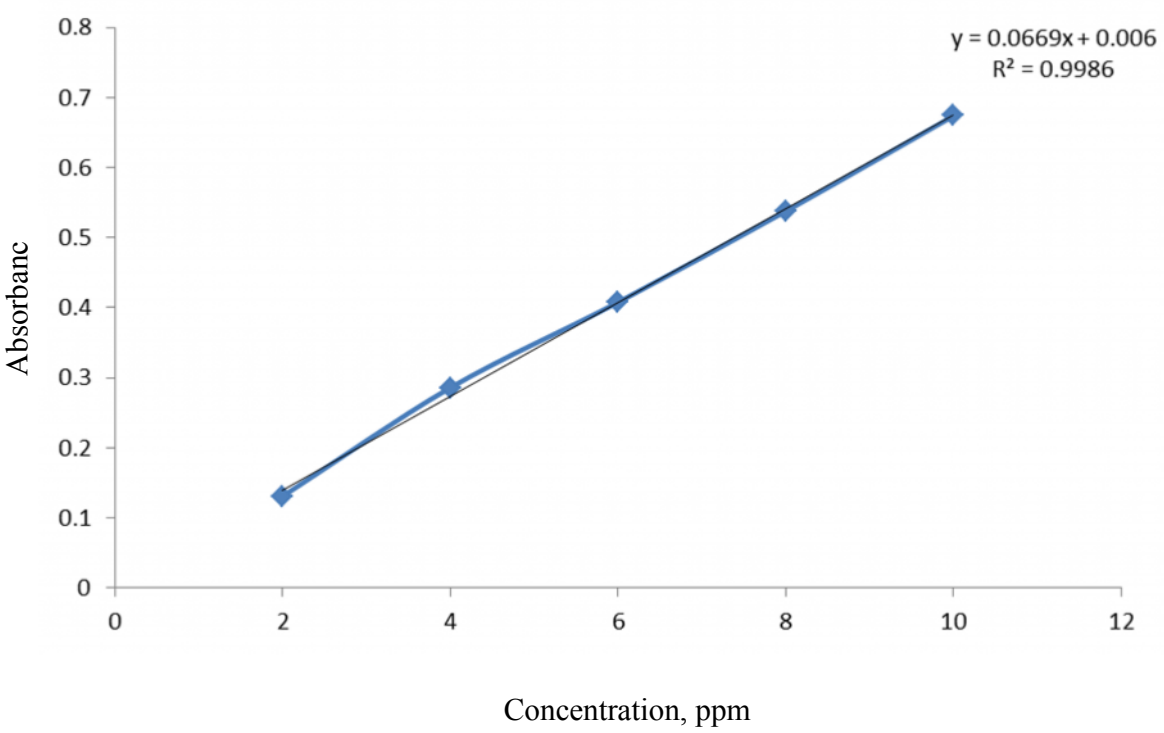

Figure 2-2: Calibration curve for methyl orange

0.015g of CR dye into 1 liter NFDW.

2- Different concentrations (2, 4, 6, 8, 10, 12 ppm) of Congo red were prepared from stock solution by a series of dilution in order to prepare the calibration curve.

3- The calibration curve was drawn by measuring absorbance at 564 nm for all prepared Congo red solutions mentioned previously in steps 1 and 2, as shown in Figure 2-3.

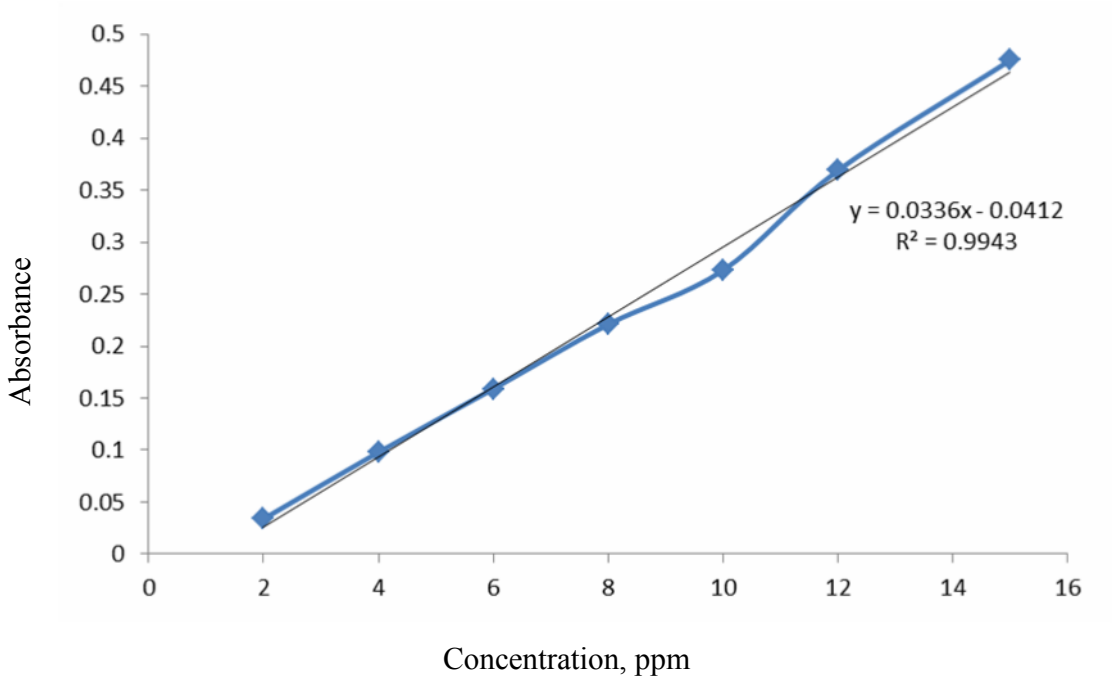

Figure 2-3: Calibration curve for Congo red

2.2.5 Testing of degradation of azo dye under visible light

The effect of visible light on degradation of azo dye was studied as follows;

1- 100 milliliter of azo dye (10 mg/L) aqueous solution was illuminated using 500W halogen lamp (Philips) at high intensity with stirring for 4 hrs.

2- At every 60 minutes of irradiation time, samples of 4 milliliter was withdrawn for analysis.

3- The disappearance of azo dye was monitored using the visible absorbance feature at λ= 465 nm as function of irradiation time.

2.2.6 Testing of degradation of azo dye by H_2O_2 and visible light

1- 100 milliliter of aqueous solution of azo dye (10 mg/L) was mixed with 2 milliliter of H_2O_2.

2- The mixture was illuminated by 500W halogen lamp (Philips) at high intensity with stirring for 4 hrs.

3- Four milliliters were drawn every 60 minutes of irradiation time for analysis.

4- Absorbance of azo dye was measured at 465 nm with the visible spectrophotometer to detect the remained concentration of remaining of the dye.

2.2.7 Testing of degradation of azo dye by H_2O_2 in dark

1- 100 milliliter of aqueous solution of azo dye (10 mg/L) was mixed with 2 milliliter of H_2O_2.

2- The mixture was stirred for 4 hrs.

3- 4 milliliters were drawn every 60 minutes of illumination time for analysis.

4- Absorbance of azo dye was measured at 465 nm with visible spectrophotometer to survey the remained concentration of methyl orange, mono azo dye.

2.2.8 Testing of degradation of azo dye by visible light in presence of N-TiO_2

1- 100 milliliter of azo dye (10 mg/L) was taken and its pH was adjusted to 2.5 using diluted HNO_3.

2- A mass of 50 mg of powder (7% N-TiO_2) was contacted with 100 milliliter of azo dyes aqueous solution.

3- The water suspension of azo dye and nanosized N-TiO_2 powder were stirred in the dark for 20 min to ensure the adsorption equilibrium was established prior to irradiation.

4- The sample was irradiated with a 500W halogen lamp (Philips) at high intensity with stirring for 4 hrs.

5- About 4 milliliter was withdrawn after every 60 minute of irradiation time.

6- The catalyst (N-TiO_2) was separated from the suspension by centrifuge for 10 minutes using 3000 RPM.

7- Absorbance of azo dye was measured to estimate the degradation percent.

2.2.9 Testing of degradation of azo dye by N doped-TiO_2 in dark

1- 100 milliliter was taken and its pH was adjusted to 2.5 with diluted HNO_3.

2- A mass of 50 mg of powder (7% N-TiO_2) was contacted with 100 milliliter of azo dye aqueous solution.

3- The water suspension of azo dye and nanosized N-TiO_2 powder were stirred in the dark for 4 hrs.

4- About 4 milliliter was withdrawn after every 60 minutes of stirring time.

5- The catalyst (N-TiO_2) was separated from the suspension by centrifuge for 10 minutes using 3000 RPM.

6- Absorbance of azo dye was measured to estimate the degradation percent.

2.2.10 Testing of degradation of azo dye by visible light in presence of N-TiO_2 and H_2O_2

1- 100 milliliter of azo dye (10 mg/L) was taken and 2 milliliter of H_2O_2 was added.

2-The pH of above solution was adjusted to 2.5 with diluted HNO_3, then 50 mg of the doped powder (7% N-TiO_2) was added.

3- The solution in the dark was stirred for 20 min to ensure the adsorption equilibrium which was established prior to irradiation.

4- The sample was Irradiated using a 500W halogen lamp (Philips) at high intensity with stirring for 4 hrs.

5- About 4 milliliter was withdrawn after every 60 minutes of irradiation time.

6- The catalyst (N-TiO_2) was separated from the suspension by centrifuge for 10 minutes using 3000 RPM.

7- The absorbance of azo dye was measured to estimate the degradation percent.

2.2.11 Effect of added electron scavengers (O_2, H_2O_2)

2.2.11.1 Effect of absence of scavengers on the degradation of azo dye

1- 100 milliliter of azo dye (10 mg/L) was taken and adjusted to pH of 2.5 using diluted HNO_3

2- A mass of 50 mg of powder (7% N-TiO_2) was contacted with 100 milliliter of azo dyes aqueous solution.

3- The water suspension of azo dye and nanosized N-TiO_2 powder was stirred in the dark for 20 min to ensure the adsorption equilibrium that was established prior to irradiation.

4- The sample was irradiated using a 500W halogen lamp at high intensity with stirring (Philips) for 4 hrs.

5- About 4 milliliter was withdrawn after every 60 minutes of irradiation time.

6- The catalyst (N-TiO_2) was separated from the suspension by centrifuge for 10 minutes using 3000 RPM.

7- Absorbance of azo dye was measured to estimate the degradation percent.

2.2.11.2 Effect of H_2O_2 on the degradation of azo dyes

1- 100 milliliter of azo dye (10 mg/L) was mixed with different volumes 0.5, 1, 2, 3, 4 and 5 milliliter of H_2O_2 then adjusted to pH of 2.5.

Note: Each volume refers to stand alone experiment.

2- 50 mg of powder (2.5% N-TiO_2) was added to above solutions.

3- The solution was stirred with O_2 bubbling in the dark for 20 minutes to ensure the adsorption equilibrium that was established prior to irradiation.

4- The sample was irradiated with a 500W halogen lamp (Philips) at high intensity with stirring for 1 hr.

5- About 4 milliliter was withdrawn after every 15 minutes of irradiation time.

6- The catalyst (N-TiO_2) was separated from the suspension by centrifugation for 10 minutes using 3000 RPM.

7- Absorbance of azo dye was measured to estimate the degradation percent.

2.2.11.3 Effect of O_2 on the degradation of azo dye

1- 100 milliliter of azo dye (10 mg/L) was taken and adjusted to pH of 2.5 with diluted HNO_3.

2- 50 mg of powder (7% N-TiO_2) was added to above solution.

3- The solution was stirred with O_2 bubbling (Note : the flow rate of O_2 is 30 ml/min) in the dark for 20 minutes.

4- The sample was irradiated with a 500W halogen lamp (Philips) at high intensity with stirring for 4 hrs.

5- About 4 milliliter was withdrawn after every 60 minutes of irradiation time.

6- The catalyst (N-TiO_2) was separated from the suspension by centrifugation for 10 minutes using 3000 RPM.

7- Absorbance of azo dye was measured to estimate the degradation percent.

2.2.11.4 Effect of H_2O_2 and O_2 on the degradation of azo dye

1- 100 milliliter of azo dye (10 mg/L) was taken and 2 milliliter of H_2O_2 was added.

2-The pH of above solution was adjusted to 2.5 with diluted HNO_3, then 50 mg of powder (7% N-TiO_2) was added.

3- The solution was stirred with O_2 bubbling in the dark for 20 minutes.

4- The sample was irradiated with a 500W halogen lamp (Philips) at high intensity with stirring for 4 hrs.

5- About 4 milliliter was withdrawn after every 60 minutes of irradiation time.

6- The catalyst (N-TiO_2) was separated from the suspension by centrifugation for 10 minutes using 3000 RPM.

7- Absorbance of azo dye was measured to estimate the degradation percent.

2.2.12 Effect of pH on the degradation of azo dye

1- 100 milliliter of azo dye (10 mg/L) was taken and 2 milliliter of H_2O_2 was added.

2- The pH of above solution was changed as follows (1.0, 2.0, 2.5, 3.0, 4.0, 5.0, 7.0, 9.0) using diluted HNO_3, then 50 mg of powder (7% N-TiO_2) was added.

3- The solution was stirred with O_2 bubbling in the dark for 20 minutes.

4- The sample was irradiated with a 500W halogen lamp (Philips) at high intensity with stirring for 4 hrs.

5- About 4 milliliter was withdrawn after every 60 minutes of irradiation time.

6- The catalyst (N-TiO_2) was separated from the suspension by centrifugation for 10 minutes using 3000 RPM.

7- The absorbance of azo dye was measured to estimate the degradation percent.

2.2.13 Effect of nitrogen content of N-TiO_2 on the degradation of azo dye

1- 100 milliliter of azo dye (10 mg/L) was mixed with 2 milliliter of H_2O_2 then adjusts pH to 2.5.

2- 50 mg of powder (N-TiO_2) was added to above solution.

a- 2.5% N-TiO_2

b- 5% N-TiO_2

c- 7% N-TiO_2

Note: Every single N-TiO_2 powder refers to separate experiment.

3- The solution was stirred with O_2 bubbling in the dark for 20 minutes to ensure the adsorption equilibrium which was established prior to irradiation.

4- The sample was irradiated with a 500W halogen lamp (Philips) at high intensity with stirring for 1 hr.

5- About 4 milliliter was withdrawn after every 15 minutes of irradiation time.

6- The catalyst (N-TiO_2) was separated from the suspension by centrifuge for 10 minutes using 3000 RPM.

7- The absorbance of azo dye was measured to estimate the degradation percent.

2.2.14 Effect of initial azo dye concentration on the rate of reaction

1- 100 milliliter of various initial concentrations of azo dye (5, 10, 15, 20, 25, 30) ppm were taken and 2 milliliter of H_2O_2 was added to each concentration then adjust pH to 2.5.

2- 50 mg of 2.5% N-TiO_2 powder was added to above solution.

3- The solution was stirred with O_2 bubbling in the dark for 20 minutes to ensure the adsorption equilibrium which was established prior to irradiation.

4- The sample was irradiated with a 500W halogen lamp (Philips) at high intensity with stirring for 1hr.

5- About 4 milliliter was withdrawn after every 15 minutes of irradiation time.

6- The catalyst (N-TiO_2) was separated from the suspension by centrifuge for 10 minutes using 3000 RPM.

7- The absorbance of azo dye was measured to estimate the degradation percent.

2.2.15 Effect of N-TiO_2 loading on the degradation of azo dye

1- 100 milliliter of azo dye (10 mg/L) was mixed in case of MO and (15 mg/L) in case of CR with 2 milliliter of H_2O_2 then adjusted to pH of 2.5.

2- 50 mg of 2.5% N-TiO_2 powder was added to above solution.

3- The solution was stirred with O_2 bubbling in the dark for 20 minutes to ensure the adsorption equilibrium that was established prior to irradiation.

4- The sample was irradiated with a 500W halogen lamp (Philips) at high intensity with stirring for 1 hr.

5- About 4 milliliter was withdrawn after every 15 minutes of irradiation time for analysis.

6- The catalyst (N-TiO_2) was separated from the suspension by centrifuge for 10 minutes using 3000 RPM.

7- The absorbance of azo dye was measured to estimate the degradation percent.

Note: all the operational conditions were fixed and replaced 50 mg N-TiO_2 by (20, 40, 60, 80, 100) mg of 2.5% N-TiO_2.

2.2.16 Effect of light intensity on the degradation of azo dye

1- 100 milliliter of azo dye (10 mg/L) was mixed with 2 milliliter of H_2O_2 then adjusts pH to 2.5.

2- 50 mg of 2.5% N-TiO_2 powder was added to above solution.

3- The solution was stirred with O_2 bubbling in the dark for 20 minutes to ensure the adsorption equilibrium which was established prior to irradiation.

4- The sample was irradiated with a 500W halogen lamp (Philips) at high intensity with stirring for 1 hr.

5- About 4 milliliter was withdrawn after every 15 minutes of irradiation time.

6- The catalyst (N-TiO_2) was separated from the suspension by centrifugation for 10 minutes using 3000 RPM.

7- The absorbance of azo dye was measured to estimate the degradation percent.

2.2.17 Effect of UV light on the degradation of azo dye

1- 100 milliliter of azo dye (10ppm) was taken and 2 milliliter H_2O_2 was added, then adjusted to pH=2.5 using dilute HNO_3.

2- 50 mg of 2.5% N-TiO_2 nano powder was added to the cell.

3- The solution was stirred with O_2 bubbling in the dark for 20 minutes to ensure the adsorption equilibrium that was established prior to irradiation.

4- The solution was irradiated by ultraviolet light for 1 hr at 14 cm cell-light source distance in the presence of O_2.

5- At one hour intervals, 4 milliliter of irradiated azo dye was taken; centrifuge for 10 minutes at 3000 RPM, then the absorbance was measured.

2.2.18 Effect of diluted H_2O_2 on the degradation of azo dye

1- 100 milliliter of azo dye was taken (10ppm) and add:

a- 1 milliliter of (0.0135N) H_2O_2

b- 2 milliliter of (0.0135N) H_2O_2

c- 3 milliliter of (0.0135N) H_2O_2

d- 4 milliliter of (0.0135N) H_2O_2

e- 5 milliliter of (0.0135N) H_2O_2

2- pH was adjusted to 2.5 using dilute HNO_3.

3- 50 mg of 2.5% N-TiO_2 powder was added to the cell.

4- The solution was stirred with O_2 bubbling in the dark for 20 minutes to ensure the adsorption equilibrium which was established prior to irradiation.

5- The sample was irradiated with a 500W halogen lamp (Philips) at high intensity with stirring for 1 hr.

6- About 4 milliliter was withdrawn after every 15 minutes of irradiation time for analysis.

7- The catalyst (N-TiO_2) was separated from the suspension by centrifugation for 10 minutes using 3000 RPM.

8- The absorbance of azo dye was measured to estimate the degradation percent.

2.2.19 Effect of some oxidants on the degradation of azo dye

1- 100 milliliter of azo dye (10ppm) was taken and 4 milliliter of 0.3 M of the oxidants (H_2O_2, $KClO_3$, $KBrO_3$ and KIO_3) was added.

Note: each type of oxidant has been employed in a separate experiment.

2- The pH was adjusted to 2.5 using dilute HNO_3.

3- 50 mg of 2.5% N-TiO_2 powder was added to the cell.

4- The solution was stirred with O_2 bubbling in the dark for 20 minutes to ensure the adsorption equilibrium that was established prior to irradiation.

5- Sample was irradiated with a 500W halogen lamp (Philips) at high intensity with stirring for 1 hr.

6- About 4 milliliter was withdrawn after every 15 minutes of irradiation time.

7- The catalyst (N-TiO_2) was separated from the suspension by centrifuge for 10 minutes using 3000 RPM.

8- The absorbance of azo dye was measured to estimate the degradation percent.

2.2.20 Determination of H_2O_2 concentration [96]

1- At first, a burette was rinsed with few milliliters of permanganate solution.

2- Burette was filled with (0.1N) permanganate solution.

3- 5 milliliter of fresh H_2O_2 was transferred to volumetric flask (250 milliliter volume) and the flask was filled with NFDW to the mark.

4- 20 milliliter of (2N) H_2SO_4 was added to Erlenmeyer flask, then 10 milliliter of H_2O_2 was added to the flask

5- The titration was conducted by adding potassium permanganate solution from a 50 milliliter glass burette until the first appearance of a faint pink color that persists for 30 seconds.

6- The volume was recorded and computed according to the following expression;

$(N \times V)_{KMnO4} = (N \times V)_{H2O2}$

$$N_{H2O2} = \frac{(N \times V)_{KMnO4}}{V_{H2O2}}$$

2.2.21 Influence of solar irradiation

1- 2 milliliter of H_2O_2 was added to 100 milliliter of (10 ppm) dye solution.

2- The pH was adjusted to 2.5 using dilute HNO_3.

3- 50 mg of N-TiO_2 nanoparticles was added to the solution.

a- 2.5% N-TiO_2

b- 5% N-TiO_2

c- 7% N-TiO_2

Note: (each type is used in a separate experiment).

4- The solution was stirred upon reaching equilibrium (20 minutes in dark).

5- It was irradiated by direct sun light.

6- At given irradiation time intervals, samples of 4 milliliter of the suspension were withdrawn and filtered post centrifugation for 10 minutes using 3000 RPM to remove the catalyst.

7- The dye concentration was determined by measuring its absorbance using a UV-VIS spectrophotometer.

Note: The sunlight experiments were carried out at 11: 15 am during August (summer season) in Baghdad city.

2.2.22 General experimental procedure at optimized conditions

Photodegradation experiments were conducted in a photoreactor (Image 2-1). This small-scale system consisted of a cylindrical Pyrex-glass cell with 150 milliliter capacity. A 500 W halogen lamp has been used as illumination source. The photocatalytic decomposition of methyl orange dye was investigated under optimum conditions: pH = 2.5, catalyst loading 50 mg and 2 ml of H_2O_2. The pH was adjusted using diluted HNO_3. For Congo Red degradation the optimum conditions was pH = 2.5, catalyst amount= 40 mg and 2 milliliter of H_2O_2. The suspension was first stirred in the dark to reach the equilibrium adsorption. All the experiments were carried out in the presence of O_2 as a scavenger for e_{cb}^-. During irradiation period, samples of 4-5 milliliter were collected at regular times, centrifuged and filtered. The discolouration was monitored spectrophotometrically by measuring the absorbance at λ_{max}. In most of the experiments, the photocatalytic process was continued until complete mineralization of the compound was achieved.

Image (2-1): Photolysis

2.3 Instruments

2.3.1 Refrigerated circulating bath. Model (WCR-P12), wisecircu.

2.3.2 Nanofiltered-deionized water supply unit. Model (Sm-11), waterpia.

2.3.3 Centrifuge (K centrifuge PLC series.).

2.3.4 Muffle furnace (SX-5-12).

2.3.5 Drying cabinet (K Hot Air Sterilizer).

2.3.6 Apel PD-303 single beam spectrophotometer has been used for visible light absorption measurements.

2.3.7 Fourier Transform Infrared (FTIR) spectrometer (IR Prestige-21 Shimadzu).

2.3.8 Double beam Shimadzu UV-VIS spectrophotometer. Model (1650 PC) has also been used throughout this work.

2.3.9 Photoreaction system

The Photoreaction configuration shown in Image (2-1), was locally made. It consists of halogen lamp 500W (Philips) which is vertically fixed

into stainless steel hollow cylinder of 10 cm in diameter and 27 cm in height. The heating effect emerged by the lamp was minimized by circulating water in the hollow cylinder through outlet and inlet slots in cylinder using circulating thermostat water bath, type Wirecircu. The internal walls of the cylinder were covered with aluminum foil to avoid radiation losses and temperature rising. Lens is used for light collection and focusing. The solutions/suspensions of azo dye and other materials (N-TiO_2, H_2O_2....etc) according to experiment were magnetically stirred. Typical irradiation done in cell (it is made of a pyrex cylindrical flask containing cover with provision for gas inlet and outlet and to withdraw samples at specific time intervals), which proved to supply enough oxygen for oxidative photodegradation (the flow rate of O_2 is 30 mL /min) with continuous stirring using a hot plate-stirrer to keep the catalyst aqueous suspension in homogeneous form during the experiments. The concentration of azo dye was determined from its visible absorbance characteristic and calibration curve method at the wavelength of maximum absorption. A single beam, Apel PD- 303 visible spectrophotometer was used through out the work.

2.3.10 X-ray Spectrometer

The X-ray diffraction (XRD) patterns were obtained on a Philips X-pert 3040/60 XRD machine using a Cu target Ka radiation (λ= 1.541A ̊) to determine the crystalline size. The accelerating voltage and the applied current were 40 kV and 30 mA, respectively. The XRD patterns was at the scanning range 2θ from 20 ^{o} to 60 ^{o}.

2.3.11 Scanning Electron Microscopy (SEM)

The Phenom™ SEM was used to characterize the morphological and structural properties of the samples. Nearly 1 mg of a sample was mounted

on a SEM sample holder and was sputtered with gold prior to analysis for better conductivity and resolution of the sample.

2.3.12 Photoluminescence (PL)

The PL spectra of the samples were measured at room temperature using a Horiba Fluoromax-4 spectrophotometer. The spectrophotometer has a 450W xenon lamp as the excitation light source (λ= 340 nm). Photoluminescence (PL) spectroscopy can provide information regarding the energy levels of different aqueous and suspended specimen.

2.3.13 Diffused Reflectance UV-VIS Spectrometer

The band gap energies of the products were determined by diffuse reflectance spectra of the samples measured using an UV–VIS spectrophotometer (Shimadzu UV-3600). The UV–VIS absorbance spectra were obtained for the dry pressed disk samples equipped with an integrating sphere assembly, using $BaSO_4$ as reflectance reference sample.

2.3.14 Brunauer Emmett Teller (BET)

Surface area and pore distribution of the samples were determined using nitrogen adsorption/desorption isotherm. Analysis was carried out on dried degassed samples using a Micromeritecs gemini surface area analyser with nitrogen as the adsorbate, and liquid nitrogen as the sample coolant (to ensure temperature stability).

2.3.15 Nuclear magnetic resonance (NMR)

Bruker ultrashield 400 plus.

2.3.16 Raman Spectrometer

Renishaw ramanscope 1000.

2.3.17 High-Performance Liquid Chromatography (HPLC)

HPLC analysis was carried out at 21.6 C^o by using Dionex-UltiMate 3000 equipped with dual wavelength UV-Vis detector and C18 column

symmetry, (4.6 x 150 mm). A sample (10 μL) was injected and dye products were allowed to separate for 29 min at flow rate 1 ml/min. Mobile phase used was methanol/H_2O. The UV-VIS detector was set at 280 and 254 nm for the study of methyl orange and Congo red, respectively.

2.3.18 Gas Chromatography–Mass Spectrometry (GC-MS)

GC-MS analysis was carried out using a Thermo Trace 1300, equipped with an intergrated gas chromotograph having a column (RXi®-5ms). Helium was used as a carrier gas at the flow rate of 1.5 mL/min. The injector temperature was maintained at 30 ^oC.

2.3.19 Time of Flight Secondary Ion Mass Spectrometry (TOF- SIMS)

Analysis was conducted using a Ga^+ ion beam, which was optimized to ensure maximum mass resolution. To ensure no fragmentation, a low current pulsed beam was used in measurements (<1013 ions/cm^2), which is known not to degrade polymer samples during measurements.

2.3.20 Energy Dispersive X-ray Spectrometer (EDXS)

(X Flash 6110) Bruker EDX coupled with (Inspect SS0) SEM (physics dept. / College of science / AL-Nahrain University) has been exploited for the sample content of the doped TiO_2.

2.3.21 Photolysis unit of UV source

The photolysis unit is laboratory-built (local market) system consisting of ultraviolet light source (125 W) medium pressure mercury lamp (MPML) fitted with a focusing lens to assure parallel beam of light.

3. Results and Discussion

3.1 Spectroscopic perspectives of azo group containing dyes

Methyl Orange ($C_{14}H_{14}N_3SO_3Na$), mono azo dye was chosen as a simple model of a series of common azo-dyes largely used in the industry. This compound, which is a well known acid-base indicator, is orange in basic medium and red in acidic medium. Its structure, shown in Figure 1-3 is characterized by a sulfonate group, which is responsible for the high solubility of these dyes in water. When dissolved in distilled water, the UV–visible spectrum of methyl orange showed two absorption maxima [97]. The first band observed at wavelength of 271 nm and the second band with higher intensity, at wavelength of 465 nm as presented in Figure 3-1. The latter band was used to monitor the photocatalytic degradation of methyl orange. The molar extinction coefficient (absorptivity, ε) of 10 ppm of methyl orange in NFDW was measured at the maximum absorption wavelength, 465 nm, using Beer-lambert equation ($A= \varepsilon bc$), where A= absorbance, b = absorption light path, 1 cm and c = molar concentration of methyl orange. The absorptivity (ε) has been $2.206 \times 10^{+4}$ $mol^{-1}.L.cm^{-1}$ for molar concentration of 3.055×10^{-5} mole/L.

Upon variation of solution pH towards lower values (protonation), with increasing the pH of solution, there exists a tautomeric equilibrium (Figure 3-2), between the ammonium form (red form) and azonium, form (yellow form) emerges that consequently lead to increase in the absorbed wavelength due to the red shift [98] . Figure 3-3 shows the standard UV-VIS scan for methyl orange at different pH.

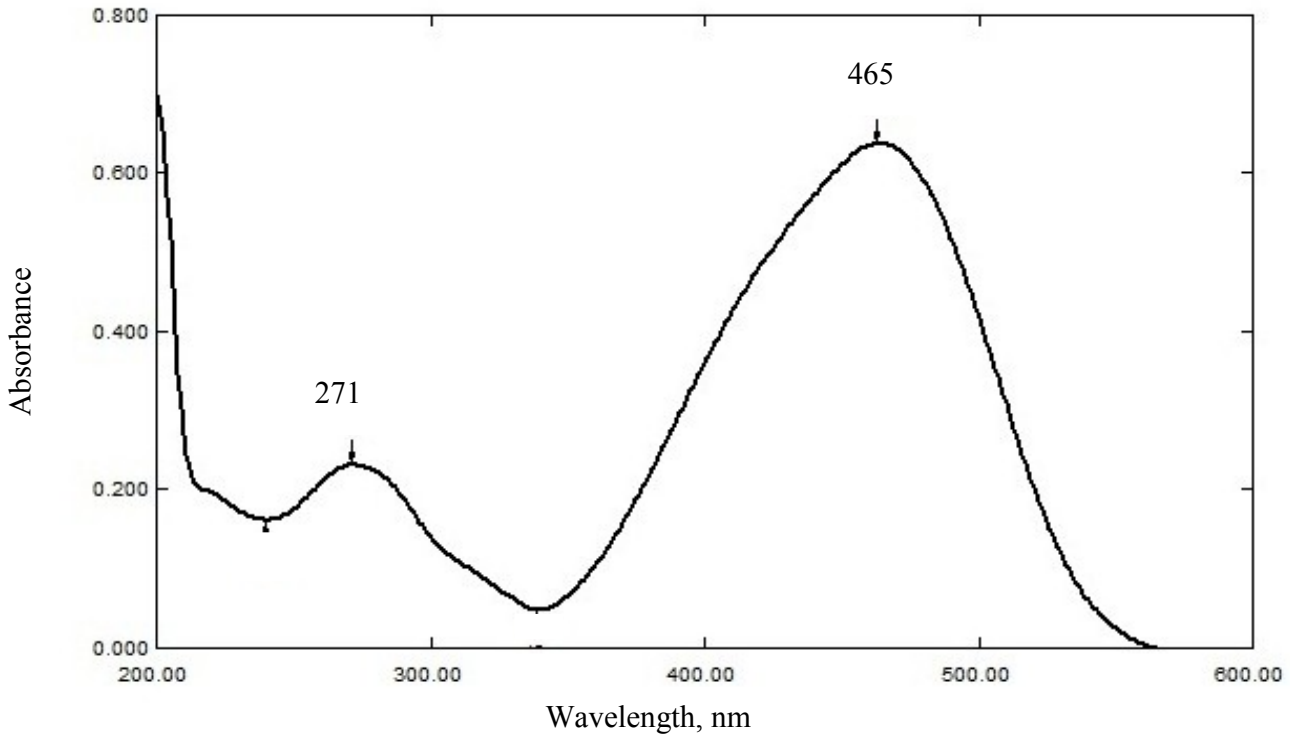

Figure 3-1: UV-VIS spectrum for methyl orange

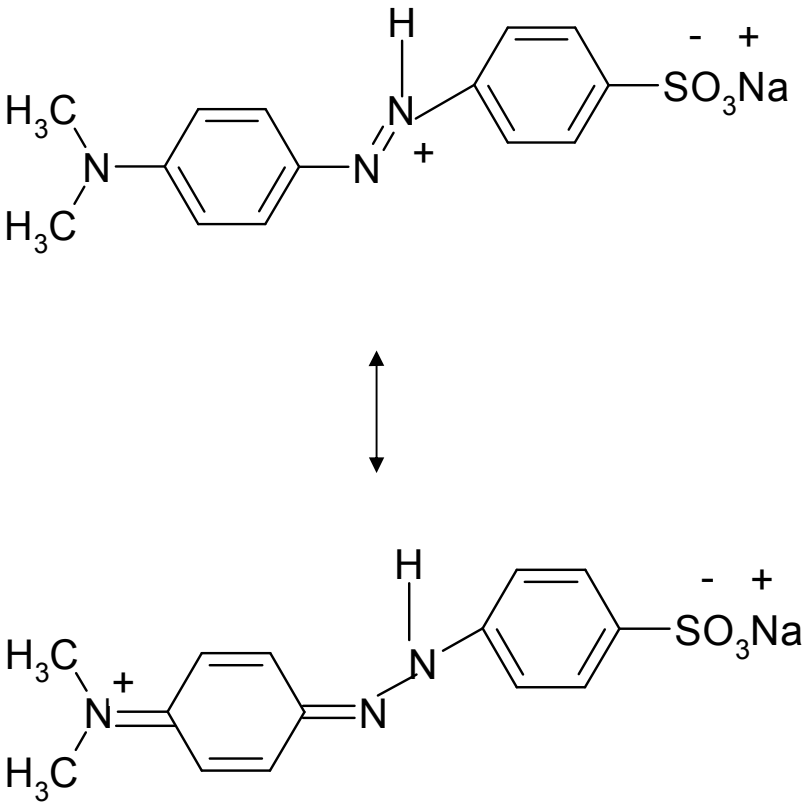

Figure 3-2: Protonation and tautomeric equilibrium of methyl orange molecule in acidic solution

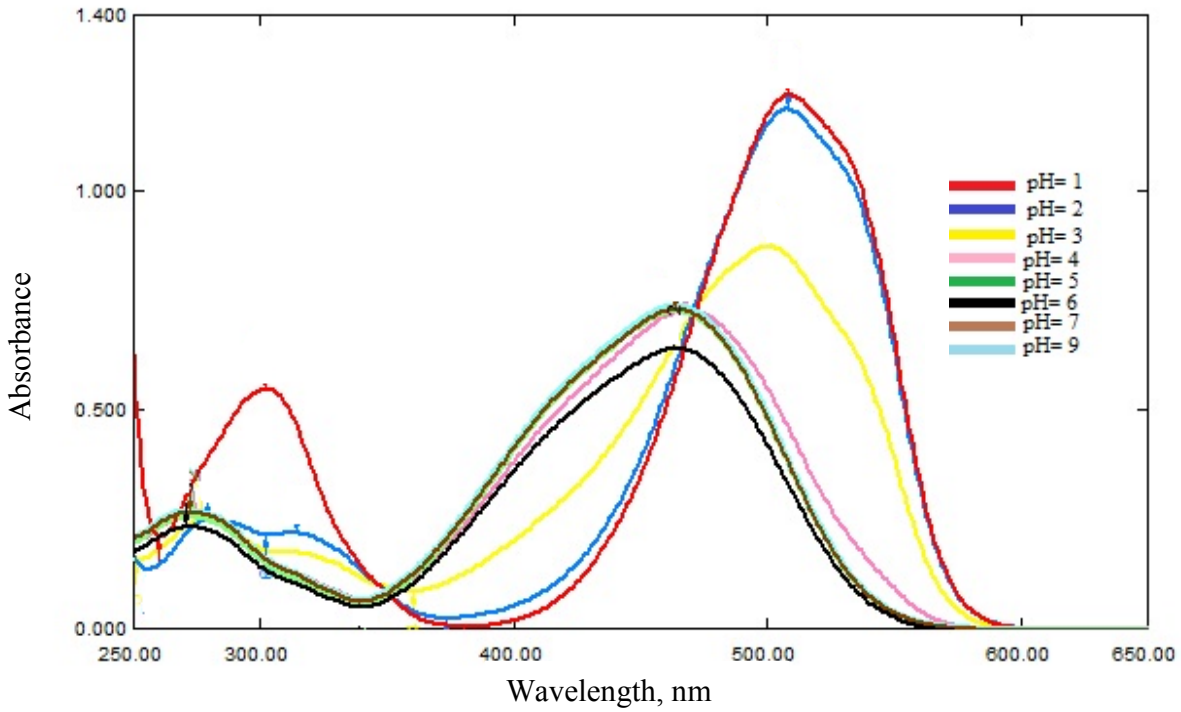

Figure 3-3: Standard scan of Methyl Orange at different pH values

This corresponds largely with behavior of congo red ($C_{32}H_{22}N_6Na_2O_6S_2$), Figure 1-3, the highly water-soluble diazo dye which has a molar extinction coefficient equals to 1.979 x 10^{+4} $mol^{-1}.L.cm^{-1}$ for molar concentration of 1.435 x 10^{-5} mole/L. congo red has a strong affinity to cellulose fibers and thus is employed in textile industries and used as an indicator of pH too [99] . Up on comparison of the UV-Vis absorption spectra for congo red at its natural pH, Figure 3-4, with the absorption spectra of congo red in aqueous solution at different pH's, Figure 3-5, the results exhibits that congo red posses important spectrophotometric properties where there is intense peak around 498 nm which is shifted to 564 nm due to the two tautomeric equilibrium forms of the protonated congo red molecule (in acidic medium), an ammonium form with the proton attached to the amino nitrogen and an azonium form, where the proton is added to the azo nitrogen, Figure 3-6 [100].

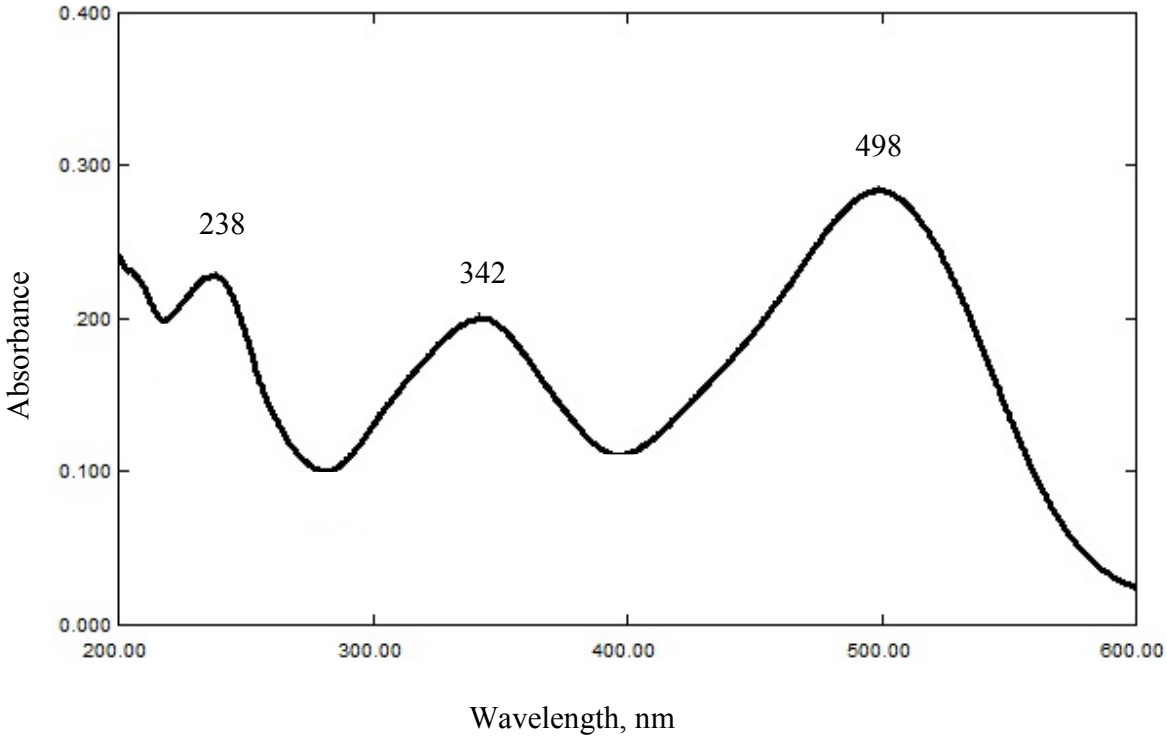

Figure 3-4: UV-VIS spectrum for Congo Red

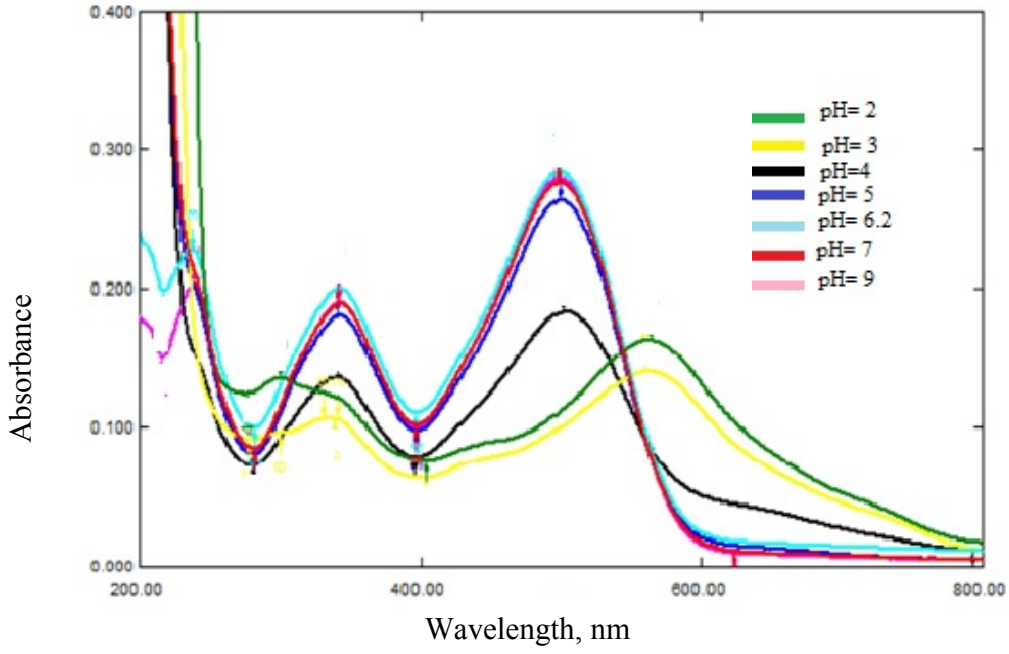

Figure 3-5: Standard scan of Congo Red at different pH values

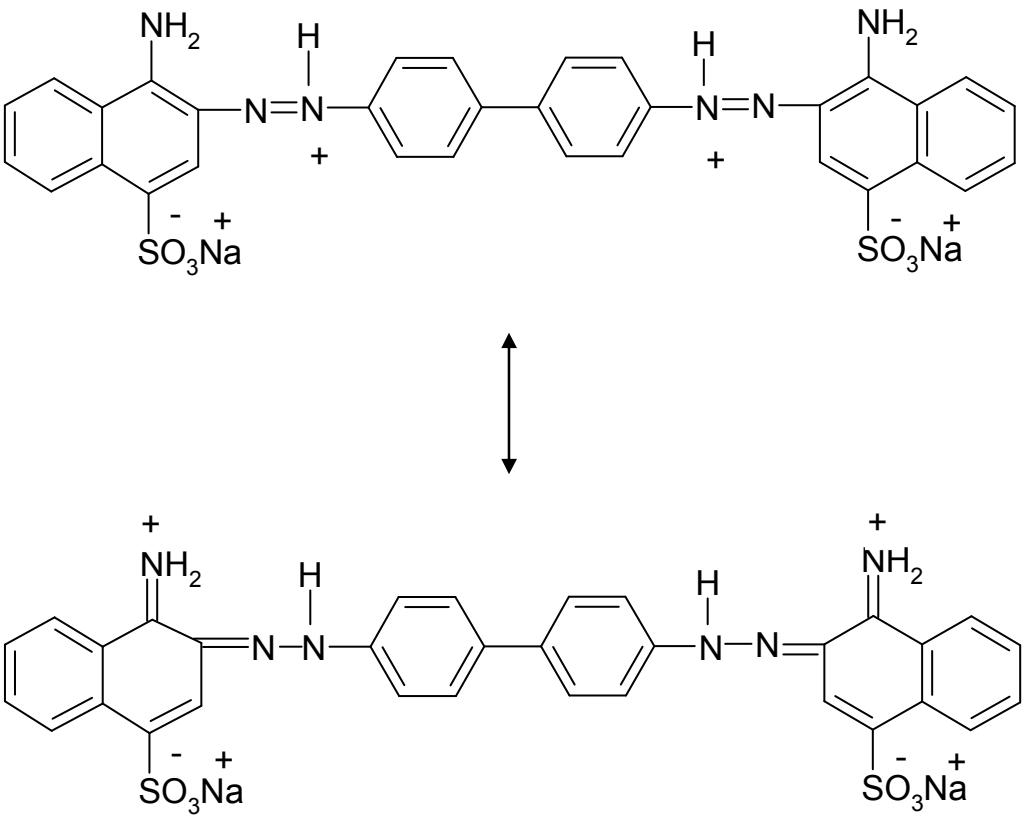

Figure 3-6: Protonation and tautomeric equilibrium of congo red molecule in acidic solution

3.2 Characterization of the synthesized anatase N-TiO_2 nanoparticles

3.2.1Characterization of morphological and structural properties of N-TiO_2 samples

Scanning electron microscope (SEM) images of undoped TiO_2 particles (anatase) revealed very smooth and homogeneous surfaces formed by very fine aggregated particles, image (A) in Figure (3-7). Whereas the N-TiO_2 particles showed slightly more compacted surface structures. Morphologies of synthesised catalysts were strongly dependent on the percent of nitrogen dopant [101-102]. In addition, the surface of the N- doped samples become a little coarser in comparison with the undoped sample, which might be due to the fact that N element was incorporated into TiO_2 lattice and led to the lattice collapse partially which is in good agreement with other reported data [103]. The surface morphology of 2.5% N-TiO_2 is characterized by

SEM, and shown in Figure 3-7, image (B). The highly ordered TiO_2 nanoparticles show that the ordered structure can sustain the impact of doping process. It also can be observed that the surface of the nanoparticles has uniform interior channels arranged parallel to each other and perpendicular to the outer surface are seen in whole material. These open ended ordered channels provide routes for light transfer and higher surface area for better adsorption, while image (C) in Figure 3-7 shows less regularly channels with holes on the surface of 5% N-TiO_2. It can be seen that there are damage of the channels and many holes or caves for 7% N-TiO_2, image (D), which mainly resulted from the increase of doping percent. These differences in the morphology of N-TiO_2 samples is reflected most clearly in the three-dimensional images in Figure 3-8.

A

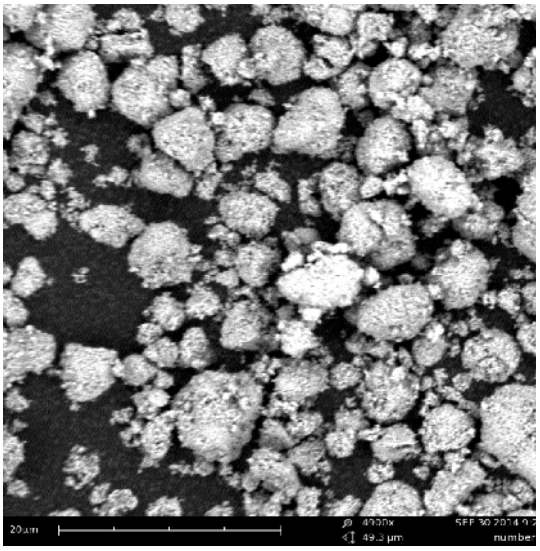

B

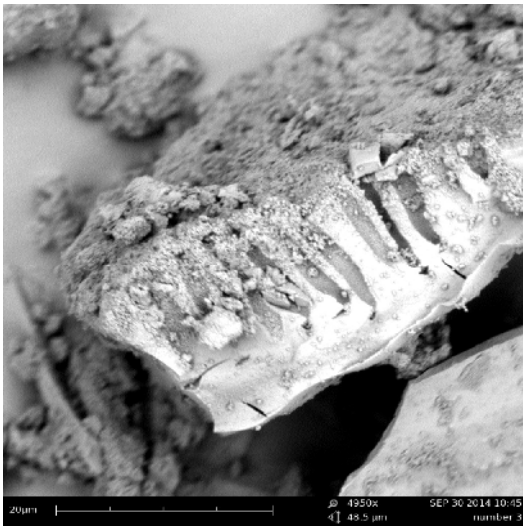

C

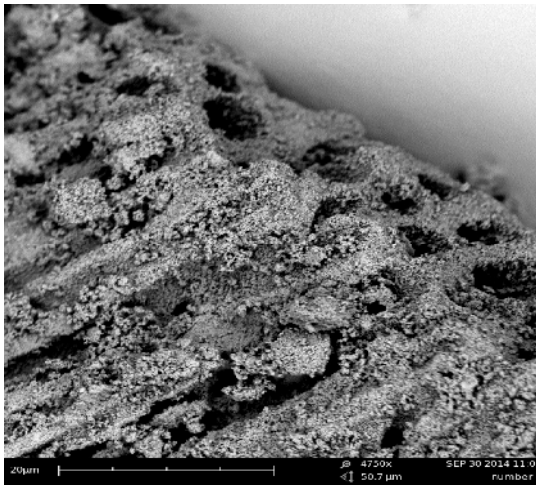

D

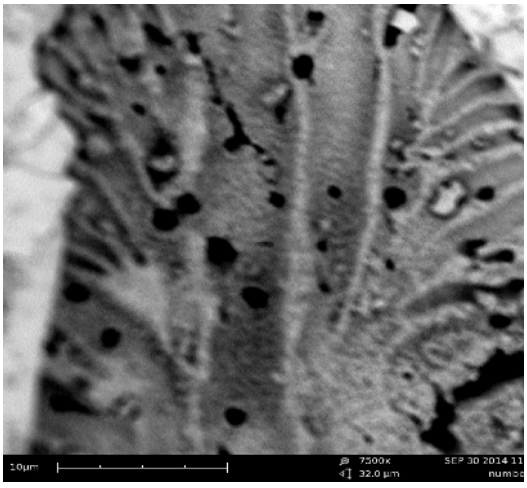

Figure 3-7: SEM images for the (A) anatase TiO_2; (B) 2.5% N-TiO_2 ; (C) 5% N-TiO_2; (D) 7% N-TiO_2

(A)

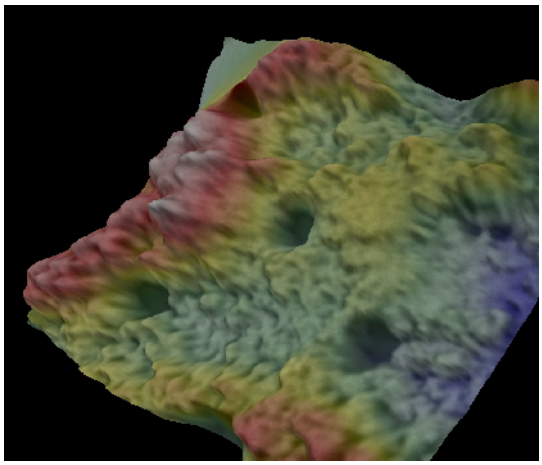

(B)

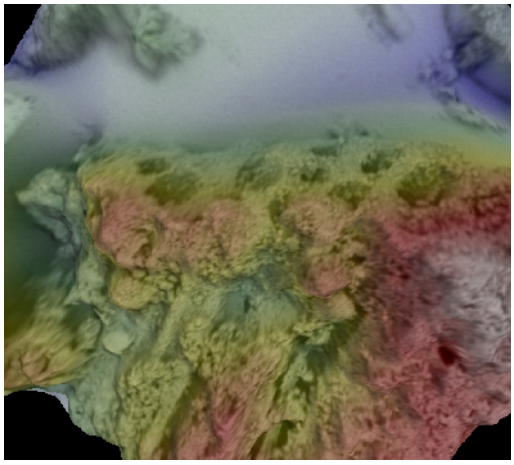

(C)

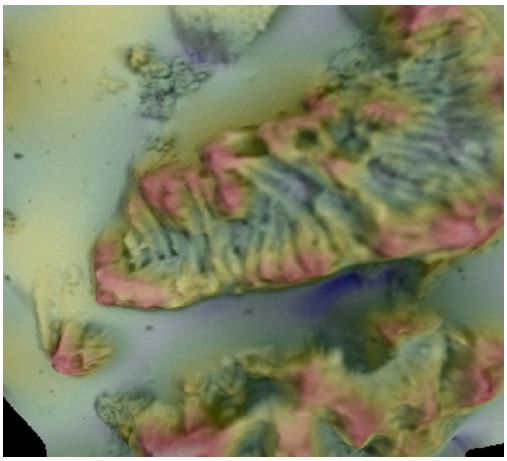

Figure 3-8: Three dimensional SEM images for the (A) 2.5% N-TiO_2; (B) 5% N-TiO_2; (C) 7% N-TiO_2

3.2.2 Optical properties

3.2.2.1 UV–VIS diffused reflectance spectra of N-TiO_2

The UV–VIS diffuse reflectance spectra (DRS) were employed to determine the effects of N doping on the light absorption of N-TiO_2 samples. Figure 3-9 shows the UV–VIS DRS spectra of the N doped TiO_2

and the undoped TiO_2 samples. As shown, the undoped TiO_2 sample depicts absorption feature in the UV region due to the inter band electronic transitions. In comparison with undoped TiO_2, all of N doped samples show light absorption band and have apparent absorption in the visible region. It is observed that with increasing nitrogen content, the band gap was narrowed. This narrowed band gap will facilitate excitation of electrons from the valence band to the conduction band in the doped oxide semiconductor under visible light illumination, which can result in higher photocatalytic activities [104]. The reduction in the band gap energy of the N-doped TiO_2 sample was determined by the following equation [105]

$E_g = h \nu = h c/ \lambda$

$E_g = 6.6 \times 10^{-34}$ J.s x 3 x 10^8 $m.s^{-1}/ \lambda$ (nm)

$E_g = 1239.8 / \lambda$

where E_g is the band gap (eV), h is Planck's constant, c is speed of light and λ is the wavelength (nm) of the absorption edge in the spectrum. The results show a clear red shift in the light absorption threshold from UV region (380) to visible region (415 nm) for 2.5% N-TiO_2.

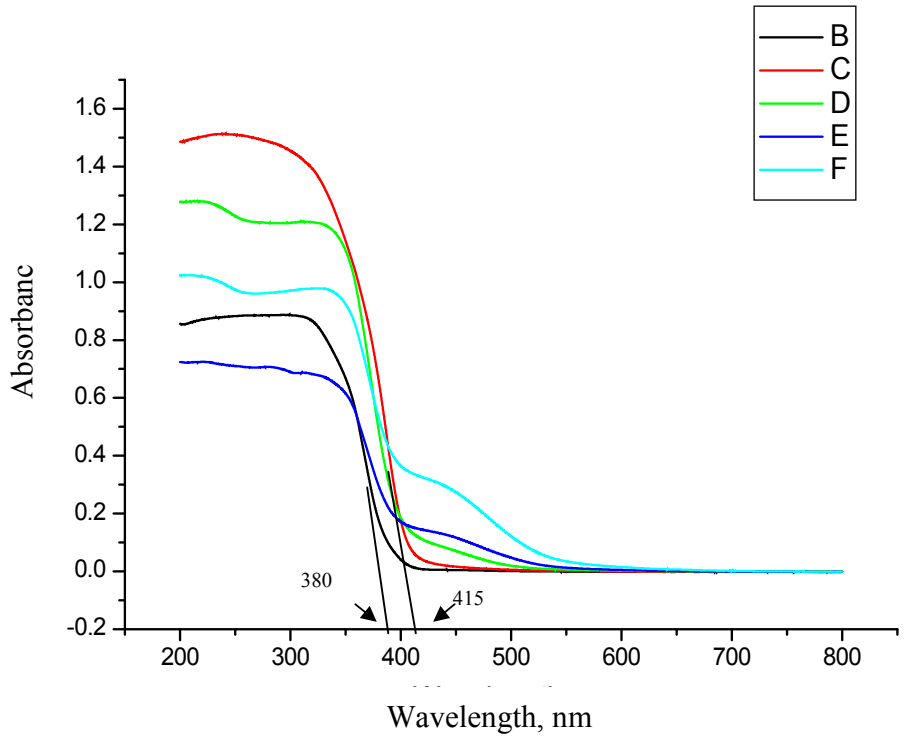

Figure 3-9: UV–vis diffused reflectance spectra of (B) undoped TiO_2 and (C) 2.5% N-dopedTiO_2; (D) 5% N-dopedTiO_2; (E) N-dopedTiO_2; (F) 7% N-dopedTiO_2

3.2.3 Photoluminescence spectra

Photoluminescence (PL) emission spectra have been widely used to investigate the recombination rate of electrons and holes [106]. To study the effect of dopants on the separation efficiency of photoinduced charges, PL spectra of as-prepared samples were investigated. Figure 3-10 illustrates PL spectra of TiO_2 nano powders doped with different amounts of N using the excitation wavelength of 340 nm. All the samples exhibit similar curve shape of PL spectra at the wavelength range from 350 to 600 nm. In general, a lower PL intensity suggests an enhanced separation and transfer of photogenerated electrons trapped in TiO_2 [103]. PL intensity obtained on 2.5% N-doped TiO_2 is lower than that on 5% and 7% N-TiO_2, indicating that N doping markedly enhances the charge separation of photogenerated

carriers of TiO_2. This phenomenon can be interpreted as the result of an appropriate content of N introbucing into the lattice of TiO_2, which formed the electron trap as mentioned in the work of Xiaoqi et al [107]. Such a structure enhanced the transfer of the energy from the matrix to the luminescence centers. The band seen around 395 nm could be assigned to the band edge emission of TiO_2 samples. The PL broad band ranging from 440 nm to 480 nm is attributed to oxygen vacancies on the surface of the N-TiO_2 while the peaks locating at 580 nm could be assigned to defect emission [103, 108].

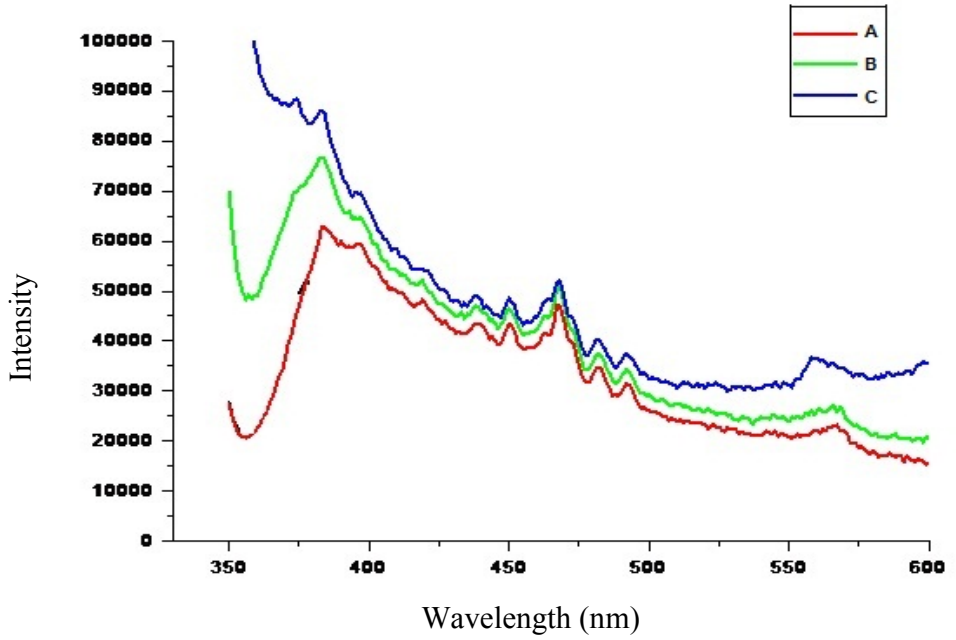

Figure 3-10: PL spectra of (a) 2.5%N-TiO_2, excitation (b) 5% N-TiO_2, (c) 7% N-TiO_2 (Xenon lamp as source of $\lambda_{exc.}$= 340 nm

3.2.4 Phase , composition features and particle size of N-TiO_2

Due to strong scattering properties of TiO_2, Raman analysis gives special spectrum of vibrational bands in which they can diagnose the

component phase of TiO_2 [109]. Figure 3-11 shows the vibrational bands of naked and N-dpoed TiO_2 at 400 cm^{-1}, 520 cm^{-1} and 640 cm^{-1} corresponding to Raman modes of B_{1g}, (A_{1g} + B_{1g}) and Eg, respectively, which are characteristic of anatase phase of TiO_2 [55, 70]. The correspondence between the spectrum of anatase TiO_2 and doped samples confirms that there is not any rutile phase in our samples.

To find out Mueller Indices of prepared samples and for comparison with standard sample (anatase TiO_2), X-ray diffraction is considered useful characterized tool for this purpose [78]. Spectrum of The XRD of TiO_2 and N-TiO_2 samples are shown in Figures 3-12, 3-13,3-14 and 3-15 respectively. As expected, the comparison with naked anatase TiO_2, did not exhibit any new XRD peak of N-TiO_2, indicating that no new phase emerged. The XRD peak at $2\theta = 25.4^o$ (101) is often taken as the characteristic peak of anatase crystal phase. The average crystallite sizes for the doped samples were estimated using the Scherrer equation [110];

$$\text{Particle Size} = B \times \lambda / F \times \cos\theta \qquad 3.1$$

where λ is the Cu Kα (0.1541 nm) radiation wavelength, F is the full width at half maximum (FWHM) of the (1 0 1) peak, θ is the half angle of the diffraction peak on the 2Theta scale [109] and B is the shape factor of the particle whose value is computed as follows[111];

$$B = 2\sqrt{\frac{\ln 2}{\Pi}} = 2\sqrt{\frac{0.693}{3.14}} = 0.94 \qquad 3.2$$

The crystallite size of all samples was shown in Table 3-1.

Table 3-1: Particle size of N-TiO_2 samples

Sample	Particle size (nm)
2.5% N-TiO_2	52.4
5% N-TiO_2	26.9
7% N-TiO_2	63.8

Energy Dispersive X-ray spectroscopy (EDX) is used to analysis the atomic composition of the N doped samples, Figure 3-16. It was confirmed that Ti and N are present. Coating of samples with gold leads to presence of signal of Au. For further analysis, we analyzed the samples using Time of Flight Secondary Ion Mass Spectrometry (TOF-SIMS) that based on the usage of pulsed primary ion beam to desorb and ionize species from the sample surface to determine chemical composition of samples. Peaks located at (46, 47, 48, 49, 50) are the known isotopes of Ti, Figure 3-17. The isotopes are in the correct ratios with one another. The peak at m/z = 69 in Figure 3-17 is Ga^+, as the analysis beam is a gallium gun. An increase of 14 due to the N doping (i.e. m/z = 60, 61, 62, 63, 64) is explicitly revealed. This gives a confirmation of the nitrogen doping in the crystal lattice of TiO_2, Figure (3-18).

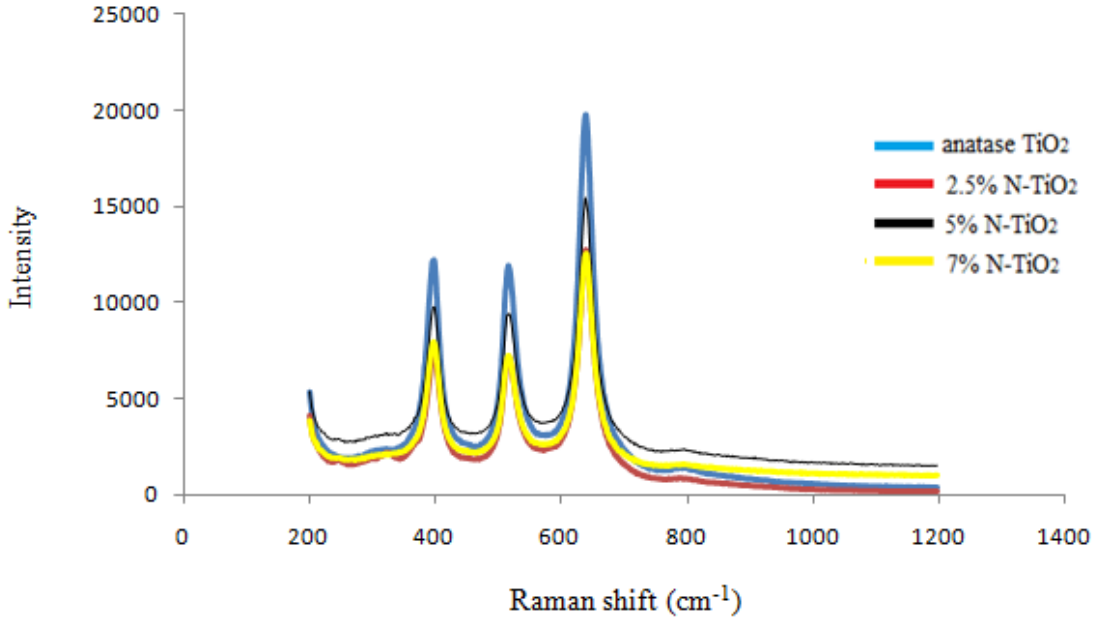

Figure 3-11: Raman spectra of anatase TiO_2 and N-doped TiO_2 with different starting N content TiO_2 powders

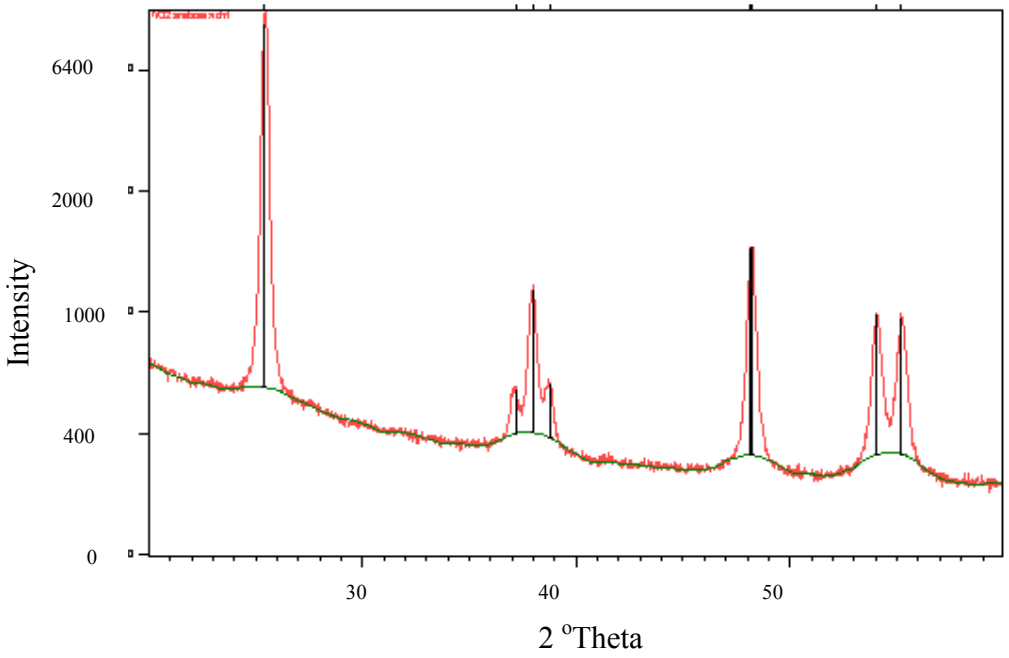

Figure 3-12: XRD pattern for anatase TiO_2

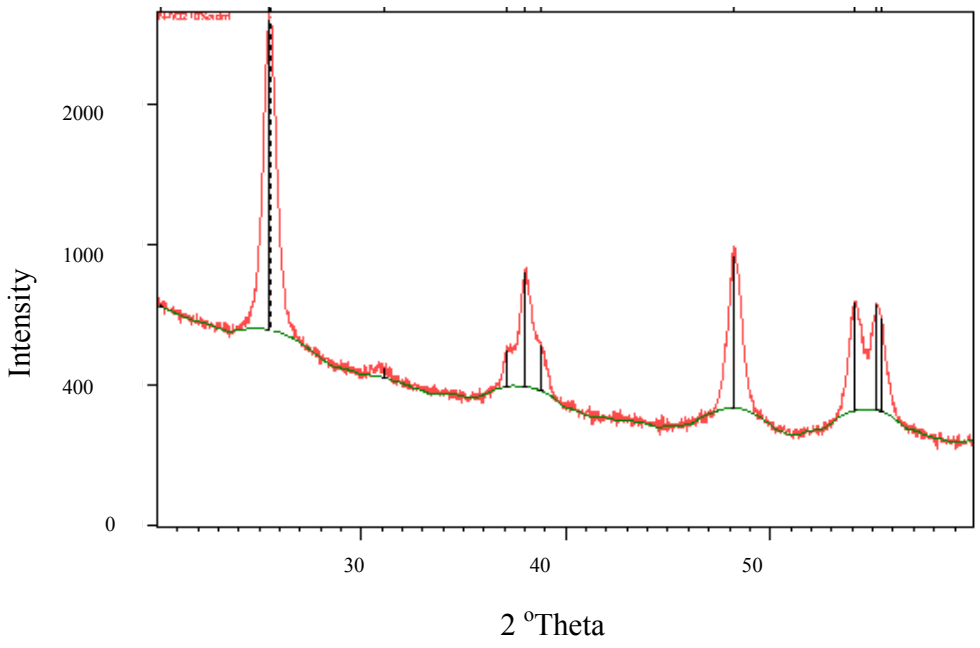

Figure 3-13: XRD pattern for prepared 2.5 % N-TiO_2

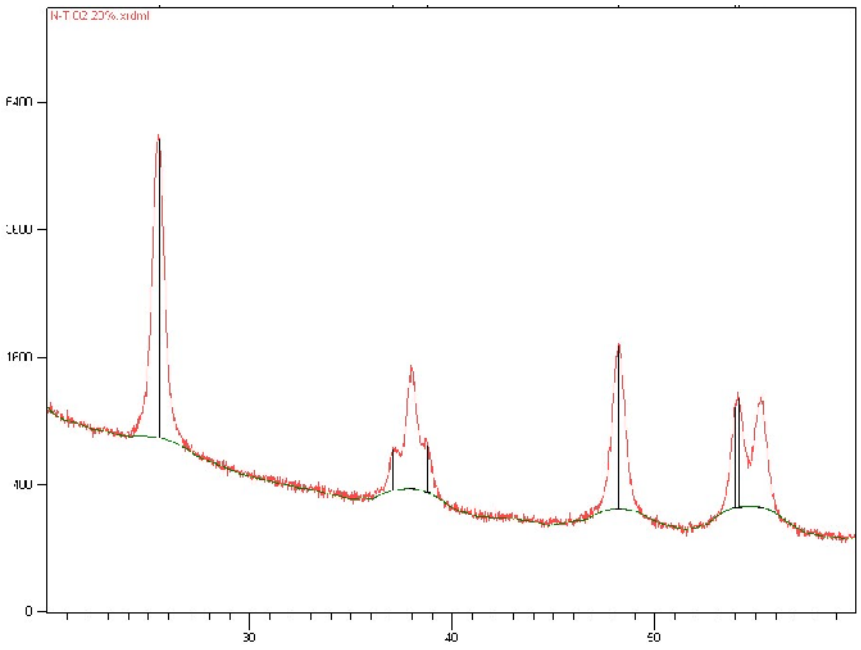

Figure 3-14: XRD pattern for prepared 5 % N-TiO_2

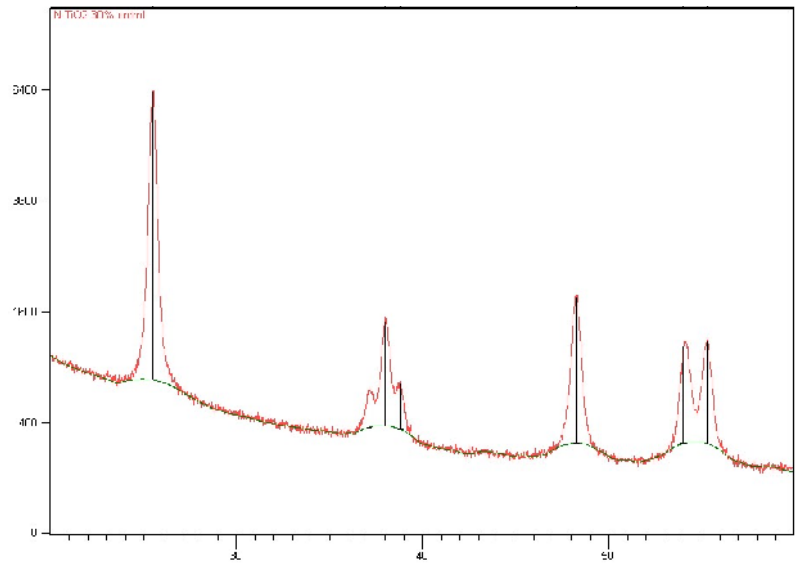

Figure 3-15: XRD pattern for prepared 7 % N-TiO_2

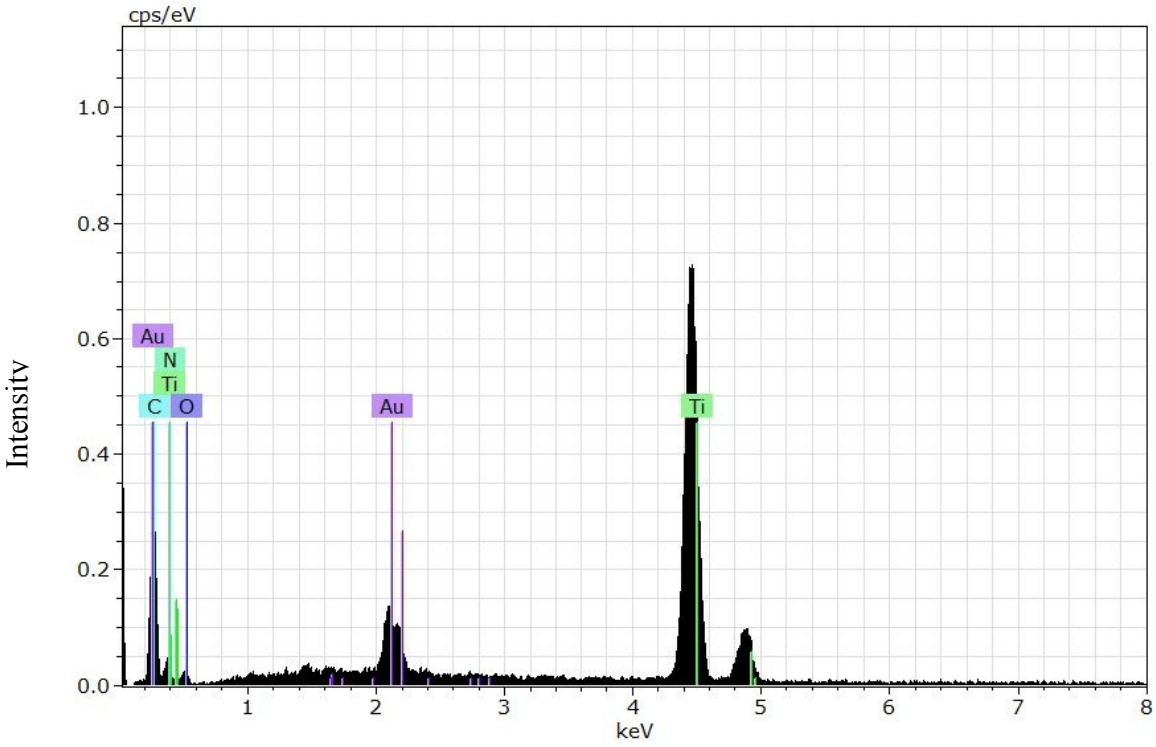

Figure 3-16: EDX analysis of 2.5% N-TiO_2

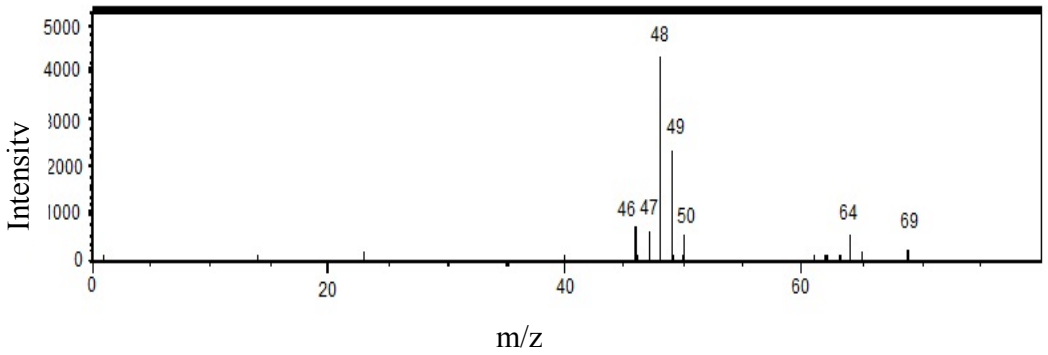

Figure 3-17: TOF-MS of undoped TiO_2

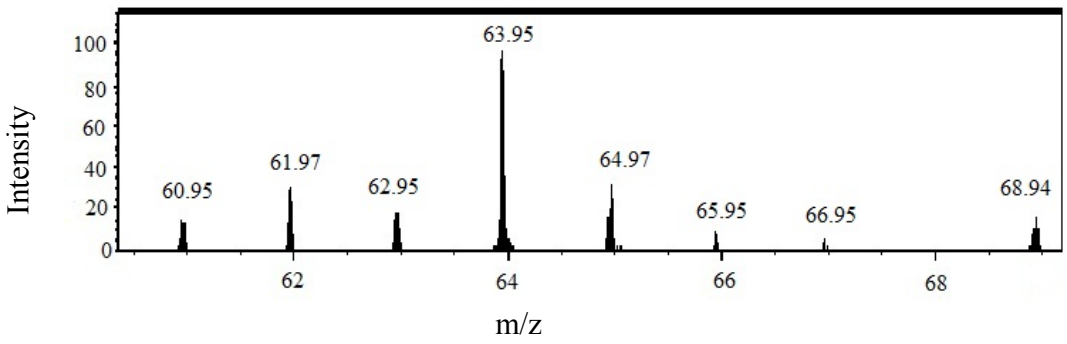

Figure 3-18: TOF-MS of 2.5% N-TiO_2

3.2.5 surface area analysis of N-doped TiO_2

The surface area of the prepared N-TiO_2 specimen has been determined based on the Brunauer, Emmett and Teller (BET) theory. The analysis scheme relies on using adsorption of molecular nitrogen gas on the surface of TiO_2. A Kaolinite calibration standard was used to calibrate the machine while the Micromeritecs Stardriver software was used to calculate surface area, through computing the volume of nitrogen adsorbed at different partial pressures. The BET surface area was increased from 41.824 to 48.412 m^2/g when increasing the nitrogen content from 0.0% to 2.5%. However, BET surface area decreased from 48.412 to 28.816 m^2/g and to 15.187 m^2/g for samples of 5% and 7% N-TiO_2, respectively. The pore diameter of the mesoporous N-TiO_2 structure was determined from the BET isotherms to be 9.966 nm compared with 6.248 nm of bare anatase TiO_2. This indicates that the surface is still of mesoporus nature. 5% and 7% of N-TiO_2 pore sizes are not known which is attributed to the machine is old and can not detect the small pore size. Some authors have reported that using of large amounts of nitrogen leads to blockage of TiO_2 pores and reduce the surface area [112-113]. Figure 3-19 shows the pore size, which verifies the mesoporosity of the prepared nano N-doped TiO_2 nanoparticles.

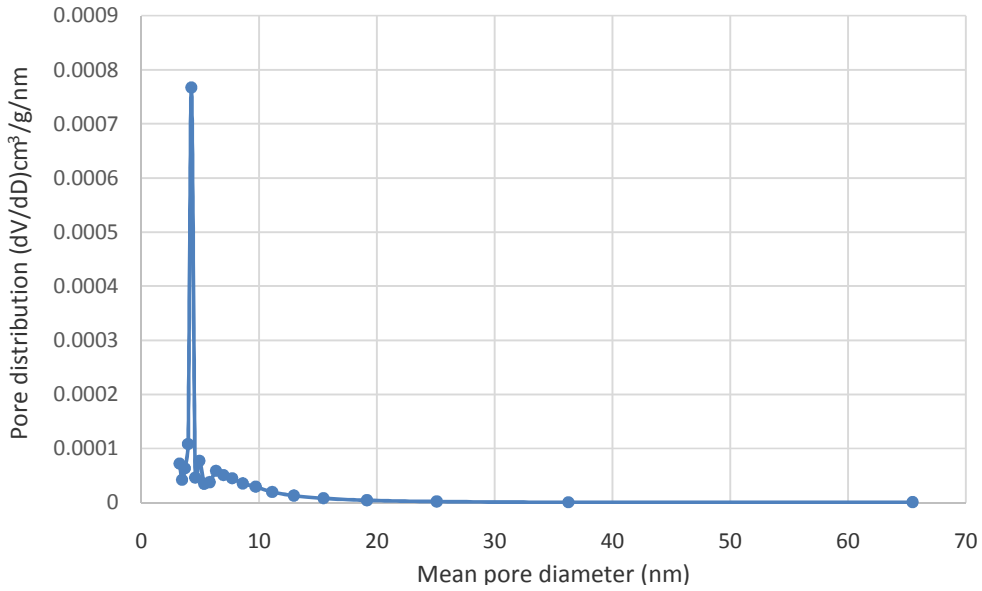

Figure 3-19: Pore size distribution graphs for the N-TiO_2 sample

3.3 Control experiments

Control experiments were carried out to verify that the color removal of the dye was truly photocatalytic and not just due to photolysis and/or ordinary adsorption. The photolysis experiments, in the absence of N-TiO_2 photocatalyst at room temperature for 240 minutes and the pH of the dye around 2.5. revealed that the self-degradation of MO was almost negligible under visible illumination and this clearly showed that homogeneous photochemical processes did not occur under the on going experimental conditions. On the other hand, the reaction of dye with peroxide in the presence of irradiation showed the signifigant role of hydrogen peroxide where the degradation percent was 34.6%. Under similar experimental conditions but in the dark, there is no change in the concentration of the dye with time, indicating that the observed changes are due to a photo-induced process. The percent was convergent when dye was mixed with catalyst

under irradiation at acidic pH = 2.5. The color removal of MO pollutant was almost complete in 60 min under halogen lamp illumination and at optimum conditions pH = 2.5, 50 mg N-TiO_2 and 2 milliliter of hydrogen peroxide.

The last experiment in the absence of irradiation and presence of catalyst at pH = 2.5 illustrated little adsorption of the dye onto N-TiO_2. This might be interpreted by the relative easiness of subsequent desorption due to adsorption-desorption equilibrium and migration of the substrate molecules from adsorption sites to the photoactive sites [114]. However, To assess the efficiency of photocatalytic reaction the extent of adsorption is very important [115]. As a result, the oxidation of the dye molecules could be only effective when the catalyst, light and hydrogen peroxide exist at optimum pH. Figure 3-20 and Table 3-2 display photodegradation experiments for the control tests listed below;

a = MO (10 ppm) +Vis light + duration 4h + pH=2.5

b = MO (10 ppm) +2 milliliter (0.675 N) H_2O_2 + duration 4hrs in dark + pH=2.5

(absence of light)

c = MO (10 ppm) + 2 milliliter (0.675 N) H_2O_2 + Vis light + duration 4hrs + pH= 2.5

d = MO (10 ppm) +50 mg N-TiO_2 + 2 milliliter (0.675 N) H_2O_2 + pH = 2.5 + duration 4hrs (absence of light)

e = MO (10 ppm) + 50 mg N-TiO_2 + Vis light + pH =2.5 + duration 4hrs

f = MO (10 ppm) + 50 mg N-TiO_2 + pH=2.5 + duration 4hrs in dark

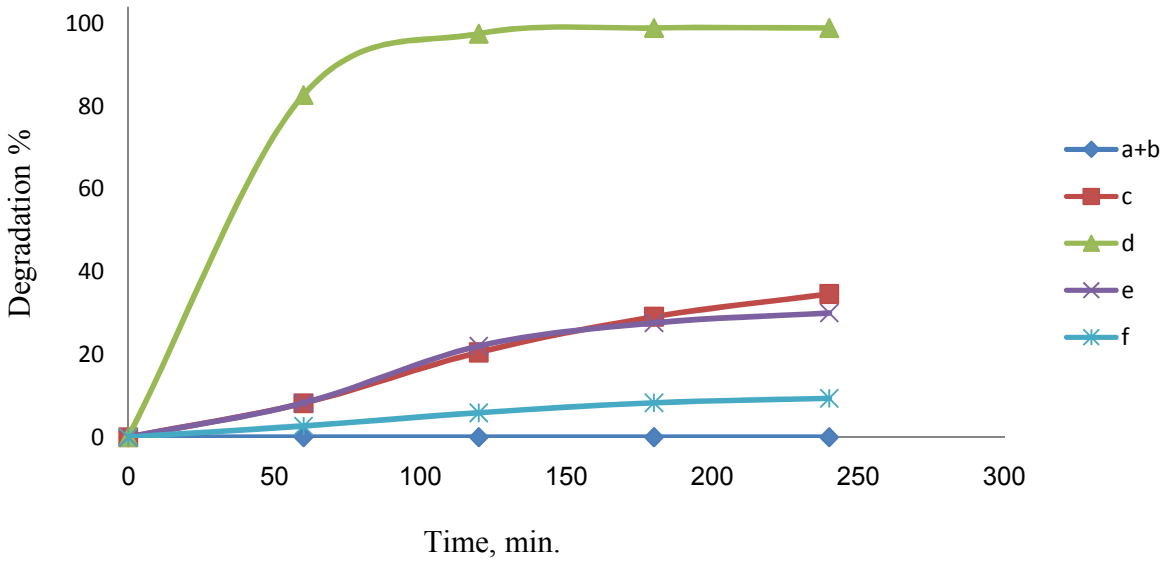

Figure 3-20: Degradation percent of methyl orange for control experiments

Table 3-2: Degradation percent of methyl orange for each control experiments

Time/ min.	a+b	c	d	e	f
0	0	0	0	0	0
60	0	8.2	82.7	8.25	2.68
120	0	20.5	97.5	22	5.89
180	0	29.1	98.9	27.6	8.31
240	0	34.6	98.9	30	9.38

3.4 Experimental optimization of photocatalysis parameters

3.4.1 Influence of initial pH on the degradation

The solution's initial pH value can directly affect the nature of the charge carried by the catalyst surface and the adsorption behavior of the pollutant on the catalyst surface. In addition, the initial solution pH also

further affects the aggregation of the semiconductor catalyst in the solution [86,116]. The isoelectric point of N-doped TiO_2 particle is 6.25 [86] and accordingly, the following equations, 3.3 and 3.4, may occur on the surface of N-doped TiO_2 at different pH values:

$$TiOH + H^+ \rightarrow TiOH^{2+} \qquad 3.3$$

$$TiOH + OH^- \rightarrow TiO^- + H_2O \qquad 3.4$$

According to above reactions, TiO_2 is carrying positive charge in acidic medium and negative charge in basic medium [62, 27, 56]. The presence of sulfonate groups that carry negative charge in methyl orange and Congo red in addition to their high electronic density because of conjugated system between π electrons in aromatic rings, it make the dyes behave as ligand that strongly attack on TiO_2 which has empty d orbital that is capable of receiving of electrons from azo dyes [18]. NMR spectrum assured this reason. The ^1H NMR spectrum of the Congo red salt, Figure 3-21, shows a signal at 7.75 ppm which is attributed to the amino group. When Congo red present in acidic medium, this signal disappears [100]. For methyl orange, Figure 3-22, the shifting of signals towards left of spectrum illustrate the impact of acidic hydrogen which consequently suggests that the dyes are protonated in acidic medium according to the pathways shown in Figures 3-23 and 3-24 for CR and MO, respectively [98, 117].

Both dyes showed better degradation results at lower pH where the rate constant of methyl orange was 0.039 min^{-1} at pH 2.5 while it was 0.021 min^{-1} for Congo red at the same pH value (Figure 3-25 and 3-26).

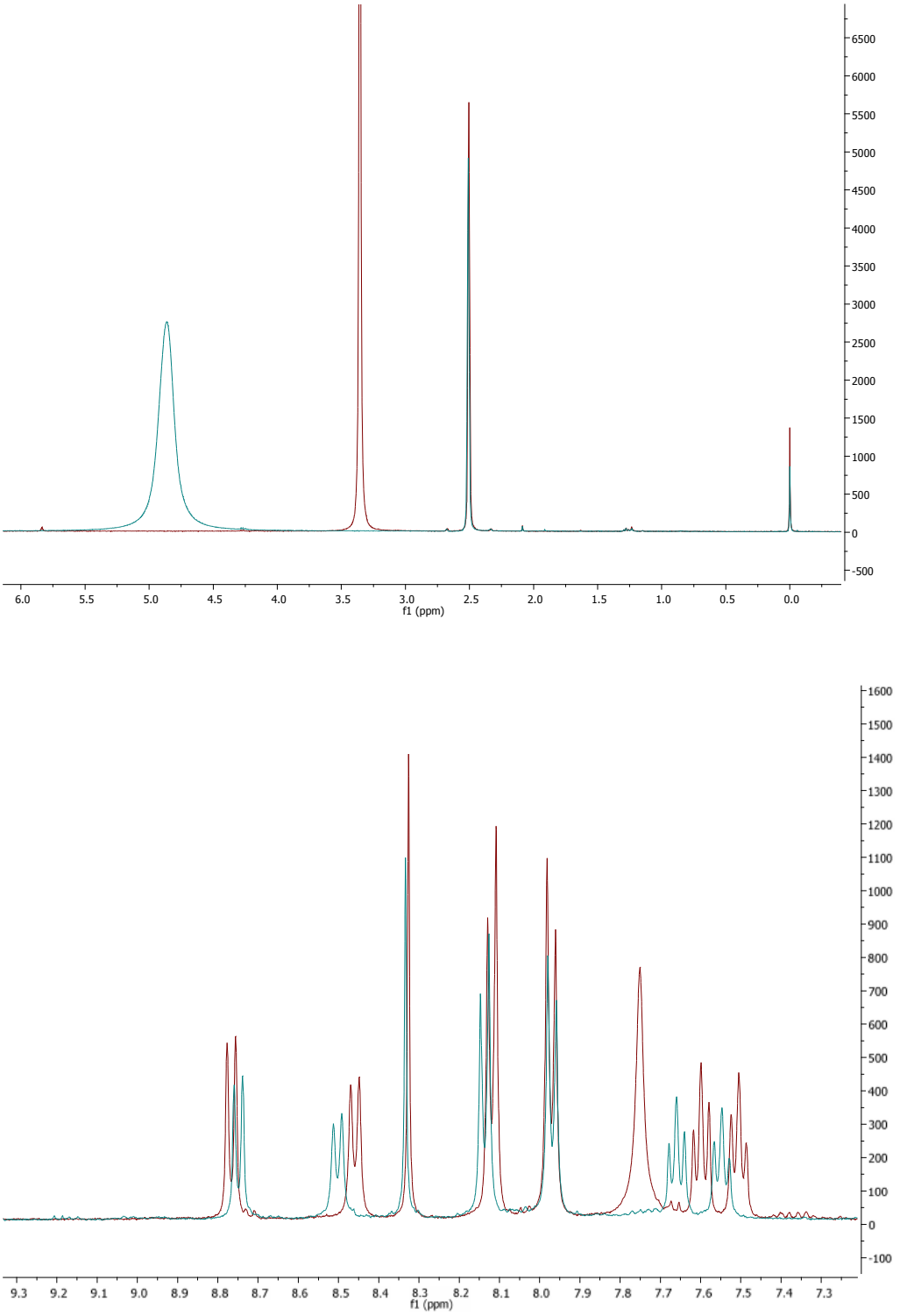

Figure 3-21: ^{1}H-NMR spectra of congo red, red signals for standard congo red and blue signals for congo red in acidic medium using DMSO_d6 solvent

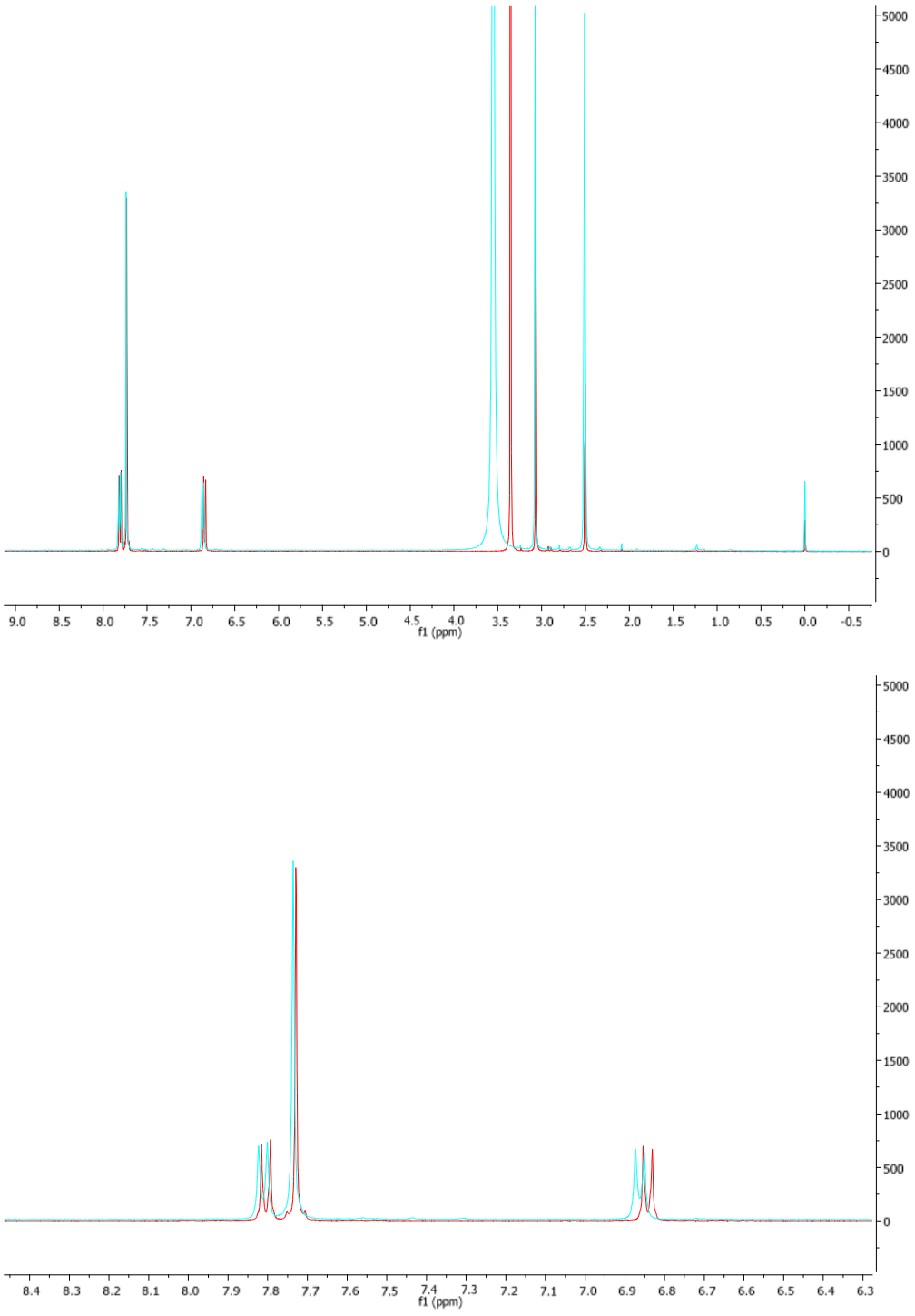

Figure 3-22: ^{1}H-NMR spectra of methyl orange, red signals for standard methyl orange and blue signals for methyl orange in acidic medium using DMSO_d6 solvent

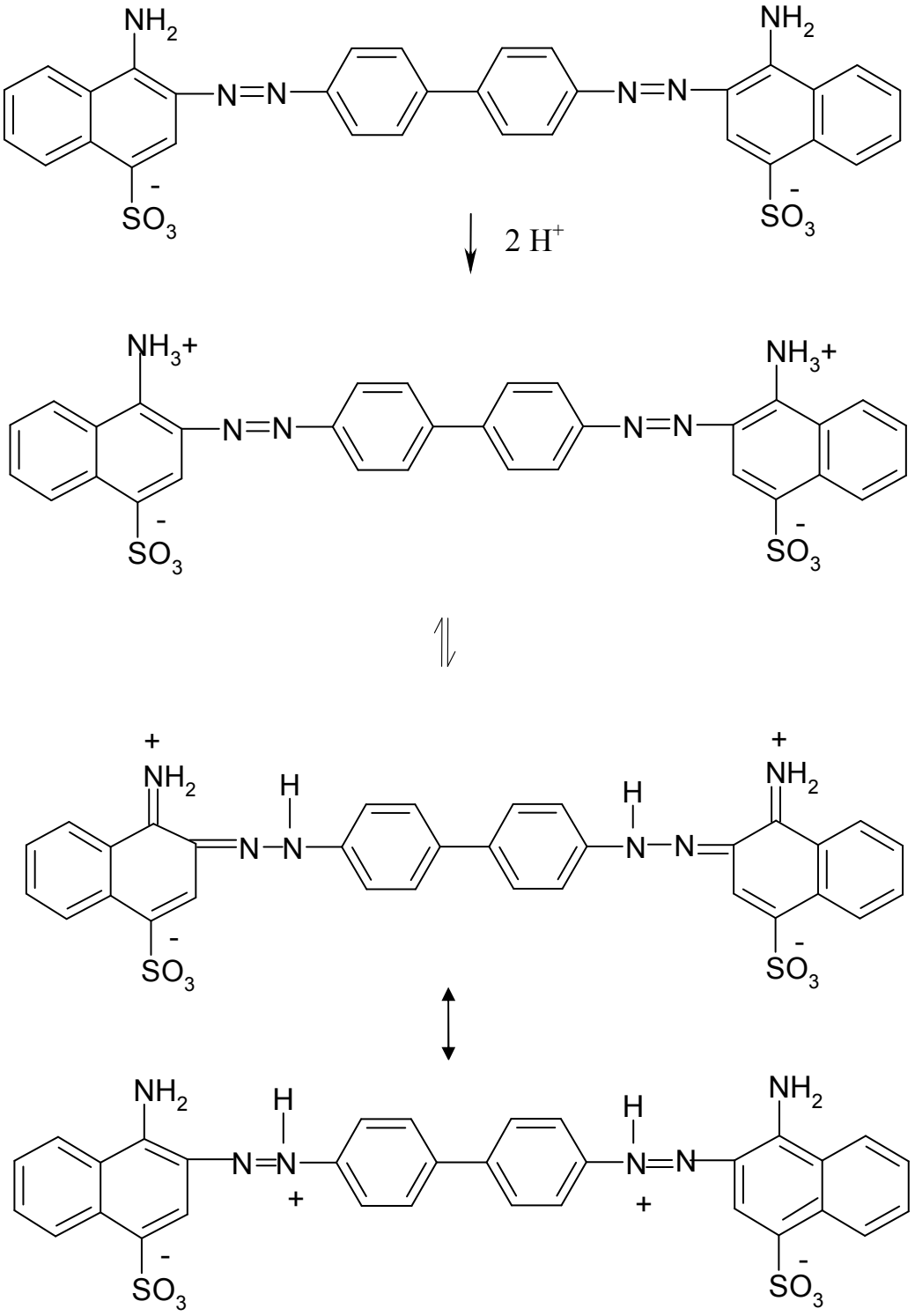

Figure 3-23: Protonation of congo red

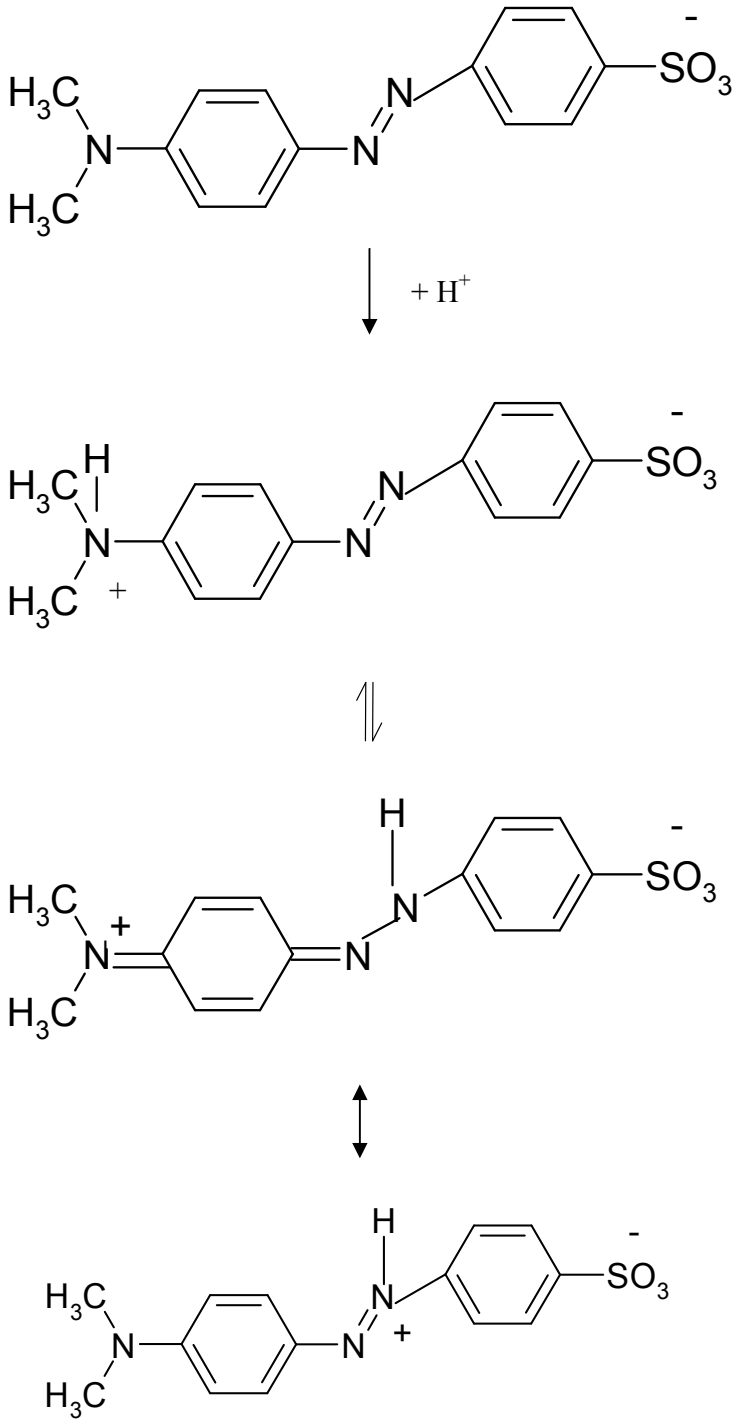

Figure 3-24: Protonation of methyl orange

k, min^{-1}	pH
0.001	9
0.002	7
0.008	5
0.013	4
0.023	3
0.039	2.5
0.03	2
0.026	1

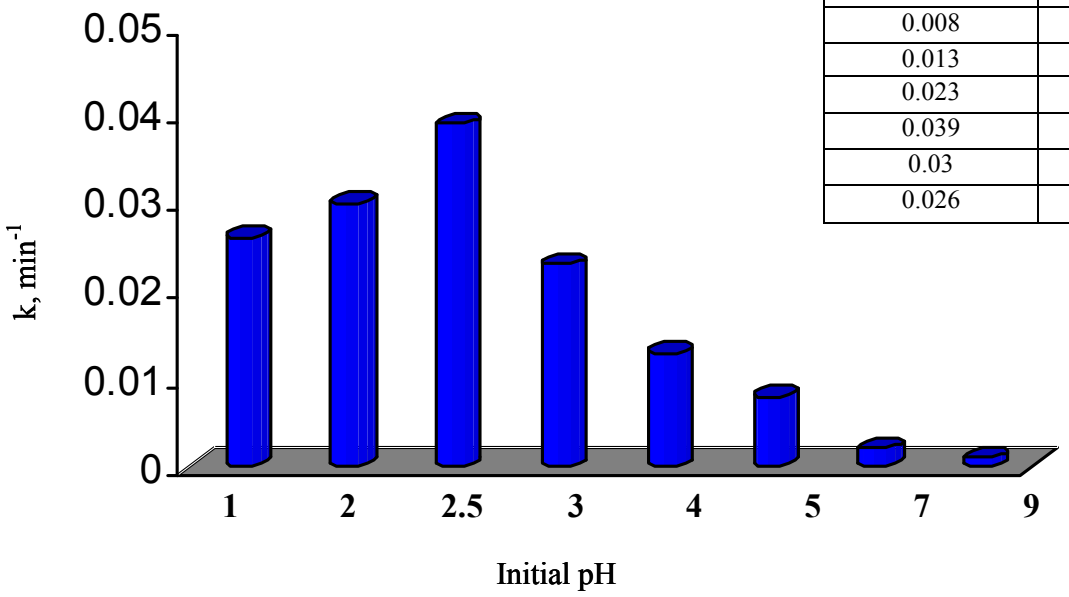

Figure 3-25: Effect of initial solution pH on the rate of phocatalysis of MO

k, min^{-1}	pH
0.021	2.5
0.016	3
0.007	4
0.005	5
0.002	7
0.002	9

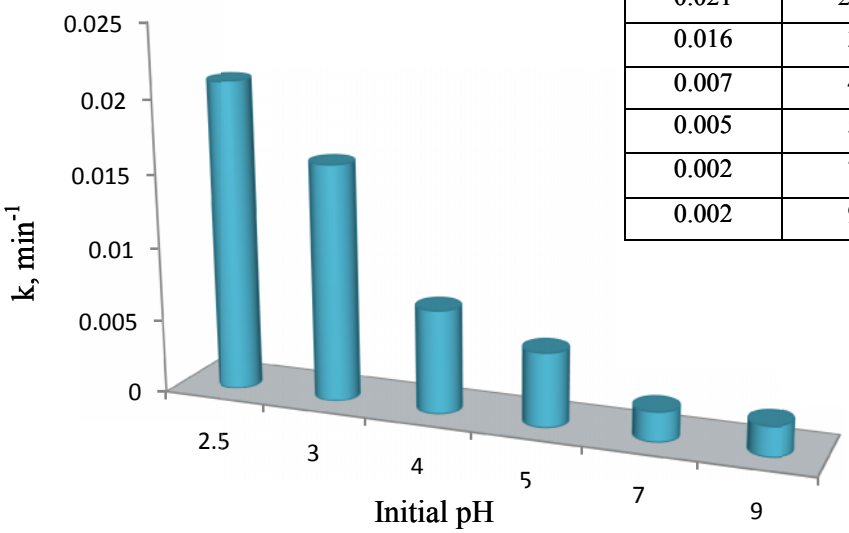

Figure 3-26: Effect of initial solution pH on the rate of phocatalysis of CR

3.4.2 Variation of pH and conductivity during photocatalysis process

The pH of the MO dye solutions before and after exposure was monitored to study the change in pH as a function of the irradiation time. The time variation of pH value of samples is shown in Figure 3-27, which indicates that the pH value of the samples slightly increases with increasing reaction time. However, no significant changes in pH were observed after 60 min of irradiation, but it can be considered that the trend of the pH change is consistent with the decolorization efficiency and indicated the organic pollutants were continuously decomposed forming simple inorganic ions, which is in accordance with the photocatalytic degradation in the presence of N-TiO_2 catalyst [118].

The conductivity or electrical current estimates the amount of dissolved ions in solution. This current depends on the temperature of the solution, ion mobility and concentration or numbers of ion present [119]. The initial conductivity was recorded prior to the irradiation of the sample and the other conductivity values were recorded after each 15 minutes of irradiation time. These results could be used to predict the degree of mineralization of the dye. Figure 3-27 shows the time variation of conductivity of dyes. It can be seen that the conductivity of dyes increases with increasing reaction time and climbs up more quickly in the first 15 minutes of the process, and the change trend is consistent with the decolorization efficiency, which means that ions in the solution augment with increasing reaction time and the dye molecules have been decomposed to ions and other substances [120].

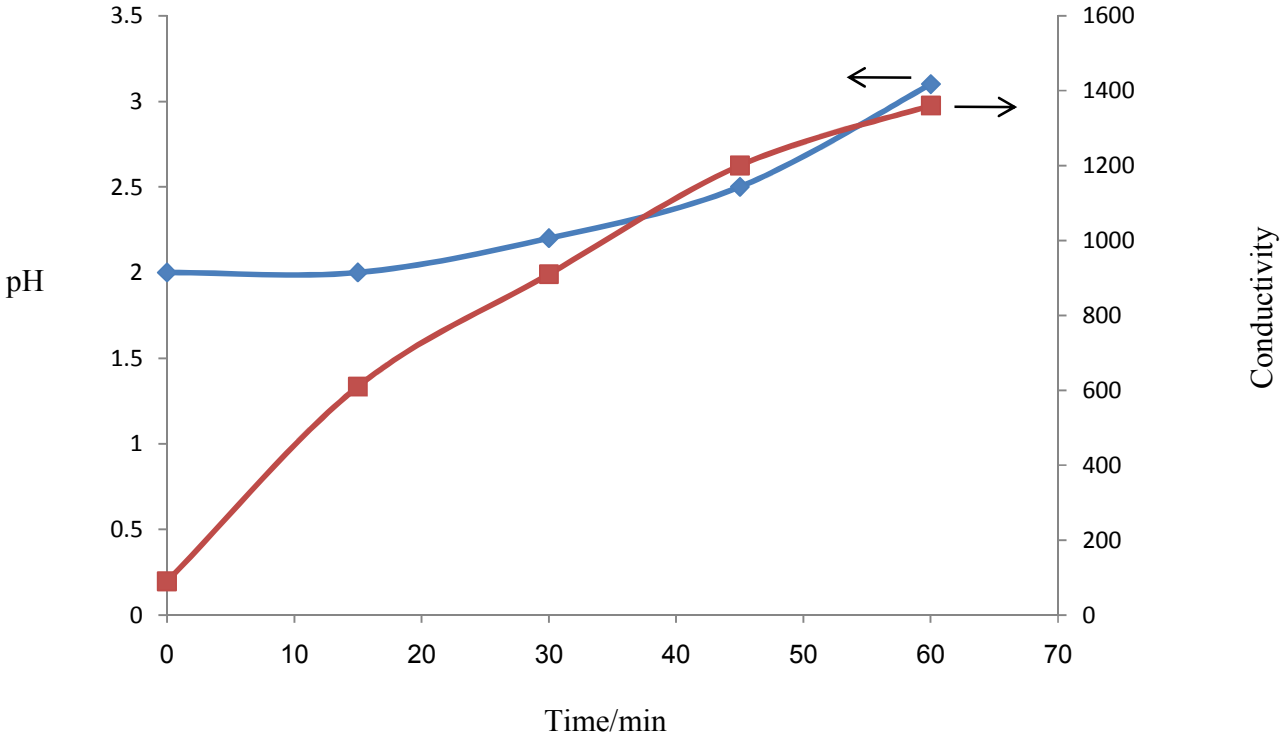

Figure 3-27: Changes of pH and conductivity during the photocatalysis process

3.4.3 Effect of catalyst loading

Using large amounts of catalyst leads to increased cost, so it is necessary to determine the optimum values of the material [9]. Increasing the catalyst loading results in increasing of active sites on the surface of catalyst and consequently increase of $^{\bullet}OH$ radicals number and as it is well known exist high concentration of hydroxyl radical is considered very important factor that effects on decoloration rate [21]. On the other hand, loading large amount of catalyst leads to decrease of degradation rate because of particle-particle interaction (agglomeration) that makes the solution turbid and eventually prevent light photons to reach into the solution [3, 18, 121].

Different amounts of catalyst from 20 mg to 100 mg were used to know the effect of loading on the reaction rate and degradation percent. From Figures 3-28 and 3-29 one could conclude that the degradation of both dyes increased significantly with increasing of catalyst concentration and then decreased with further increase of the catalyst concentration due to light scattering and screening effect. Some researchers suggest that there is no significant affect on the dye degradation at higher addition of photocatalyst quantities [122]. This agrees well with our results of Congo red. It is also noted by others [122-123] that there is fluctuation of degradation percent with further increases of catalyst concentration. Wang et al. [118] reported that with ascending added amount of catalyst lead to gradual increase in the degradation ratio due to the increase of the surface area and then high adsorbability of dye in case of rutile and even though we used anatase, but this may be the reason. Therefore, the existence of an optimum value in this reaction system is essential. The observed optimum concentration of the catalyst has been about 50 mg for a given concentration of 10 ppm of methyl orange solution and 40 mg for 15 ppm of Congo red. From a practical application point of view, the concentration of 50 mg and 40 mg are moderate quantities.

N-TiO_2 loading (mg)/L	Degradation%
20	91.4
40	95.6
50	98
60	96
80	90.6
100	86.2

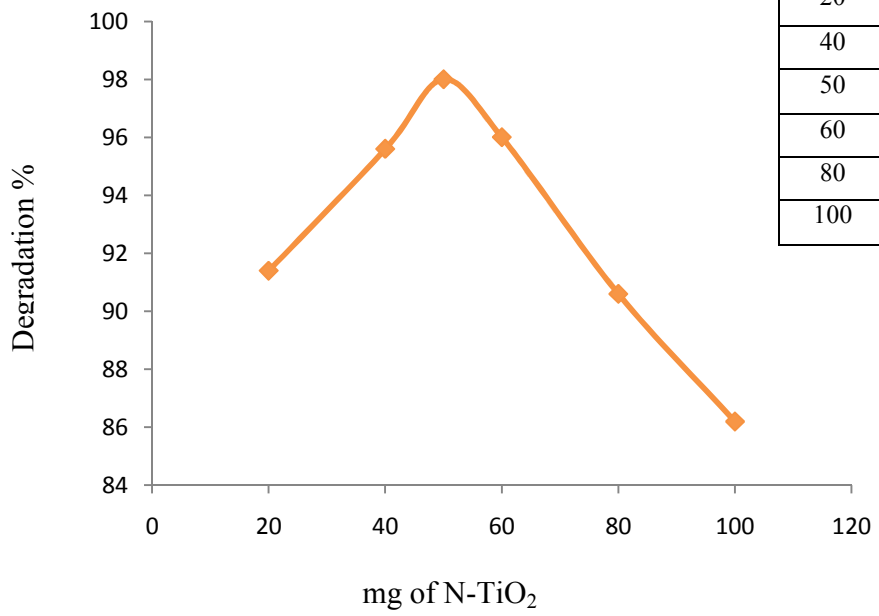

Figure 3-28: Effect of N-TiO_2 loading on the removal of methyl orange

N-TiO_2 loading (mg)/L	Degradation%
20	92.4
40	97
50	94
60	86.6
80	91
100	89.5

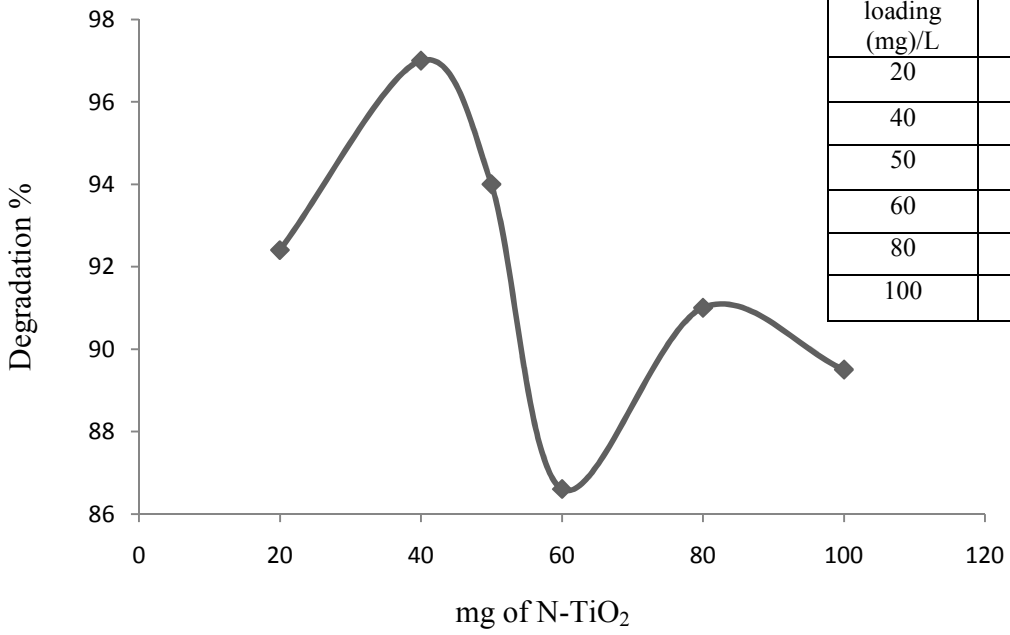

Figure 3-29: Effect of N-TiO_2 loading on the removal of congo red

3.4.4 Effect of initial dye concentration on the degradation

The effect of initial methyl orange concentration in water on the photocatalytic effectiveness of the process was examined. The photocatalytic

decomposition of the dye was studied by varying the initial concentration from 5 to 30 mg. L^{-1}. For the concentration of 15 mg/L complete discolouration of the solution was observed (98-97%) after 60 min of illumination. For concentration of methyl orange below 15 mg/L, practically the totality of the dye disappeared with 97.4 % and the solution becomes completely transparent. Similar observations are made in the case of congo red and the results are shown in Figures 3-30 and 3-31 for MO and CR, respectively. At initial dye concentration of 30 mg/L, the rate of elimination reached hardly 50% for a total time of 60 min. However better results can be obtained by extension of reaction time. Beyond 20 mg/L, degradation becomes very slow. The rate of degradation relates to the probability of $^{\bullet}OH$ radicals formation on the catalyst surface and to the probability of $^{\bullet}OH$ radicals reacting with dye molecules [27]. Once the concentration of dye is increased; firstly, the adsorption amounts of catalyst attain the saturation for superfluous dye. Secondly, the mutual screens among dye molecules also increase along with the concentration rising of dye. Thus, once the concentration of dye is increased, it also causes the dye molecules to absorb light and the photons never reach the photocatalyst surface and therefore less $^{\bullet}OH$ are formed, thus resulting in less degradation percentage [122, 124]. Additionally, according to Beer–Lambert law, by increasing the molecules of the dye, penetration of photons into the solution decreases, which causes lower photonic adsorption on the nano photocatalyst and consequently a reduction in the efficiency of (e^-_{CB}/h^+_{VB}) pair formation [22].

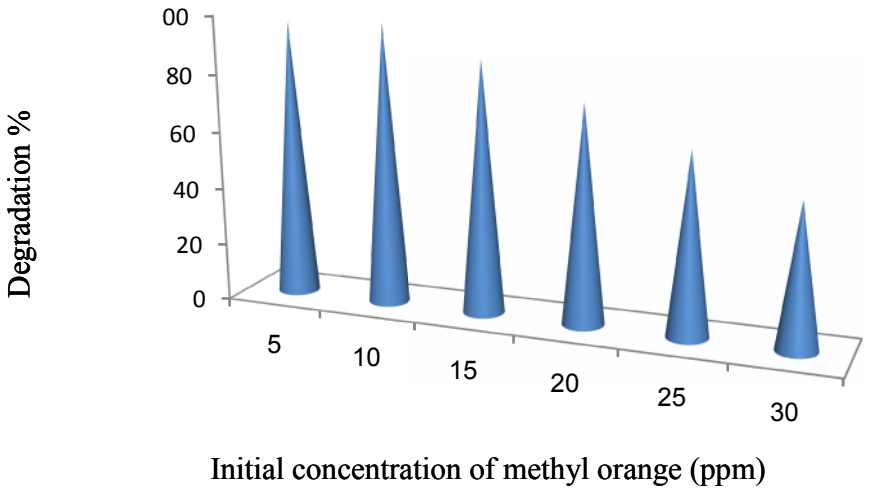

Conc. of MO (ppm)	Degradation%
5	96.6
10	98
15	87.5
20	75.6
25	63
30	49.9

Figure 3-30: Effect of initial methyl orange concentration on photodegradation efficiency

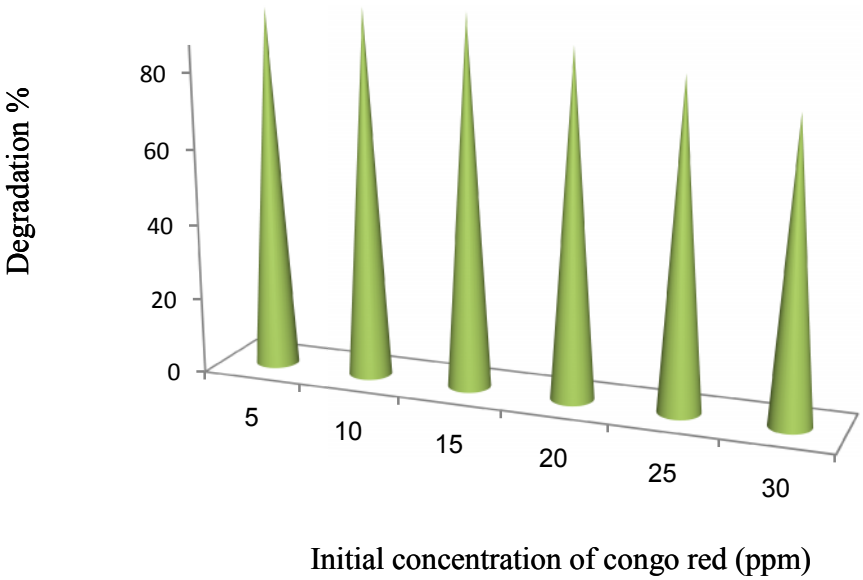

Conc. of C.R (ppm)	degradation%
5	95.3
10	96.7
15	97
20	90.3
25	85.2
30	78

Figure 3-31: Effect of initial congo red concentration on photodegradation efficiency

3.4.5 Effect of H_2O_2 concentration variation

The effective prevention of photogenerated electrons and holes recombination is of critical importance to improve photocatalytic ability of N-TiO_2 catalyst [125-126]. In most cases, dissolved oxygen is used as electron scavenger in these processes and several works have been implemented on its efficiency as oxidant agent to complete organic matter mineralization [127-128]. Nevertheless, it has been demonstrated that only low mineralization is reached when dissolved oxygen is used as oxidant agent in, for example, the photoassisted degradation of pesticide [127], suggesting that the decoloration reaction can be further promoted by the addition of hydrogen peroxide. The improvement of photocatalytic rates using H_2O_2 has been attributed to many factors, mainly: hydrogen peroxide is better electro acceptor than oxygen; its potential for reduction is 1.76 V while this value for oxygen reduction is -0.13 V. This simple peroxide is considered as environmentally friendly and of great interest for "green" chemistry and engineering applications [125, 129]. Addition of hydrogen peroxide will increase the rate of decoloration because of increasing of hydroxyl radical concentration through three main reactions. Either through reaction with conduction band electron, equation 3.5, or reaction with superoxide anion, equation 3.6, or by direct photolysis of H_2O_2 at low concentration, equation 3.7, [126, 129].

$$e_{CB}^{-} + H_2O_2 \rightarrow OH^- + {}^{\bullet}OH \qquad 3.5$$

$$O_2^{\bullet -} + H_2O_2 \rightarrow OH^- + {}^{\bullet}OH + O_2 \qquad 3.6$$

$$H_2O_2 + h\nu \rightarrow 2\,{}^{\bullet}OH \qquad 3.7$$

Using high concentration of H_2O_2 plays negative role in photocatalytic process where H_2O_2 can scavenge $^{\bullet}OH$, equations 3.8 and 3.9, and trap the holes that formed from illumination of catalyst, equation 3.10. Despite of formation of superoxide anion and hydroperoxyl radical at high concentrations of H_2O_2, but these radicals are not compared with $^{\bullet}OH$ that has oxidation potential equal to +3.06 V [125-126, 130- 131].

$$^{\bullet}OH + H_2O_2 \rightarrow H_2O + HO_2^{\bullet}/O_2^{\bullet -} \qquad 3.8$$

$$^{\bullet}HO_2 + {}^{\bullet}OH \rightarrow H_2O + O_2 \qquad 3.9$$

$$h_{CB}^{+} + H_2O_2 \rightarrow H^{+} + {}^{\bullet}HO_2 \qquad 3.10$$

In order to deepen our understanding, various volumes of hydrogen peroxide were added to the dye solution in the concentration of 0.675N and the photocatalytic studies were performed after each addition of hydrogen peroxide. The results are presented in Figure 3-32. Complete degradation has been achieved within 60 min irradiation in the presence of 2 milliliter of hydrogen peroxide. A quantitative degradation (98.8%) of MO has been found to be possible in the presence of hydrogen peroxide in comparison with the results in the absence of hydrogen peroxide.

Milliliter of conc. H_2O_2	Degradation%
0.5	93.6
1	96.7
2	98
3	98
3.5	94.9
4	94.7
5	92.9

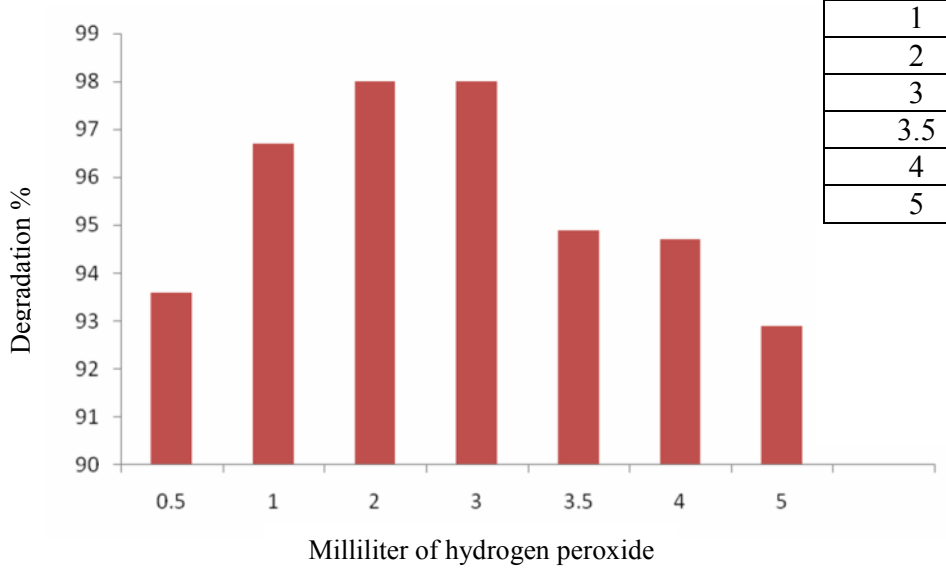

Figure 3-32: Effect of different amount of H_2O_2 on degradation of MO at optimum condition

3.4.6 Effect of the presence of some oxidants

As expected, oxygen showed low activity where the reaction needs 60 min in order to reach 9.3% of dye degradation. This behavior can be ascribed to the low reduction potential value of oxygen (–0.13V), therefore low mineralization is reached when dissolved oxygen is used solely as oxidant agent [127]. Accordingly, the impact of diluted hydrogen peroxide has been studied using 0.0135N mol/l of peroxide. The degradation percent attained 57.1 % at 4 milliliter addition of diluted H_2O_2 as explicitly shown in Figure 3-33. Based on the results, the impact of other oxidants has been investigated using the same concentration of hydrogen peroxide.

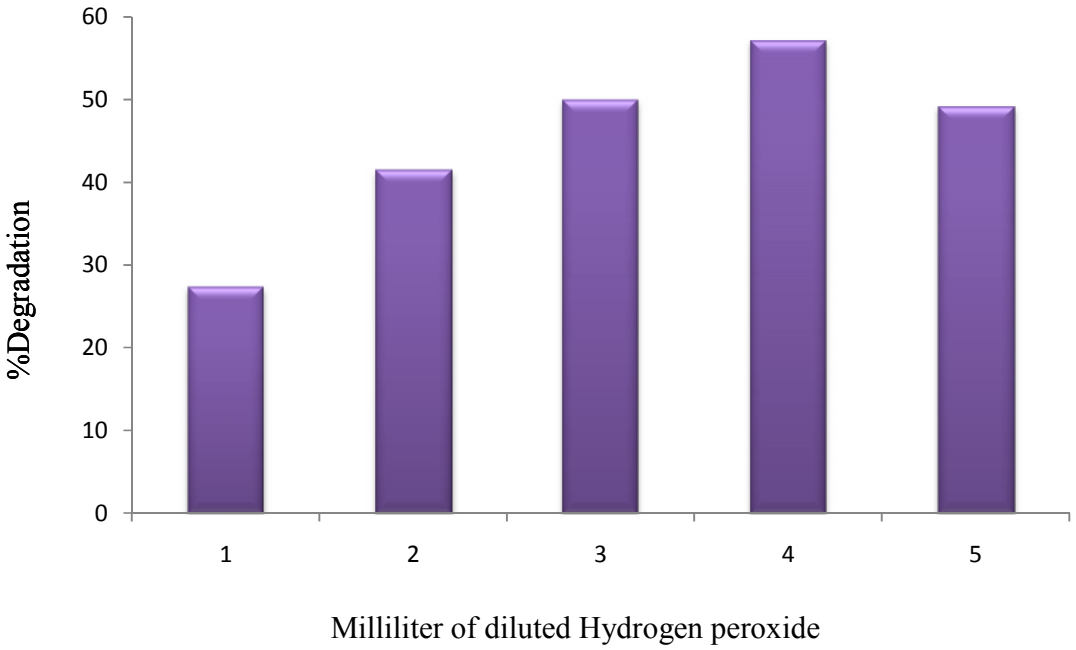

Figure 3-33: Degradation of methyl orange at optimum condition at different diluted amount of H_2O_2

From Figure 3-34, it is noted that the decoloration of MO increased in the presence of $S_2O_8^{2-}$ more than that attained by H_2O_2. This could be due to the effect of SO_3 in which the O–O bond is longer and consequently the bond energy is less. The bond distance of the O–O in H_2O_2 and $S_2O_8^{2-}$ are 1.460 and 1.497Å, respectively. The bond energy in $S_2O_8^{2-}$ is estimated as 140 kJ/mol, while in H_2O_2 is 213 kJ/mol [132]. This suggests that persulphate is cleaved more easily than hydrogen peroxide, and thus the resulting sulphate radicals might be formed more readily than hydroxyl radicals. Additionally, persulfate ($S_2O_8^{2-}$) has higher potential (E_o= 2.01 V) than H_2O_2 (E_o = 1.76 V) [132]. This interpretation is in a geed accordance with other reported conclusions [95, 133].

The effectiveness of the inorganic oxidants ($KClO_3$, $KBrO_3$, KIO_3) tested in our system (VIS/TiO_2). Halogen atom in these compounds can act as electron trapping because of it's high electropositivity [134]. BrO_3^- was the best oxidant compared with ClO_3^- and IO_3^- where about 94% of MO was

degraded in 60 minutes of irradiation time when BrO_3^- was used while IO_3^- came in the second order, the degradation percent of MO was 72% in presence of IO_3^-. The small atomic radius of Cl increases the steric factor by oxygen atoms and thus retards the ability of Cl to capture the electron that produced from illumination of N-TiO_2 [134]. For this reason only 44% degradation of MO was achieved during similar processing time. However, some authors [135] found that the effectiveness of oxyhalogenes was in this order IO_3^-> BrO_3^-> ClO_3^- but Bayat et al. [136] reported that $KBrO_3^-$ is an effective agent for debenzylation as compared with other oxidative agents, and this is consistent with our findings.

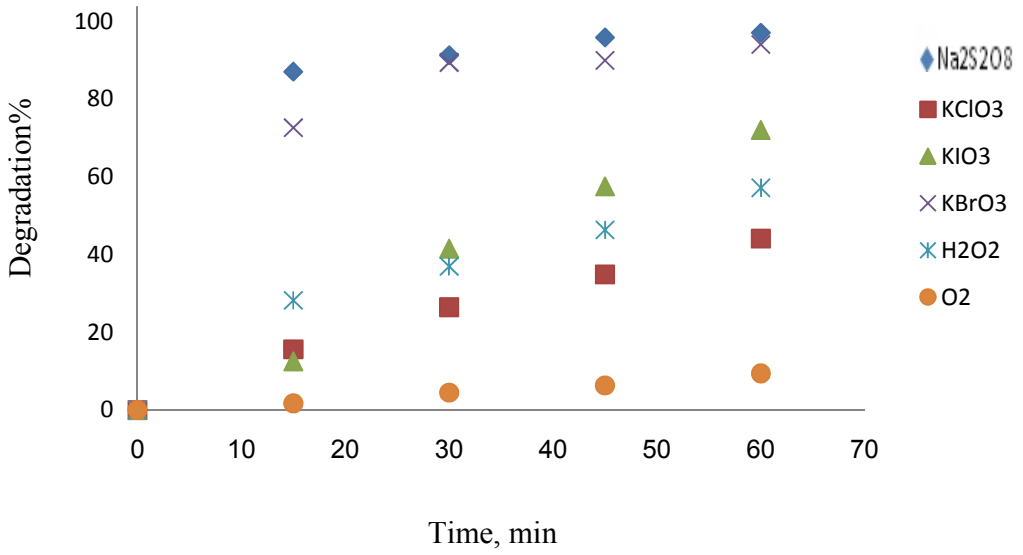

Figure 3-34: Degradation of methyl orange using different types of oxidants

3.4.7 Effect of N doping on photocatalytic activity

The introduction or doping of nitrogen atoms into network of TiO_2 in certain amount leads to several advantages [118] :

1- Dopants act as active sites of substrate that leads to increase of adsorption capacity and then increase of reaction rate.
2- Narrowing of band gap energy and region of space-charge, consequently, enhancement of electron-hole separation.

Using excess amount of dopant results in reduction of activity of catalyst because of:

1- Prevention of oxygen adsorption on TiO_2 and thus precludes trapping of electron by oxygen so decreasing of oxidizing agent number according to what Yong et al reported [137].
2- Akpan et al. [89] mentioned that increasing of dopant content creates recombination centers of e^--h^+ and thus causes screening of the catalyst.
3- More reduction of band gap energy and further reduction of space-charge layer with increase of photoinduced charge carrier and hence inducement recombination process because there is no driving force to e^--h^+ separation [78]. Figure 3-35 shows the relationship between concentration of N and rate of degradation percent of the dye. It is observed that the decolorization rate decreases with the increase of the amount of doping .

In this study, the optimal nitrogen content has been 2.5%. The maximal degradation efficiency of MO is up to 98% within 60 minute. The apparent rate constants k_{app} (Figure 3-35) of 2.5% N-iO_2, 7% N-TiO_2, and 30% N-TiO_2 samples are 0.085 min^{-1}, 0.064 min^{-1} and 0.035 min^{-1} respectively. It can be seen that the apparent rate constant of 2.5% N doped TiO_2 sample is higher than others. This could be explained concurrently via the results of N-doped samples characterization, as previously mentioned in SEM, BET and PL, and photocatalytic activity of N-TiO_2 samples. 2.5% N-TiO_2 revealed

lower PL intensity, that means it is most photo efficient compared with 5% N-TiO_2 and 7% N-TiO_2. On the other side, the surface feature of 2.5% N-TiO_2 was more ordered than that of the other samples as SEM presented. Finally, 2.5% N-TiO_2 has higher surface area according to BET.

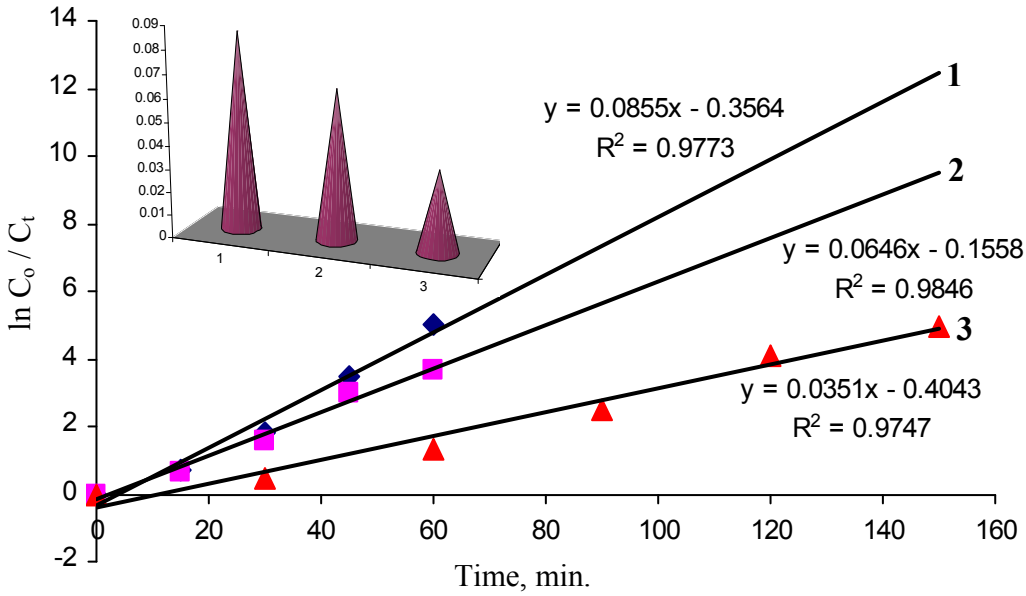

Figure 3-35: Relation of N doping with rate of photodecolorization of MO; (1) 2.5% N-TiO_2 ;(2) 5% N-TiO_2; (3) 7% N-TiO_2: inset shows variation of rate constant (k) with N doping content

3.4.8 Effect of radiation dose on dye removal

Photocatalytic reaction rate depends largely on the radiation absorption of the photocatalyst [9]. As would be expected, increasing the radiation dose dramatically increases the rate of dye degradation. At a higher radiation dose, number of photons increases to reach the active site of catalyst so number of excited catalyst molecules increases and consequently the number of hydroxyl radicals and rate of degradation of dye molecules also increase [129, 138-139]. It has been shown [18] that at low light intensities (0–20 mW/cm^2), the rate would increase linearly with increasing light intensity (first order), whereas at intermediate light intensities (25 mW/cm^2) the rate

would depend on the square root of the light intensity (half order), and at high light intensities the rate is independent of light intensity. The authors [18] stated that at low light intensity, reactions involving electron–hole formation are predominant and electron–hole recombination is negligible. As the intensity of light increases the competition between separation and recombination of electron and hole increases too [27, 140]. Mechanism of reaction is not affected by light type [9]. The influence of visible-lamp power on methyl orange decoloration in 60 minutes is shown in Figure (3-36). The degradation rate was appreciably higher under higher intensity of halogen lamp (5.55×10^{-7} mol l^{-1} sec^{-1}) than of an intermediate and low intensities of visible light (2.3×10^{-7} mol l^{-1} sec^{-1}) and (2.1×10^{-7} mol $l^{-1}sec^{-1}$), respectively. Increase the intensity of the light increases the number of photons and the number of photogenerated species and consequently increasing of oxidizing agent number according to theoretical study [125]. Therefore, it is expected that the kinetic rate constant k for methyl orange degradation is directly proportional to the light intensity I_o. The calculated first-order rate constant, k, of methyl orange degradation under high intensity of a halogen-lamp, 3.9×10^{-7} mol / L min, is significantly higher than that under the intermediate and low intensities of the visible lamp 5×10^{-9} mol /L.min and 10^{-9} mol /L.min, respectively validating the theoretical reasoning above. Additionally, Figure 3-37 reveals stand alone ratification for the better degradation yield percent in case of high incident light intensity comparing to the intermediate and low visible light intensities. The relation between degradation rate and square root of intensity is showd in Figure (3-38).

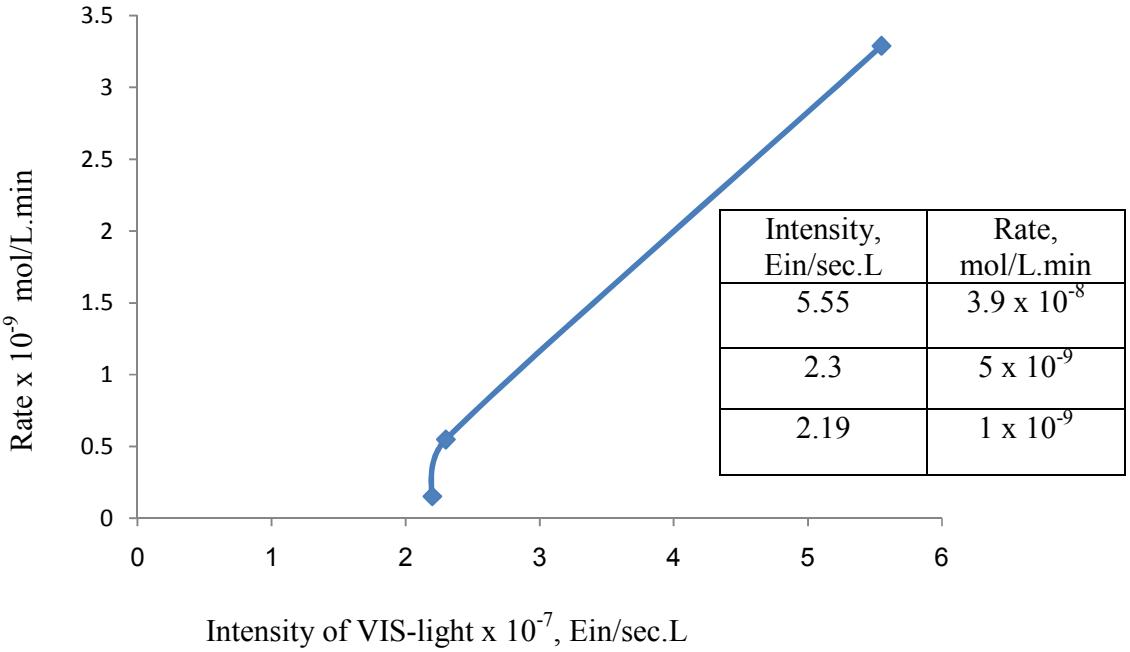

Intensity, Ein/sec.L	Rate, mol/L.min
5.55	3.9×10^{-8}
2.3	5×10^{-9}
2.19	1×10^{-9}

Figure 3-36: Variation of the initial rates as function of light source intensity

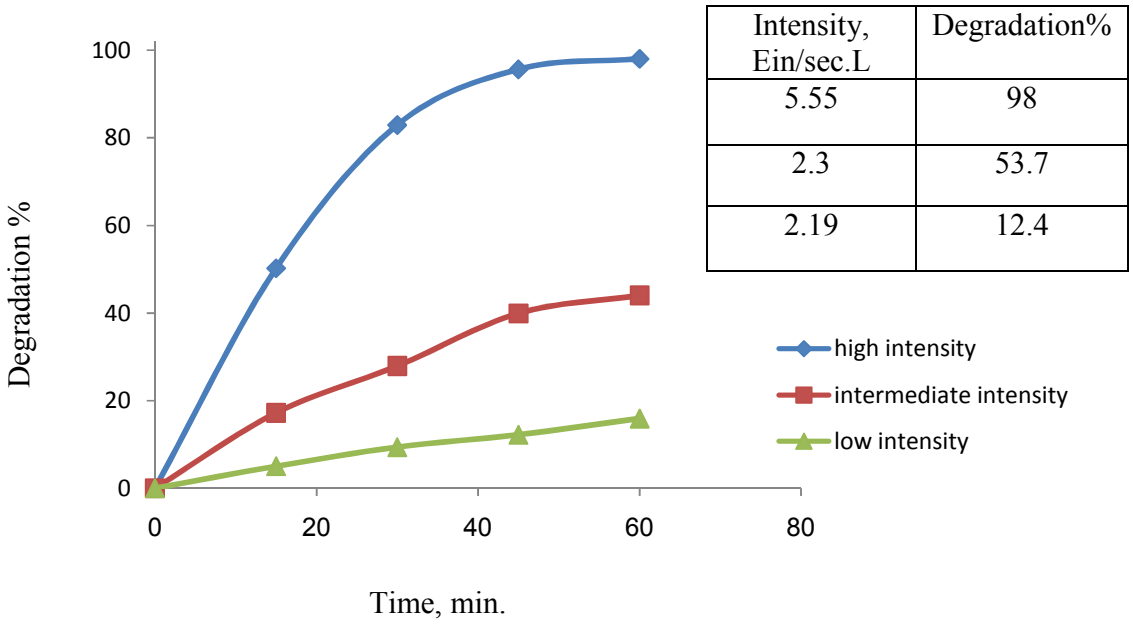

Intensity, Ein/sec.L	Degradation%
5.55	98
2.3	53.7
2.19	12.4

Figure 3-37: Degradation yield percent at different light intensities

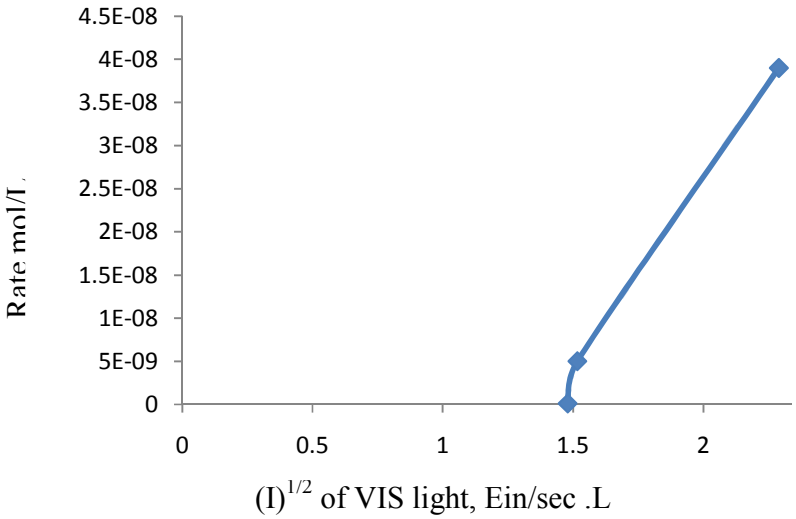

Figure 3-38: relationship between square root of light intensity and reaction rate

3.5 Kinetic study

3.5.1 Influence of irradiation time on the reaction kinetics

Figures 3-39 and 3-40 show the effect of light irradiation time on the decline of azo dyes concentration. 98% of the methyl orange and 97% of congo red were degraded, after an irradiation time of 60 minutes, 90 minutes, respectively. It is also evident that the percentage of decolorization and photodegradation increases with increasing irradiation time. The photocatalytic decolourisation of the dye occurs on the surface of N-TiO_2, where the $^{\bullet}OH$ and $O_2^{\bullet-}$ radicals are trapped by the holes of the reactive species, as oxygen and water are essential for photocatalytic decolourisation. The $^{\bullet}OH$ radicals are strong enough to break the bonds of the dye molecules absorbed on the surface of N-TiO_2. When the intensity of light and dye concentration are constant, the number of $^{\bullet}OH$ and $O_2^{\bullet-}$ radicals increases with an increase in the irradiation period, and hence, the dye molecules are completely decolorized [141].

The reaction rate decreases with irradiation time since it follows apparent first-order kinetics and additionally a competition for degradation may occur between the reactant and the intermediate products. The slow

kinetics of dyes degradation after certain time limit is due to: (a) the difficulty in converting the N-atoms of dye into oxidized nitrogen compounds, (b) the slow reaction of short chain aliphatic moieties with ˙OH radicals, and (c) the short life-time of photocatalyst because of active sites deactivation by strong by-products deposition [18, 27, 142- 143].

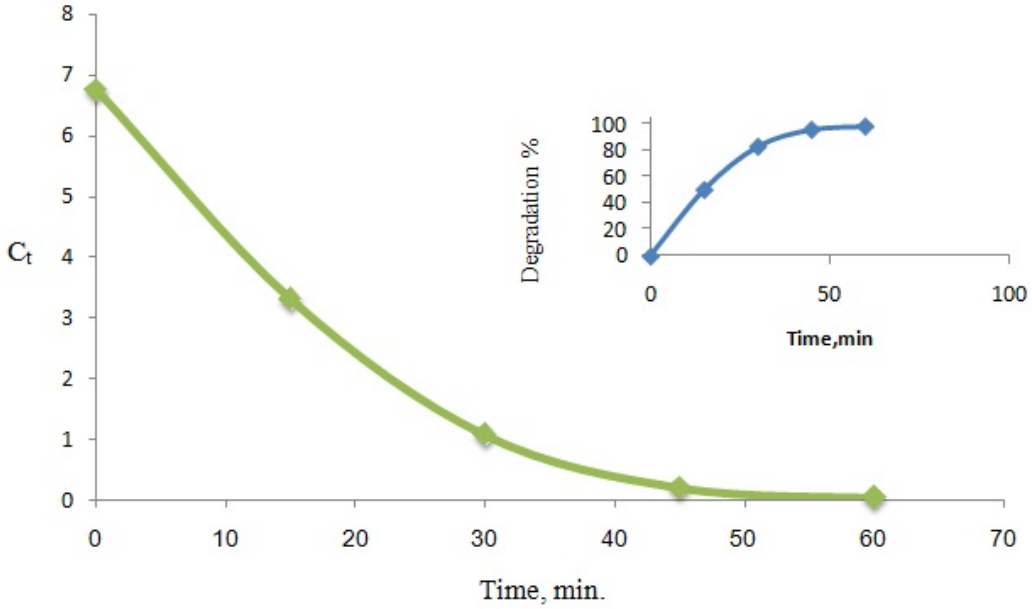

Figure 3-39: Correlation of methyl orange concentration with irradiation time

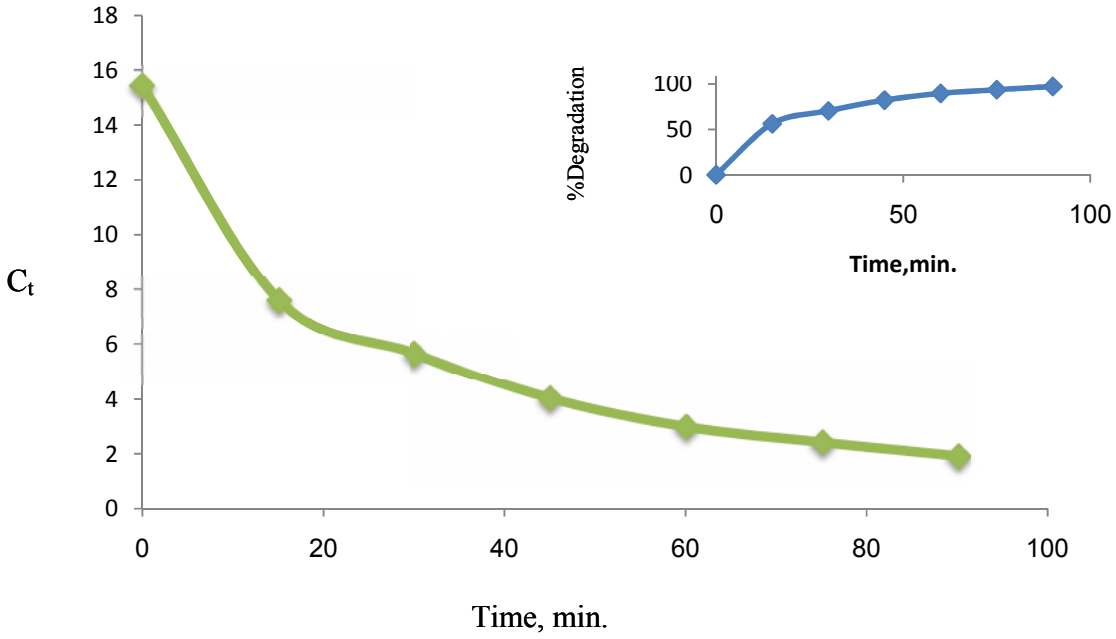

Figure 3-40: Correlation of congo red concentration with irradiation time

3.5.2 Kinetic model

In order to investigate the overall order of reaction with respect to the initial dye concentration, it was necessary to determine the kinetic order and apparent rate constant for the degradation of the methyl orange. The degradation experiments by visible irradiation of azo dye aqueous solution containing N-TiO_2 follow the pseudo-first-order kinetics with respect to the concentration of the dye.

$r = - dC/dt = k_{app}C$

Integration of this equation (with the same restriction of $C = C_o$ at $t = 0$, with C_o being the initial concentration of dye and t the reaction time) will lead to the expected relation:

$\ln C_o/C_t = k_{app}t$

in which C_o is the initial concentration of the reactant, C_t is the concentration of the reactant at any time, t the irradiation time and k_{app} is the apparent pseudo-first-order rate constant and is affected by dye concentration. A plot of $\ln (C_o/C_t)$ versus time, Figures 3-41 and 3-42, exhibit a straight line, the

slope of which upon linear regression equals the apparent first-order rate constant k_{app} [144]. One of the most useful indications to evaluate the reaction rate of first order kinetic is the calculation of half-life time reaction which is calculated as follows;

$t_{1/2} = 0.693/ k_{app}$

here, $t_{1/2}$ is the half-life time of reaction calculated from k_{app}. $t_{1/2}$ equals to 8 minutes for methyl orange and 33 minutes for congo red.

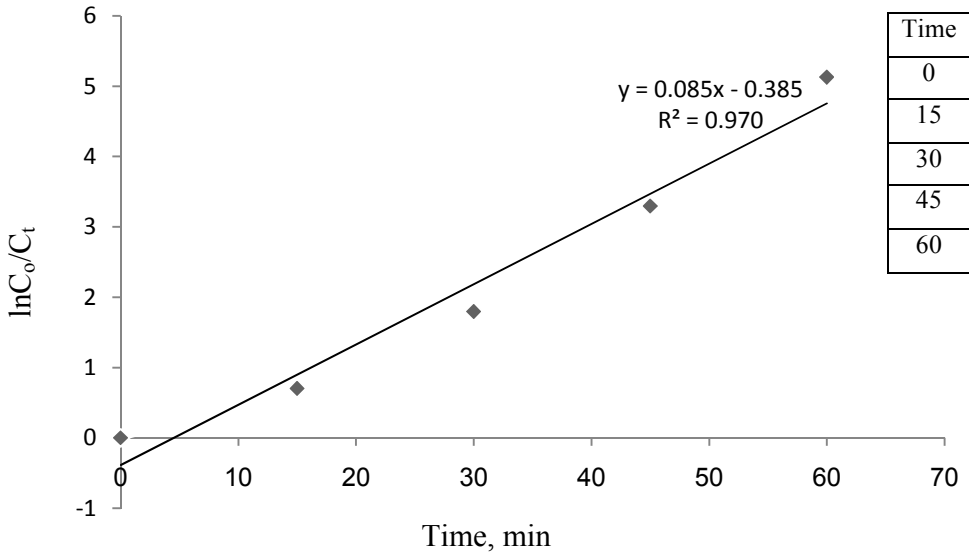

Time	ln Co/Ct
0	0
15	0.703
30	1.796
45	3.295
60	5.128

Figure 3-41:Degradation rate of methyl orange at optimum conditions

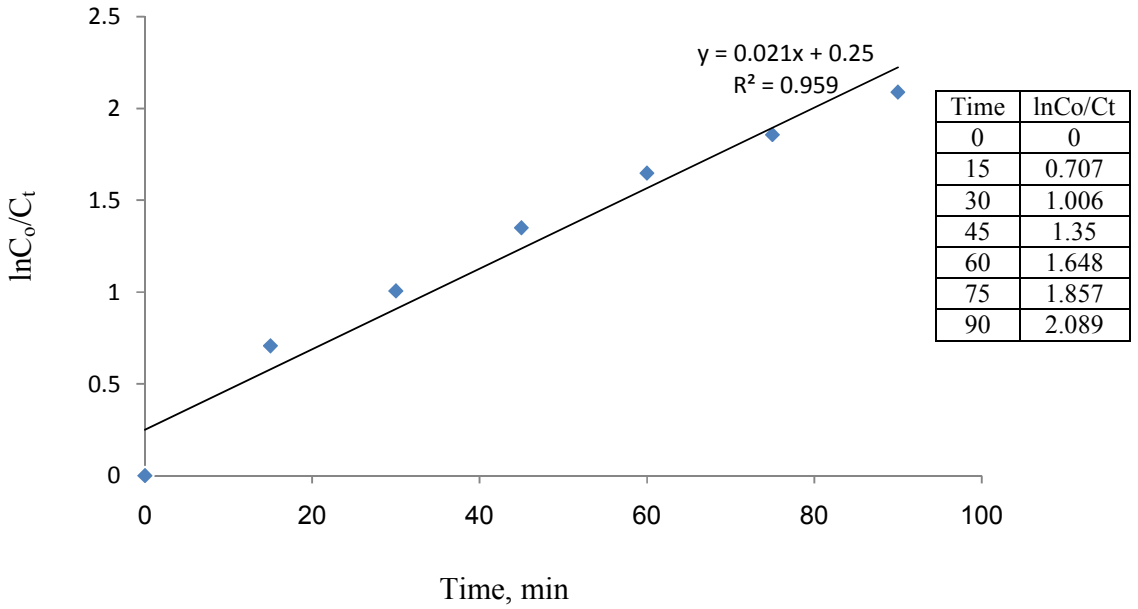

Time	lnCo/Ct
0	0
15	0.707
30	1.006
45	1.35
60	1.648
75	1.857
90	2.089

Figure 3-42: Degradation rate of congo red at optimum conditions

3.5.3 Determination of remaining amount of H_2O_2 at the end of reaction

The remaining amount of H_2O_2 at the end of reaction was determined using a titration method as described in chapter two. The color of the sample changed to light pink with the first drop. The volume of the titrating solution was recorded and the remaining amount of H_2O_2 was calculated based on the following chemical equation;

$$5H_2O_2 + 2KMnO_{4\,(aq)} + 3H_2SO_4 \rightarrow 5O_2 + 2MnSO_{4\,(aq)} + K_2SO_4 + 8H_2O \quad 3.11$$

This result indicates that the treatment associating VIS/N-TiO_2/H_2O_2 has consumed the added peroxide completely. Furthermore, the VIS/N-TiO_2/H_2O_2 treatment has the advantage of leads to a final nontoxic residue due to the absence of residual peroxide. This confirms that the interaction actually goes through the pseudo first order as stated previously in this work. Similar results have also been made by Garcia et al. [145] in their work on the comparative study of the degradation of real textile effluents by photocatalytic reactions involving UV/TiO_2/H_2O_2 and UV/Fe^{+2}/H_2O_2 systems.

3.5.4 Langmuir-Hinshelwood kinetic model for the Photocatalysis of azo dyes

As reported in several papers, decolorization kinetics of most dyes by the heterogeneous photocatalytic method fitted with the Langmuir–Hinshelwood (L–H) kinetic model represented in Equation 3.12 [146-147].

$$r = dC / dt = k_r K_{ad} C / (1 + KC) \qquad 3.12$$

where r is the oxidation rate of the reactant (mg/l min), C is the concentration of the reactant (mg/l), t is the illumination time, k is the reaction rate constant (mg/l min) and K is the adsorption coefficient of the reactant (l/mg). When the concentration of the dye is sufficiently low, the equation can be simplified to an apparent first-order equation [27].

$$\ln (C_o/C_t) = kKt = K_{app}t \qquad 3.13$$

or

$$Ct = C_o e^{-k_{app}.t} \qquad 3.14$$

A plot of $\ln C_o/Ct$ versus time represents a straight line, the slope of which upon linear regression equals the apparent first-order rate constant k_{app}. Depending on that we can say, The L–H model was established to describe the dependence of the observed reaction rate on the initial solute concentrations and to describe the solid–liquid reaction [27].

Many researchers agreed that when the following assumptions were established, heterogeneous photocatalysis could be analyzed using the Langmuir-Hinshelwood model: (i) at equilibrium, the number of catalyst surface adsorption sites is fixed, (ii) the catalyst surface can be covered to the maximum by one layer; only one substrate may bind at each surface site, (iii) there is reversible adsorption reaction, (iv) the surface of catalyst is homogeneous and (v) there is no interaction between adjacent adsorbed molecules [147].

From Figures 3-43 and 3-44 one could determine rate constants of adsorbed dyes and the adsorption constants K_{ads}. These values are reported in Table 3-12.

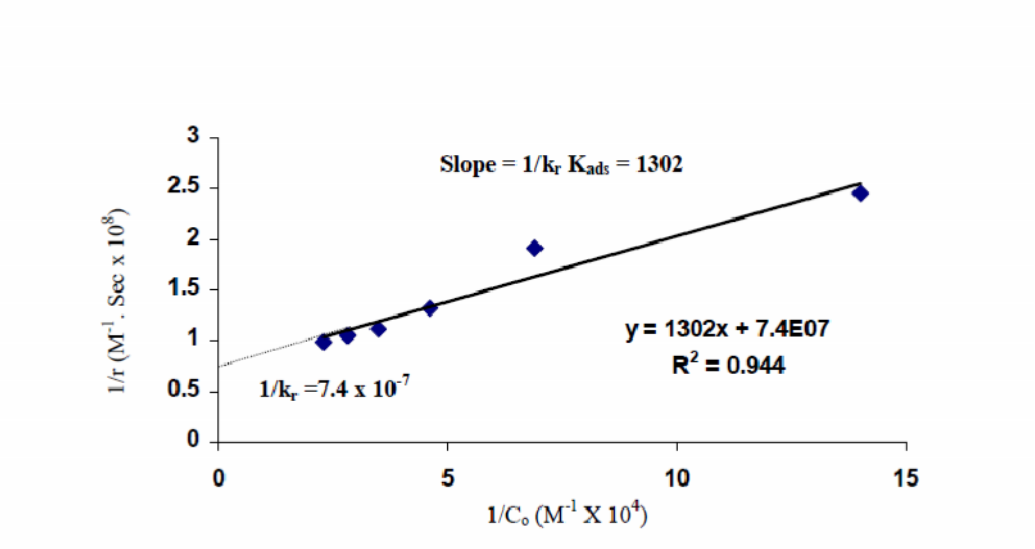

Figure 3- 43: Langmuir-Hinshelwood model outcomes for the photobleaching of congo red at different initial concentrations; N-TiO_2 loading = 40 mg; pH = 2.5

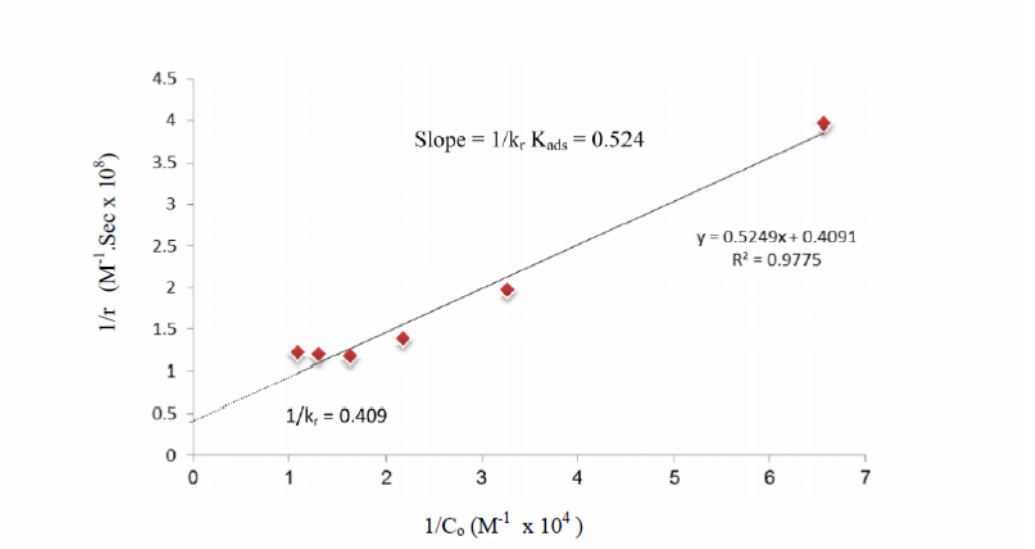

Figure 3- 44: Langmuir-Hinshelwood model outcomes for the photobleaching of methyl orange at different initial concentrations; N-TiO_2 loading = 50 mg; pH = 2.5

Table 3-3: Rate constants and adsorption coefficients of the dyes

Dye	K_{ads} (μM^{-1})	k ($\mu M.\ sec^{-1}$)
Methyl orange	0.007	0.025
Congo red	0.0569	0.0135

From Table 3-3, one could observe the higher adsorption coefficient value for CR in comparison to that of MO. This observation is ascribed to the higher electron density of aromatic ring due to extended conjugation in CR and further the existence of diazo groups which increase the chelation and lead consequently to stronger adsorption onto (Ti^{+4}) sites at the N-TiO_2 surface [148]. Correspondingly, one might conclude that the relatively high value of adsorption coefficient, K, reflects the importance of the direct photolytic reaction of the adsorbed CR moiety on the photocatalyst surface, beside its oxidation by hydroxyl radical and superoxide anion radical (generated on photocatalyst surface) in solution bulk. However and also from Table 3-2 , the lower k value for CR relatively to that of MO could be attributed to higher number of produced intermediates which contribute significantly in the consumption of incident photons and active adsorption sites on the photocatalyst on one hand, and the large moieties need normally longer time for decomposition, on the other hand [17].

3.6 Evaluation of the photodegradation system via quantum yield calculations

The quantum yield, Φ, is defined as the number of moles of the reacted species via photophysical or photochemical process divided by the number of moles of photons that actually contributed in promotion of

molecules. Also, it could be translated as the rate of photochemical reaction divided by the light intensity [149];

Φ = number photoreacted or photoproduced molecules/ number of absorbed photons

= process rate / light intensity

For several photochemical reactions, the high quantum yield is 10^6 and low quantum yield is 10^{-2} [150]. Quantum yield or quantum efficiency is considered as a substantial quantity in photochemistry, because it provides essential information regarding the nature and mechanism of the photochemical reaction. Hence, it is necessary to measure quantum yield in the studies of photochemical reactions [150] in order to explore the efficiency of a photodegradation reaction and to have an idea about the number of photons which are really involved in the transformation process [123].

Any chemical compound that possess known quantum yield, do not suffer side reaction, not sensitive to presence of oxygen or impurity, stable thermally during reaction and insensitive to wavelength change can be used to determine light intensity [151-152]. In this work Ferrioxalate $[Fe(C_2O_4)_3]^{3-}$ is used as actinometer. This actinometer is the most common actinometer and most accurate which cover wide range of wavelength from 250 nm to 577 nm [150].

In heterogeneous semiconductor photocatalysis, the measurement of $\Phi_{overall}$ is very difficult and, as a consequence is rare. The most obvious reason is that the rate of absorption of photons is very difficult to assess, as long as the semiconductor particles absorb, scatter, reflect and transmit the light. It is usually assumed that all the light is absorbed and the efficiency is quoted as an apparent quantum yield [52, 151-153].

Effect of several factors on the quantum yield was studied to investigate of photocatalytic efficiency. Figures 3-45a and 3-46a show quantum yields increase with increasing N-TiO_2 dose, but beyond the optimum value of catalyst amount it decreases because of aggregation of catalyst particles that decrease the number of active sites and on the other side increase the turbidity of solution and light scattering and then diminishing the quantum yield value.

Quantum yield decreases from 0.038 to 0.029 when the concentration of MO increases from 5 ppm to 30 ppm as shown in Figure 3-45b. This may be due to lowering of the number of reached photons into solution because of screening effect as the concentration of dyes increases and eventually Φ decreases [154]. However, in case of CR, the results were different where the quantum yield increased from 0.0073 to 0.0181 with increasing the CR initial concentration from 5 ppm to 30 ppm, Figure 3-46b. This can be interpreted on the basis of that with the increase in initial concentration of dye, while the Visible light irradiation period and catalyst dose are kept constant, more dye molecules are adsorbed onto the surface of catalyst and hence the amount of decomposed dye has increased [95, 123].

The initial solution pH is another important variable in the evaluation of photocatalytic efficiency. The relationship between pH and Φ is shown in Figures 3-45c and 3-46c. It could be concluded that the pH variation could result in enhancement of the efficiency of photo removal of organic pollutants in presence N-TiO_2 [155].

Finally, the quantum yield of 2.5% N-TiO_2 is much higher than that of 5% and 7% N-TiO_2. The photocatalytic performance of N-doped TiO_2 revealed dependence of Φ on the N dopant amount as shown in Figure 3-45d. This is a stand alone verification for our previous observation in which

the increase of the nitrogen content lowers the quantum yield under illumination, and further is consistent with other reported data [156].

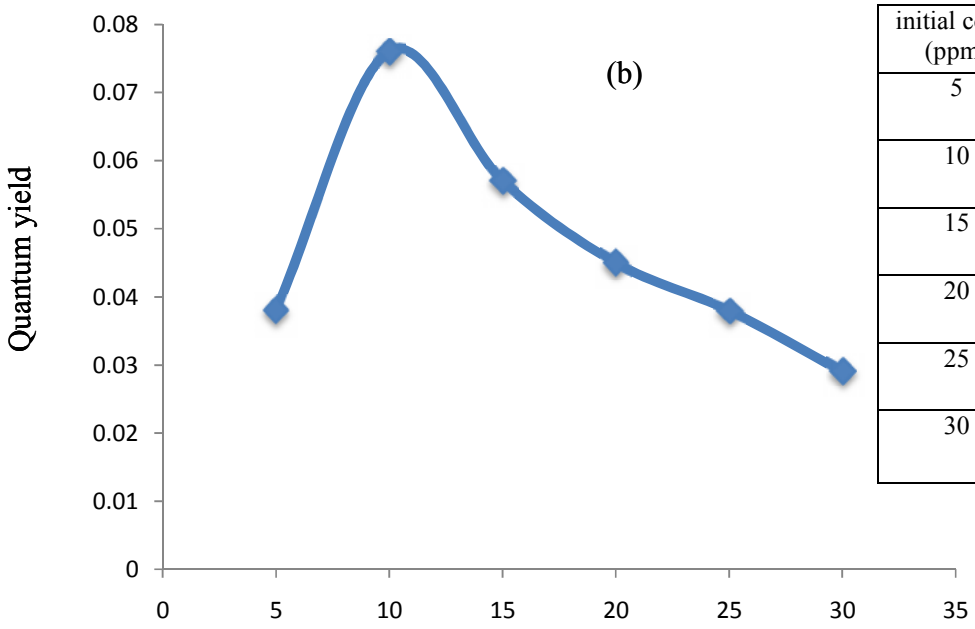

initial conc. (ppm)	Quantum yield
5	0.038
10	0.076
15	0.057
20	0.045
25	0.038
30	0.029

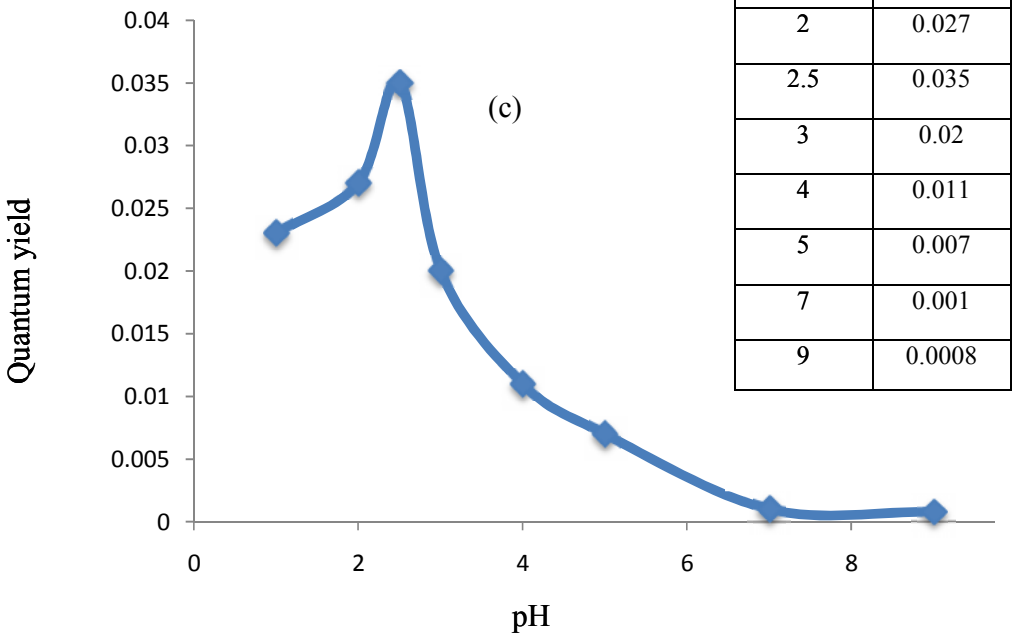

pH	Quantum yield
1	0.023
2	0.027
2.5	0.035
3	0.02
4	0.011
5	0.007
7	0.001
9	0.0008

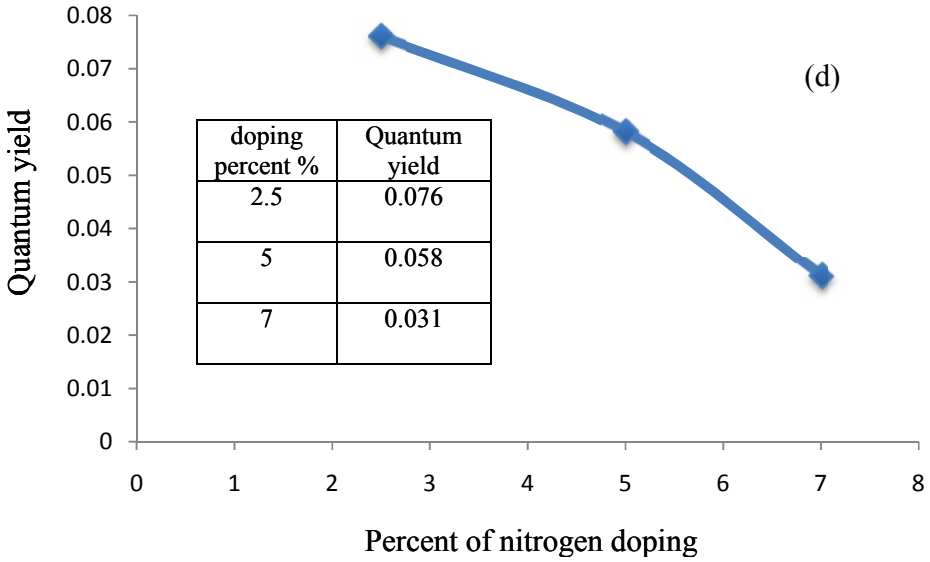

doping percent %	Quantum yield
2.5	0.076
5	0.058
7	0.031

Figure 3-45: Effect of (a) N-TiO_2 loading (b) methyl orange initial concentration (c) pH and (d) percent of nitrogen doping on the quantum yield of photocatalytic reaction

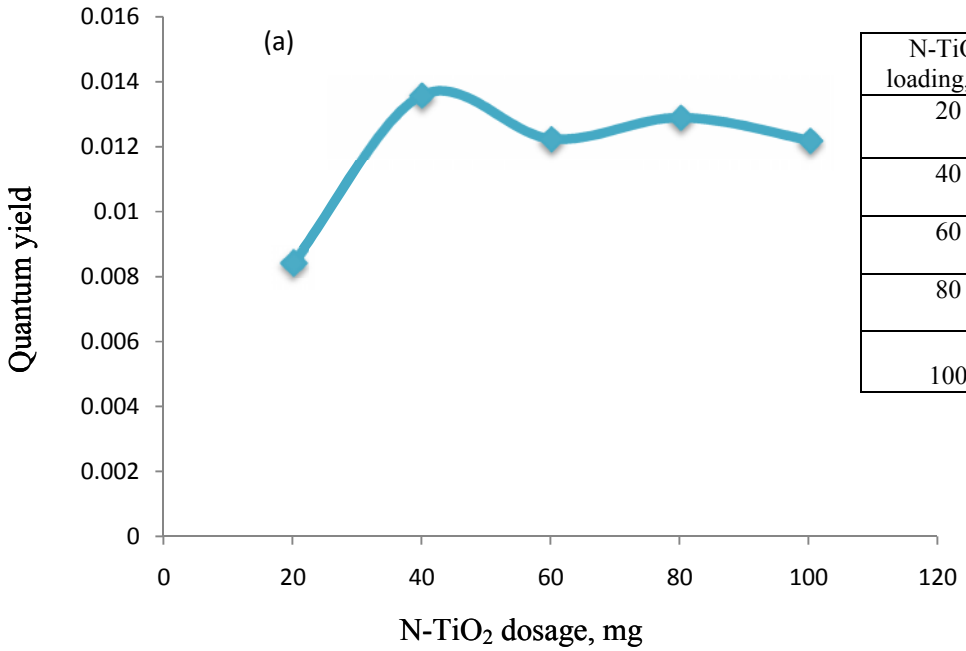

N-TiO_2 loading, mg	Quantum yield
20	0.008401
40	0.01357
60	0.01225
80	0.0129
100	0.0122

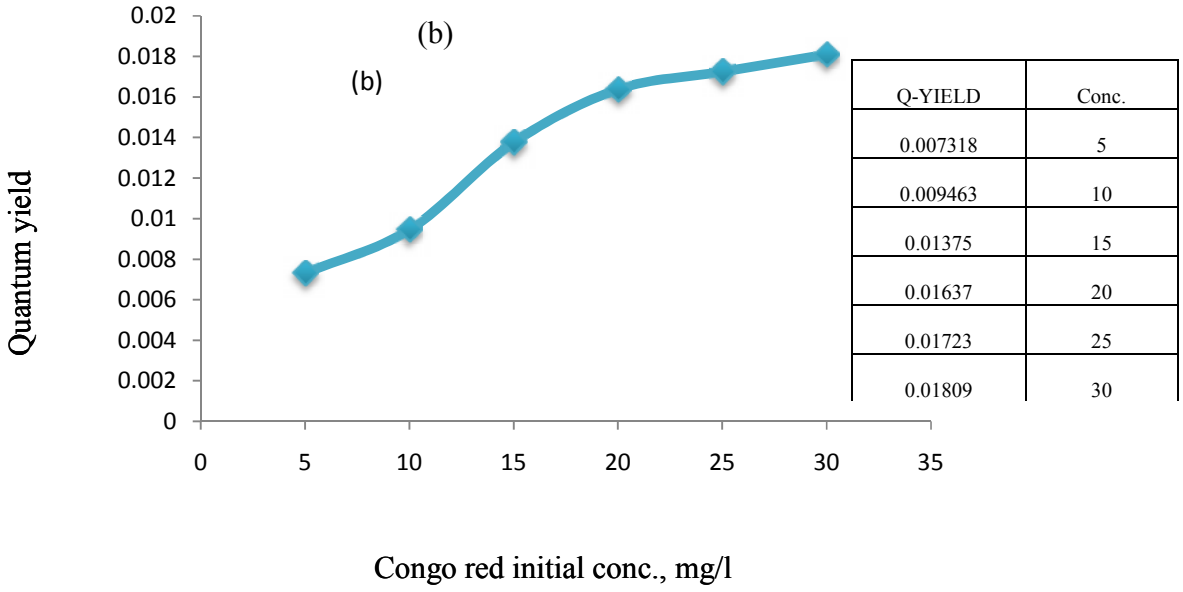

Q-YIELD	Conc.
0.007318	5
0.009463	10
0.01375	15
0.01637	20
0.01723	25
0.01809	30

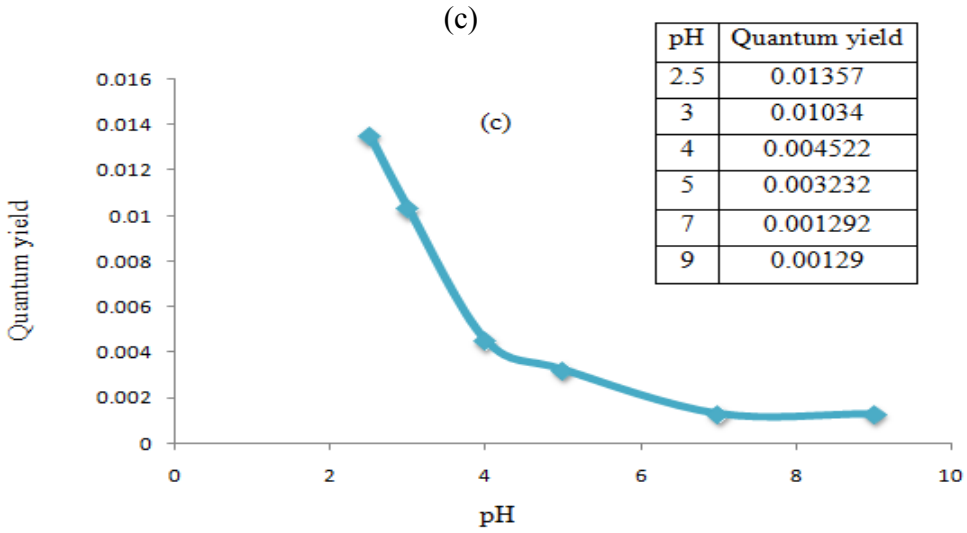

pH	Quantum yield
2.5	0.01357
3	0.01034
4	0.004522
5	0.003232
7	0.001292
9	0.00129

Figure 3-46: Effect of (a) N-TiO_2 loading (b) congo red initial concentration and (c) pH on the quantum yield of photocatalytic reaction

3.7 Effect of temperature and thermodynamic parameters

Although the temperature influences the e^--h^+ separation and the adsorption process of organic substrate, but it can not affect seriously the photocatalytic reaction [157, 158-159]. Dependence of methyl orange photodegradation on temperature was studied in the range of 20 C^o to 45C^o. From Figure 3-47 we can conclude that the degradation percent increases with the increased temperature.

The reaction rate constant, k_{app}, can be derived from the Arrhenius equation as follows [160];

$$K_{app} = A\, e^{-Ea/RT} \qquad 3.15$$

where k_{app} is the apparent rate constant; A is pre exponential factor ; E_a is the activation energy; R is the universal gas constant (8.314 J/mol. K) and T is temperature (K). The activation energy (E_a) was obtained from a plot of ln k_{app} versus 1/T as shown in Figures 3-47 and 3-48 for MO and CR, respectively. Linearization of equation 3.15 resulted in the following expression;

$$\ln k_{app} = \ln A - E_a /RT \qquad 3.16$$

The other thermodynamic parameters, free energy, enthalpy and entropy of activation were calculated as presented in Tables 3.3 and 3.4 for MO and CR, respectively. The value of $\Delta G^{\#}$ (the free energy of activation) may be determined from following equations [161]:

$$k_{app} = kBT/h \text{ exponential } (-\Delta G^{\#}/RT) \qquad 3.17$$

$$\Delta G^{\#} = RT \times [\ln (kBT/h) - \ln k_{app}] \qquad 3.18$$

where kB is Bolzmann constant (1.3805x 10^{-23} J K^{-1}) and h is Planck constant. The introduction of the constant values, leads to:

$$\Delta G^{\#} = RT \times (23.76 + \ln T - \ln k_{app}) \quad 3.19$$

The enthalpy ($\Delta H^{\#}$) and entropy ($\Delta S^{\#}$) of activation are derived from equations 3.17 and 3.18, leading to the final relations;

$$\ln k_{app} = \ln A - E_a / RT \quad 3.20$$

$$d(\ln k_{app}) / dT = E_a / RT^2 \quad 3.21$$

likewise, equation (3.19) is rewritten as:

$$\ln k_{app} = \ln (kBT/h) - \Delta H^{\#} / RT + \Delta S^{\#} / R \quad 3.22$$

$$d(\ln k_{app}) / dT = 1 / T + \Delta H^{\#} / RT^2 = (\Delta H^{\#} + RT) / RT^2 \quad 3.23$$

Solving equations 3.21 and 3.23for the activation enthalpy gives

$$\Delta H^{\#} = Ea - RT \quad 3.24$$

finally giving access to the entropy of activation

$$\Delta S^{\#} = (\Delta H^{\#} - \Delta G^{\#}) / T \quad 3.25$$

From Tables 3-4 and 3-5, it can be concluded that the higher temperature can increase the degradation rate. This fact indicates that the mobility of dye molecules increased with the temperature [162] that leads to increase collision frequency of molecules in solution due to molecules possessing more kinetic energy and moving faster. Additionally, the number of molecules possessing enough energy to overcome the activation energy is also increased [163] and according to collision theory, the rate of change in the molar concentration of a molecule is the product of the collision density and the probability that a collision occurs with sufficient energy [149]. Most authors stated that the optimum temperature is generally between 20 and 80 C^o [11, 135] and this agrees well with our results.

The desorption of adsorbed substrate and recombination process are so affected by temperature change because of E_a barrier presence in a photocatalytic process [155, 164]. According to literature, when temperature becomes close to the water boiling temperature, the adsorption of substrate is lowered and the process becomes exothermic. [11].

The positive values of $\Delta G^{\#}$ gives an indication of non-spontaneous process as one expected. The process was endothermic due to positive values of $\Delta H^{\#}$ i.e., that higher temperatures are favored for enhanced removal of organic pollutant. The negative values of $\Delta S^{\#}$ suggest the decreased randomness at the solid/ solution interface during the adsorption of azo dye on catalyst and further ratification for the non spontaneous process.

The relatively higher activation energy of CR (33.8 kJ/mol) in comparison to that of MO (25.8 kJ/mol) could be, most likely, another endorsing sign for the lower degradation rate of CR which was observed and reported earlier in this thesis.

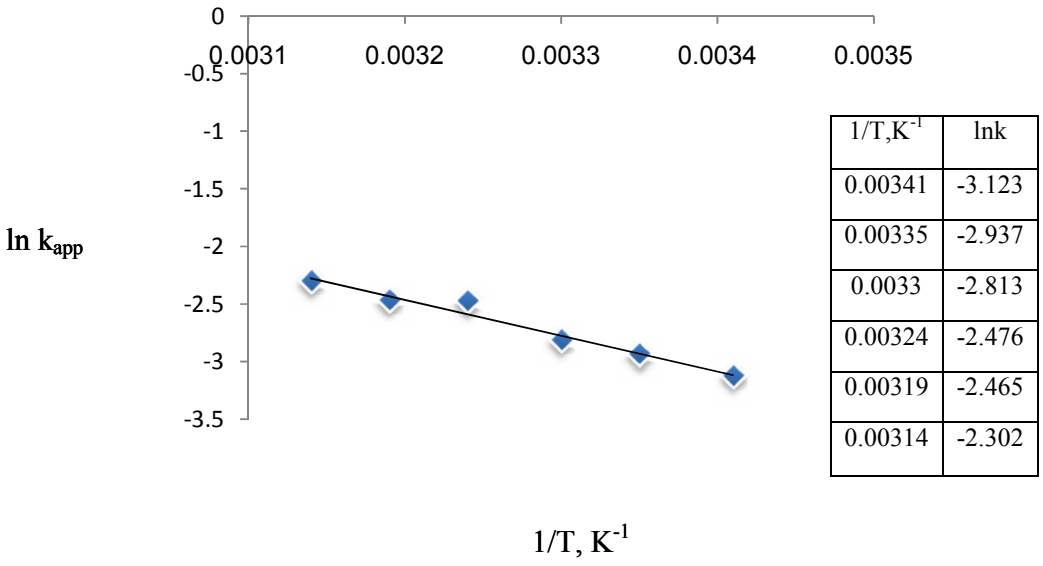

1/T,K^{-1}	lnk
0.00341	-3.123
0.00335	-2.937
0.0033	-2.813
0.00324	-2.476
0.00319	-2.465
0.00314	-2.302

Figure 3-47: Arrhenius plot of rate constant versus reciprocal of reaction temperature for degradation of methyl orange

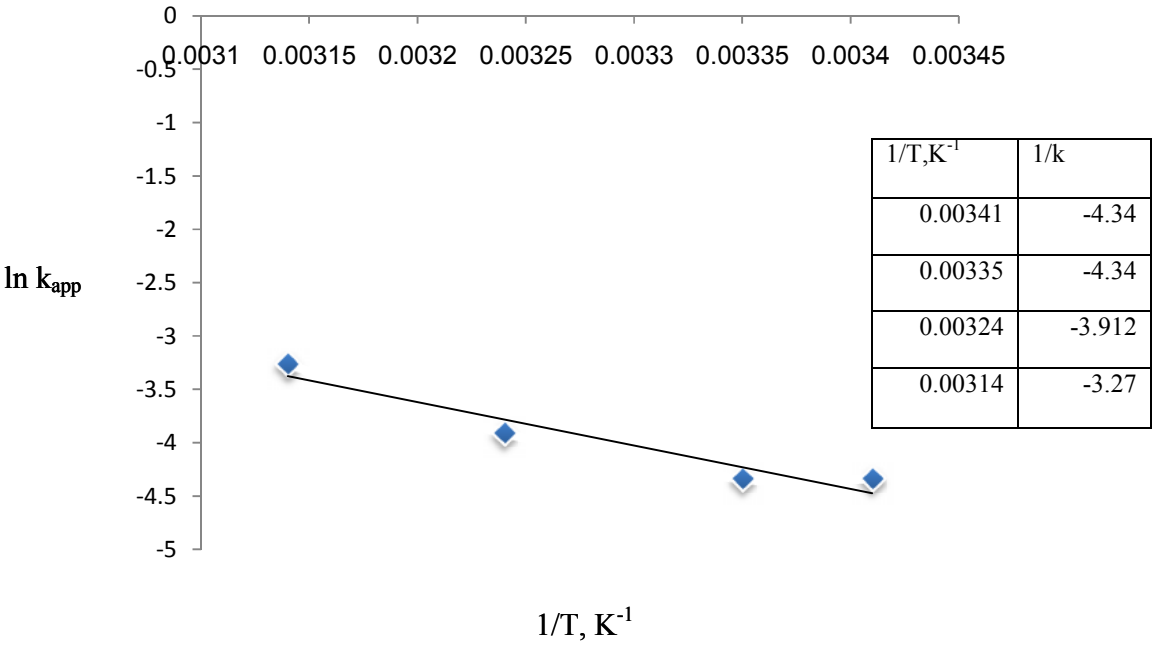

1/T,K^{-1}	1/k
0.00341	-4.34
0.00335	-4.34
0.00324	-3.912
0.00314	-3.27

Figure 3-48: Arrhenius plot of rate constant versus reciprocal of reaction temperature for degradation of congo red

Table 3-4: Thermodynamic parameters for the photocatalytic degradation of methyl orange

T (K)	E_a (kJ mol^{-1})	$\Delta G^{\#}$ (kJ mol^{-1})	$\Delta H^{\#}$ (kJ mol^{-1})	$\Delta S^{\#}$ (JK^{-1} mol^{-1})
293	25.8	89.298	23.363	-225.03
298		90.404	23.322	-225.107
303		91.649	23.28	-225.64
308		92.341	23.239	-225.356
313		93.864	23.197	-225.77
318		94.975	23.156	-225.845

Table 3-5: Thermodynamic parameters for the photocatalytic degradation of congo red

T (K)	E_a (kJ mol^{-1})	$\Delta G^{\#}$ (kJ mol^{-1})	$\Delta H^{\#}$ (kJ mol^{-1})	$\Delta S^{\#}$ (JK^{-1} mol^{-1})
293	33.8	92.276	31.539	-207.907
298		93.893	31.318	-209.983
308		96.019	31.235	-210.337
318		98.737	31.332	-211.965

3.8 Comparison of photocatalytic activity of N-TiO_2 nanoparticles under UV, VIS and Solar light irradiation

The photocatalytic activity of N-TiO_2 catalyst was estimated by measuring the decomposition rate and degradation percent of the dye under sun light. All the experiments were performed on the days when the intensity of sunlight was relatively high during the period between 11:15 am to 12:00 am during the days of August (summer season). It was noticed that N-TiO_2 2.5% and 5% N-TiO_2 achieved 94.5% and 91.1% degradation for methyl orange within 15 minutes, while 7 % N doped TiO_2 degraded about 92% of methyl orange during 35 minutes.

Figure 3-49 shows photodegradation rate of methyl orange under sun light and in presence of 2.5, 5, 7 % N-doped TiO_2. This faster degradation rate of methyl orange under sun light irradiation using N-doped TiO_2 is attributed mainly to the existence of about 5% UV light within the solar light in addition to previous reported reasons in this thesis regarding N occurrence in the photocatalyst powder.

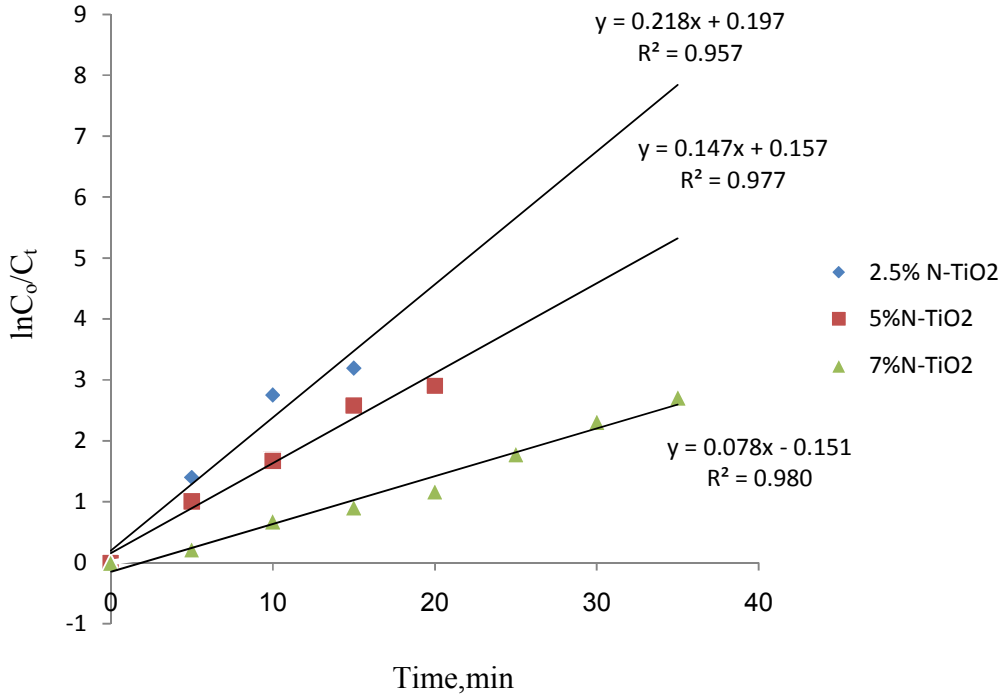

Figure 3-49: Degradation rate of methyl orange using different doping percents of N-TiO_2 under solar light

2.5% N-TiO_2 was chosen as a comparison model for the photobleaching under three UV, VIS and solar radiation sources. N doped TiO_2 shows lower photodegradation efficiency of methyl orange under UV light exposure as compared to its efficiency under sun light or visible light by using halogen lamp due to the faster recombination of electron–hole pair as a result of the absorption characteristics caused by the N doping [131, 165]. Under UV light irradiation, a large amount of electrons and holes were generated in short time because the energy of UV irradiation is large compared to band gap energy of the catalysts., meaning high recombination rate of electrons and holes [31, 156]. N-TiO_2 nanoparticles conferred significantly higher photocatalytic activity under visible compared to UV light towards the photocatalytic degradation of methyl orange. It is considered that nitrogen modification is responsible for lowering the bandgap energy of N-TiO_2 nanoparticles (red-shift of the energy band gap to the visible range),

consequently significant enhancement in the photoactivity was obtained [166]. High photocatalytic efficiency is exhibited by catalyst under solar light which might be due to their capability to absorb both UV and visible light radiations of solar light where visible light accounts for 45% while the UV-light occupying 5% of the incident sunlight [167-168]. Under the higher intensity of light irradiation, the enhancement was considerably higher because the electron–hole formation is predominant and, hence, electron–hole recombination is negligible [31]. Figures 3-50 and 3-51 show different rates and percents of degradation of methyl orange under ultra violet and visible lightening.

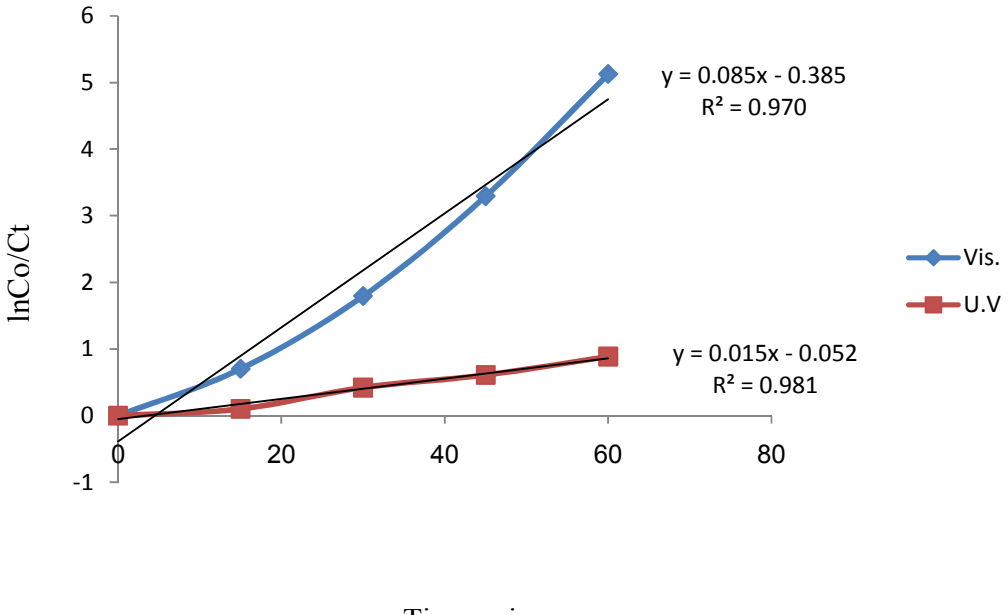

Figure 3-50: Rate of photodegradation of methyl orange at optimum conditions under visible light and ultra violet light

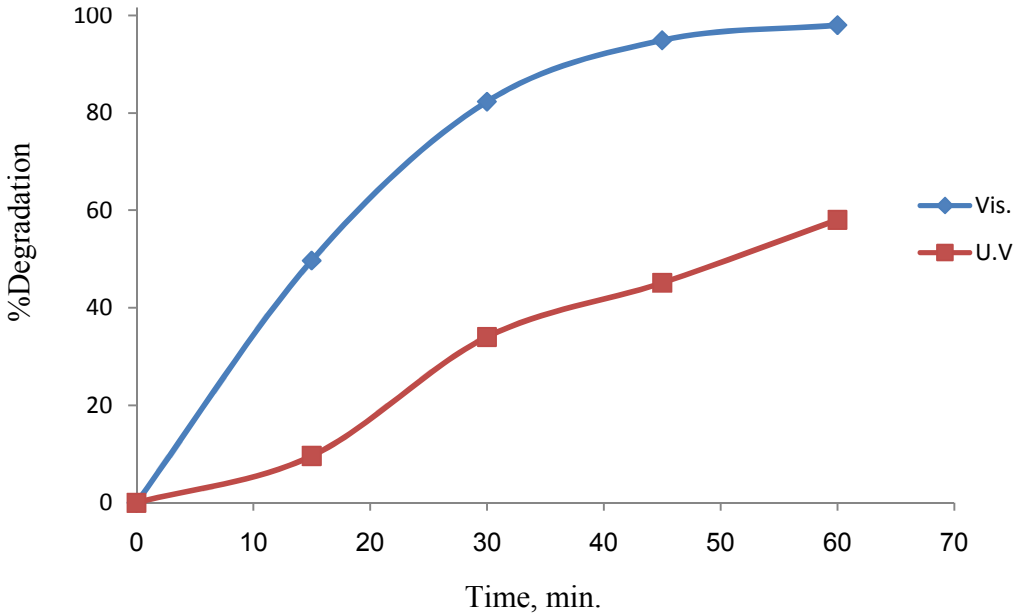

Figure 3-51: Comparison between degradation percent of methyl orange under VIS and UV light

3.9 Suggested mechanism for azo dye photocatalytic degradation in TiO_2/VIS/H_2O_2 system

One of the heterogeneous system disadvantages is that the mechanism is complicated therefore the heterogeneous AOP is still in the early stages of development and implementation [95] and hence, there have not yet been the ready made mechanism and satisfying explanation on the photocatalytic degradation of organic pollutants in the presence of a nanometers TiO_2 catalyst [169]. However, the following data and their interpretation are possibly acceptable for the elucidation of the mechanism of photocatalytic degradation of congo red and methyl orange.

In UV-vis, it is interesting to note from Figures 3-52 and 3-53 that the absorption of characteristic visible bands of the studied dyes decreased with time of irradiation and finally disappeared which indicates that the whole

dye in aqueous solution are degraded completely. Furthermore, no new absorption bands appeared in either the visible or the UV spectra region.

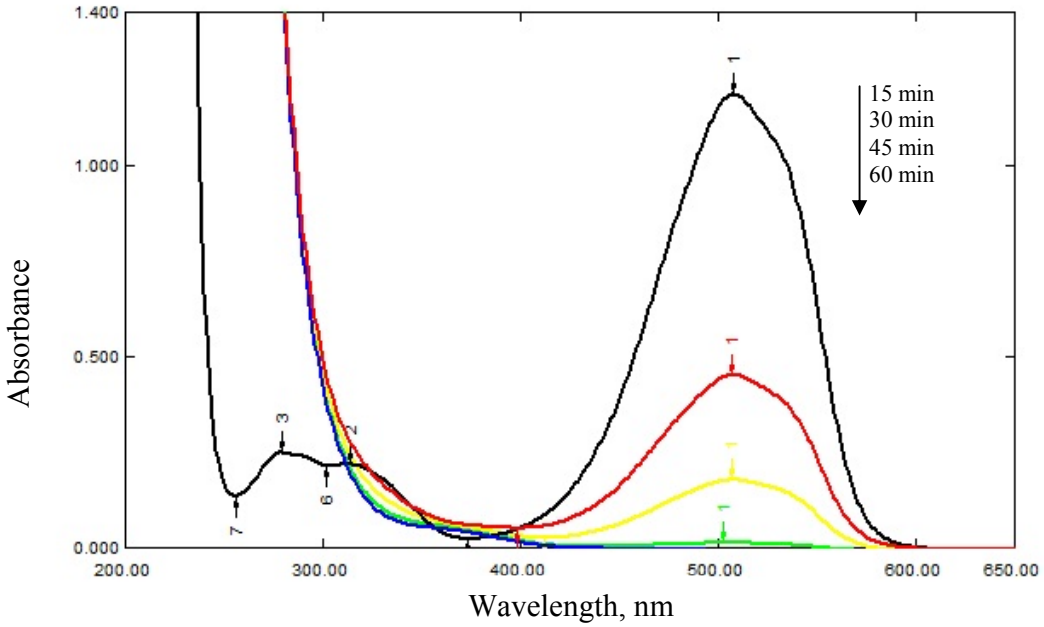

Figure 3-52: UV-VIS spectra changes of methyl orange at varying times

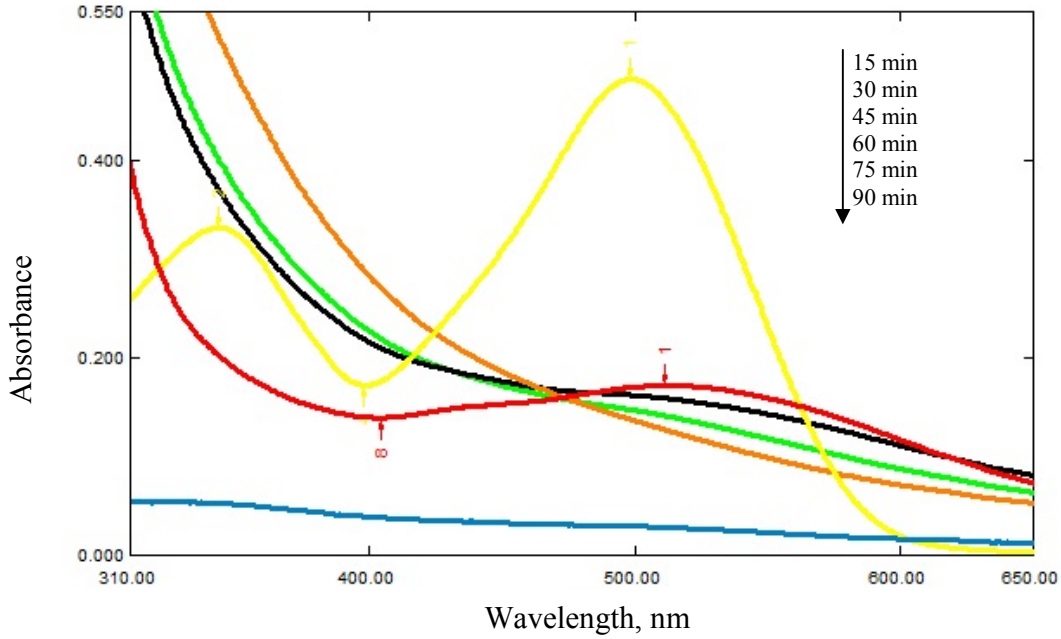

Figure 3-53: UV-VIS spectra changes of congo red at varying times

The chromatograms of dyes are consistent dramatically with UV-VIS results. Figures 3-54 and 3-55 report the HPLC profiles corresponding to solutions of congo red and methyl orange degraded at zero time, half time and full time of degradation, respectively. The chromatograms show clearly the appearance of peaks corresponding to the by-products of the degradation of the parent dye. As can be seen from Figures 3-56 and 3-57, the peaks of parent dyes are disappeared and many new peaks of the intermediates are appeared due to irradiation. At the end of illumination no peaks are observed which indicates that the dyes are completely degraded.

The FTIR spectrum obtained from the azo dyes powder are shown in Figures 3-56 and 3-57. Several bands can be distinguished in the region of 2000–1000 cm^{-1}, which can be assigned as follows, the intense bands at 1519 cm^{-1}(CR) and 1607 cm^{-1} (MO) are attributed to the –N=N– bond vibrations or to aromatic ring vibrations sensitive to the interaction with the azo bond [170]. The bands located at (1000-1300) cm^{-1} are assigned to S=O stretching [170-171]. This distinctive bands disappear after irradiation of dyes with appearance of new band at 2084 cm^{-1} for degraded MO and at 2093 $cm^{-1}$for degraded CR which are attributed to N≡N group [172]. Simultaneously, there is a broad band above 3400 cm^{-1} for both degraded dyes that is assigned to OH group [173].

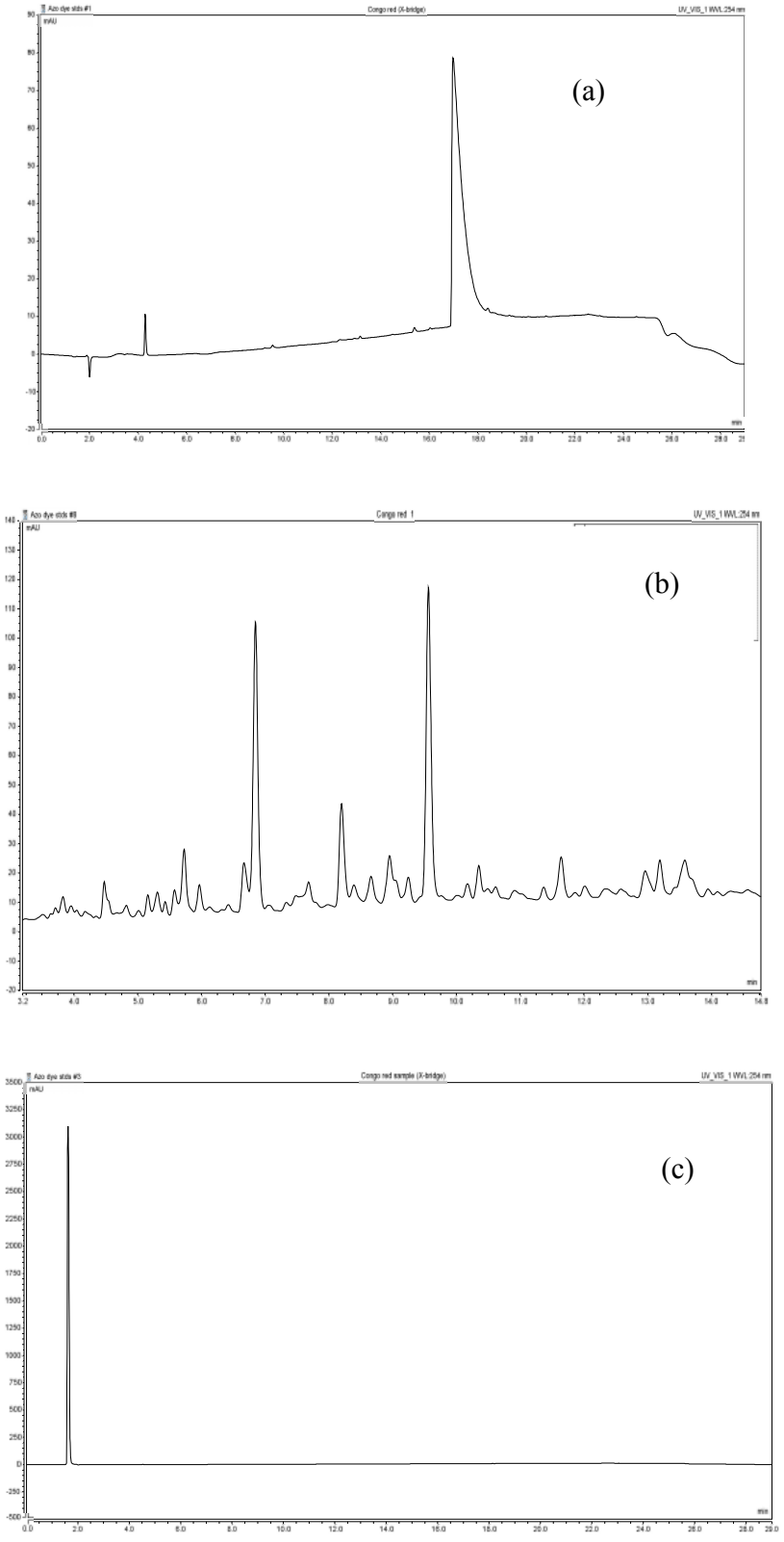

Figure 3-54: HPLC chromatograms of CR degraded at (a) zero, (b) half time and (c) full time of irradiation.

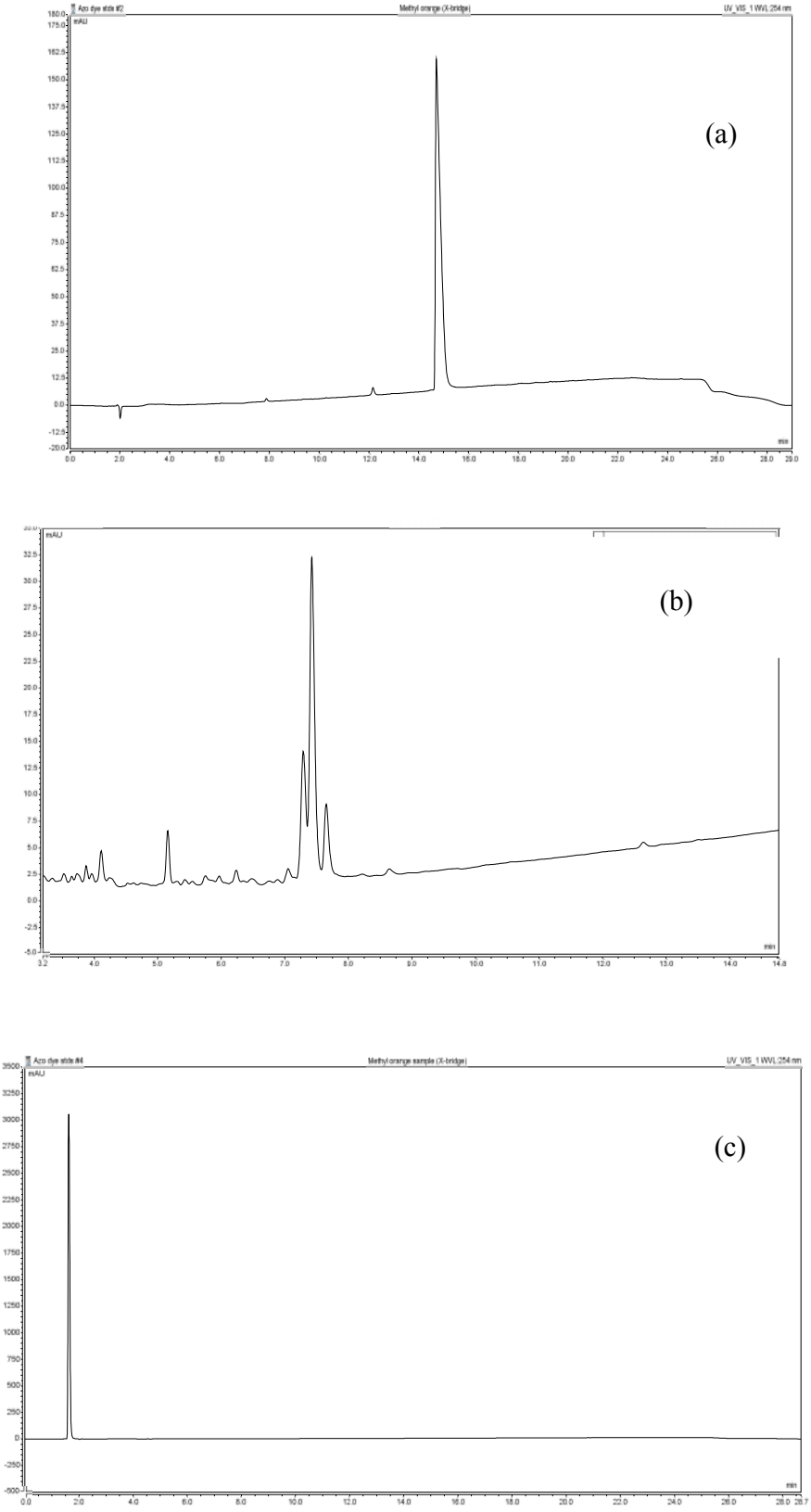

Figure 3-55: HPLC chromotograms of MO degraded at (a) zero, (b) half time and (c) full time of irradiation

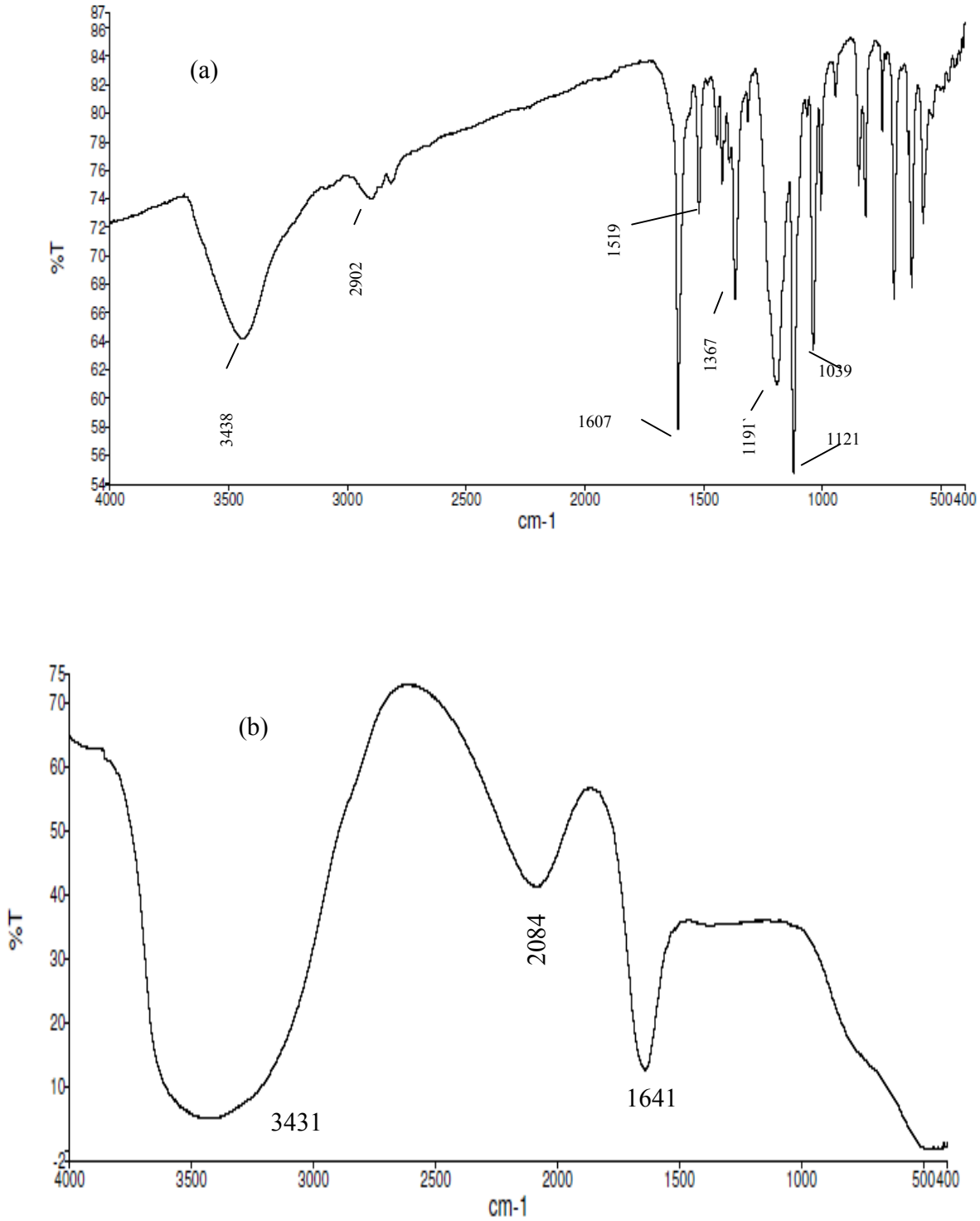

Figure 3-56: FT-IR spectra of (a) pure methyl orange and (b) degraded methyl orange

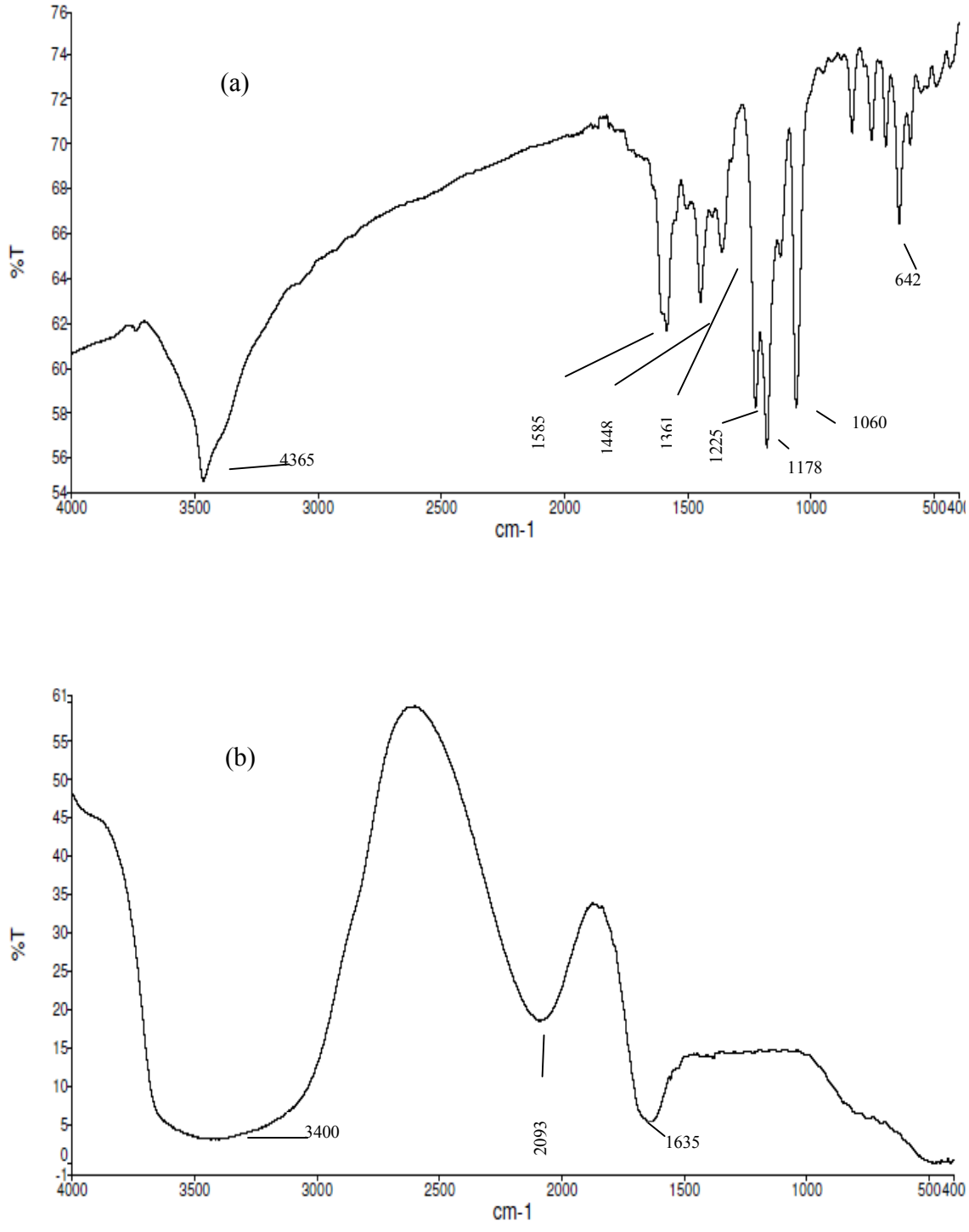

Figure 3-57: FT-IR spectra of (a) pure congo red and (b) degraded congo red

In order to broaden our insight on the degradation pathway of the dyes, mass spectroscopic the analysis was conducted. Based upon the m/z values, some intermediates have been identified and are presented in Figures 3-58 and 3-59.The degradation of MO is initiated, most by the probably, attack of $^{\cdot}OH$ radicals resulting in aromatic substitution with hydroxyl group in acidic medium to show a compound at 355 m/z. Some researchers [174-175] have mentioned that there is a demethylation reaction which occurrsduring degradation of methyl orange, therefore the product that has m/z = 327 may be formed by cleaving a methyl group from the MO molecule. Further, there are cleavage of azo bond and N-C bond to give rise other intermediates. The progress of illumination would definitely results in further degradation of the intermediates leading to lower molecular weight degradation products and afterwards to complete mineralization. The possible species formed after degradation of congo red suggest that the degradation of congo red follows the cleavage of azo linkage and also the cleavage of various C-C and C-N bonds of CR as a result of crucial effect of OH radical ending eventually with evolution of CO_2 and H_2O [176]. The most possible and photodegradation pathways for MO and CR are proposed as shown in Figures 3-60 and 3-61, respectively.

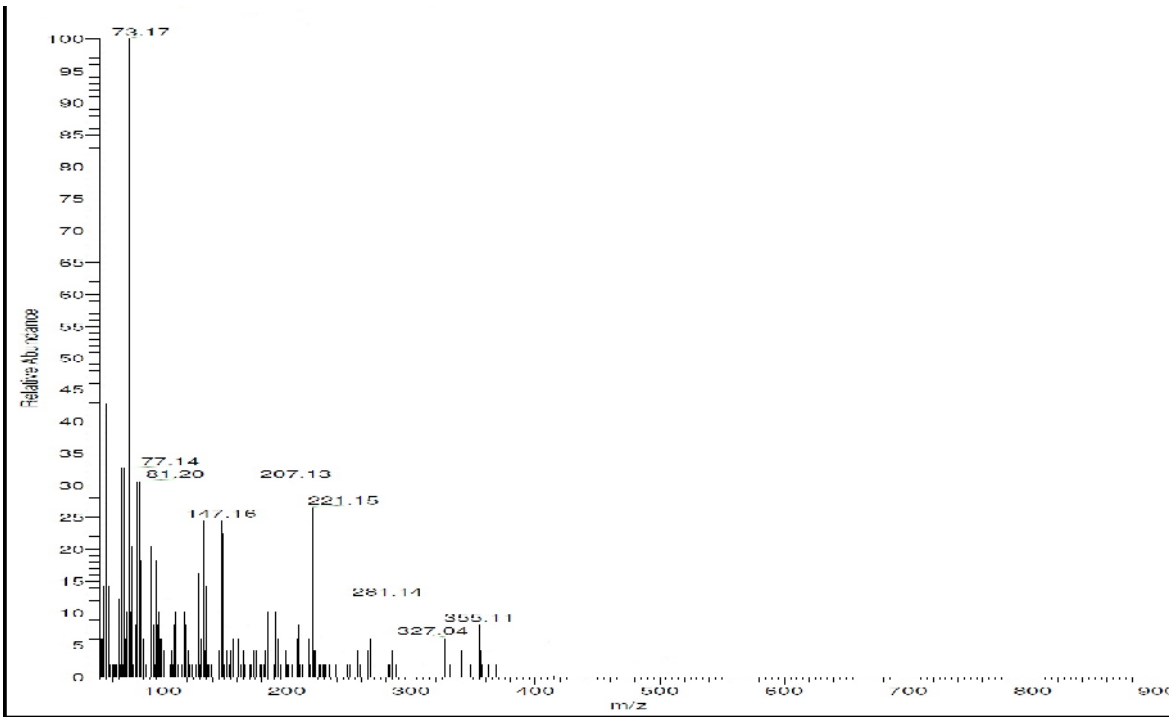

Figure 3-58: Mass spectra of methyl orange after complete degradation

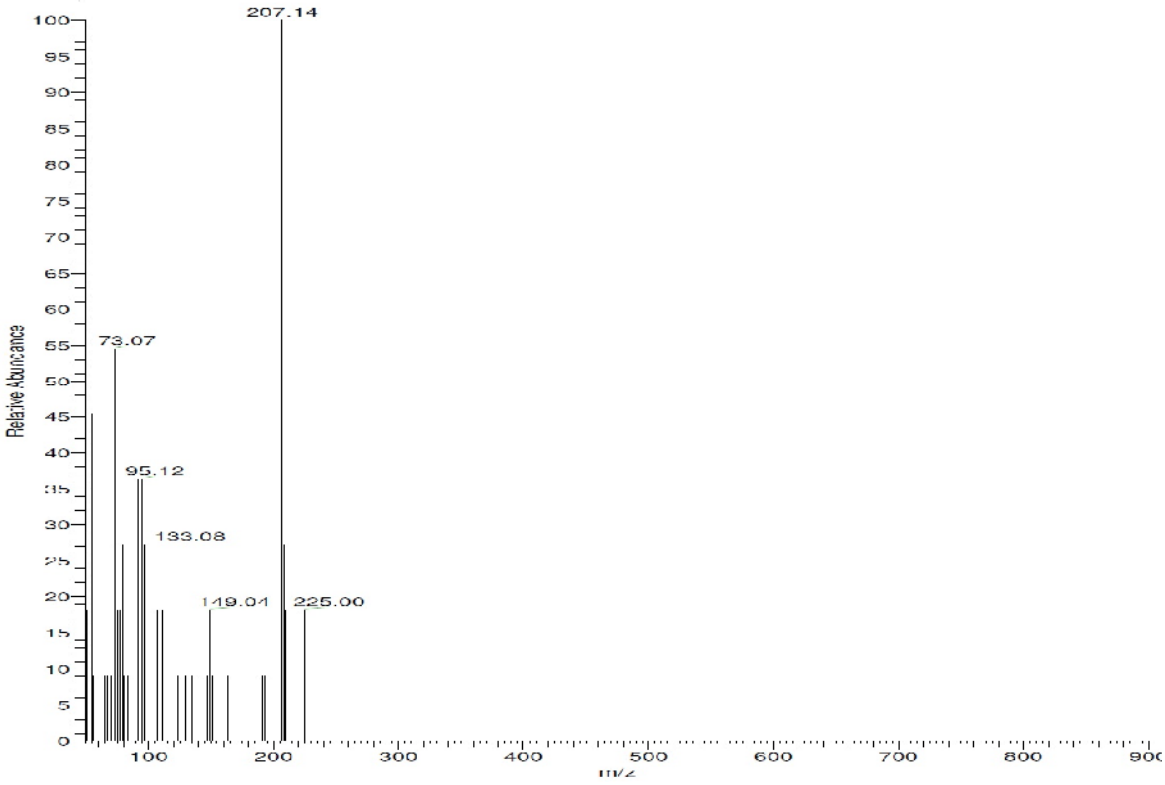

Figure 3-59: Mass spectra of congo red after complete degradation

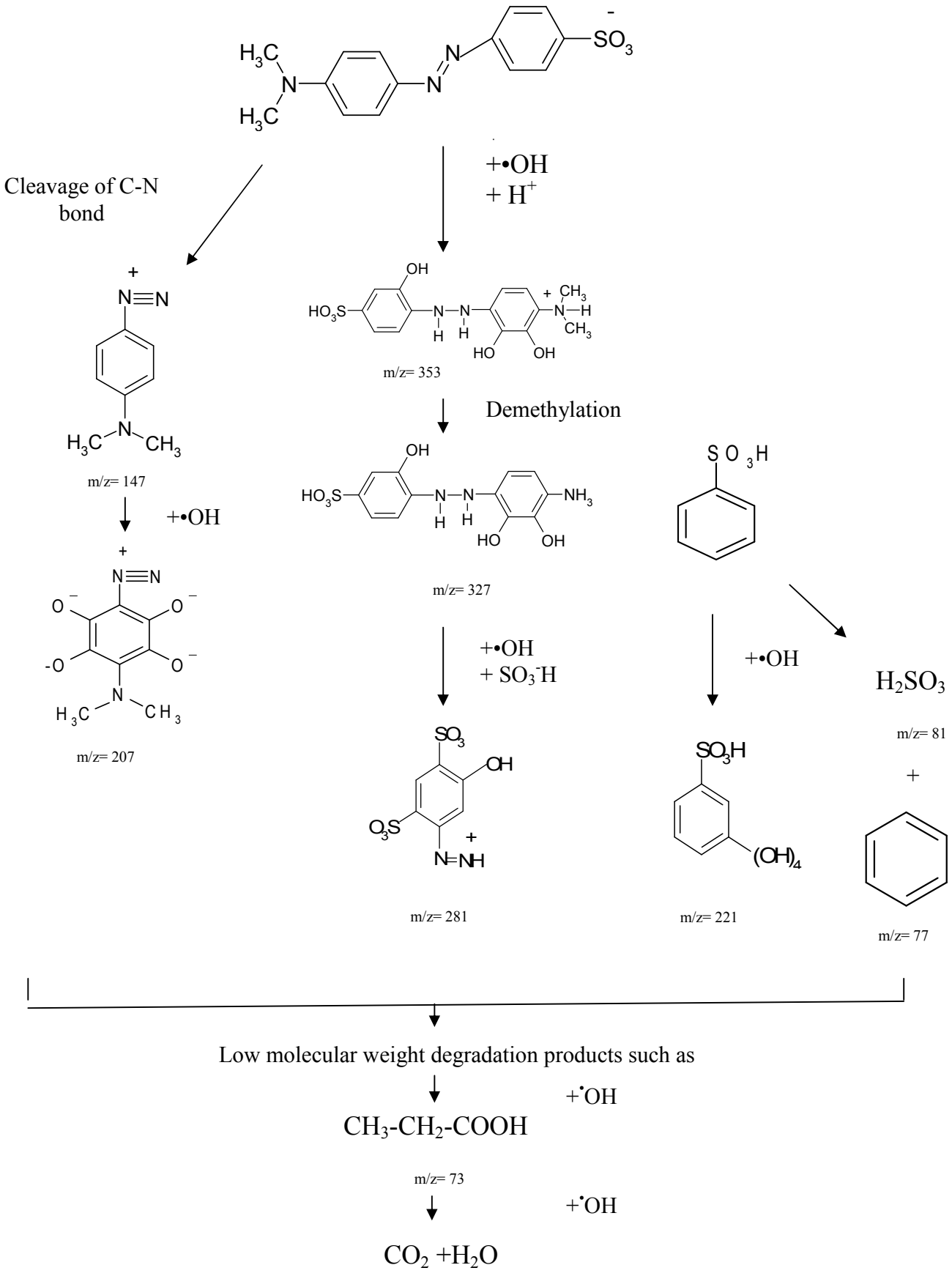

Figure 3-62: Proposed pathway for the photocatalytic degradation of MO

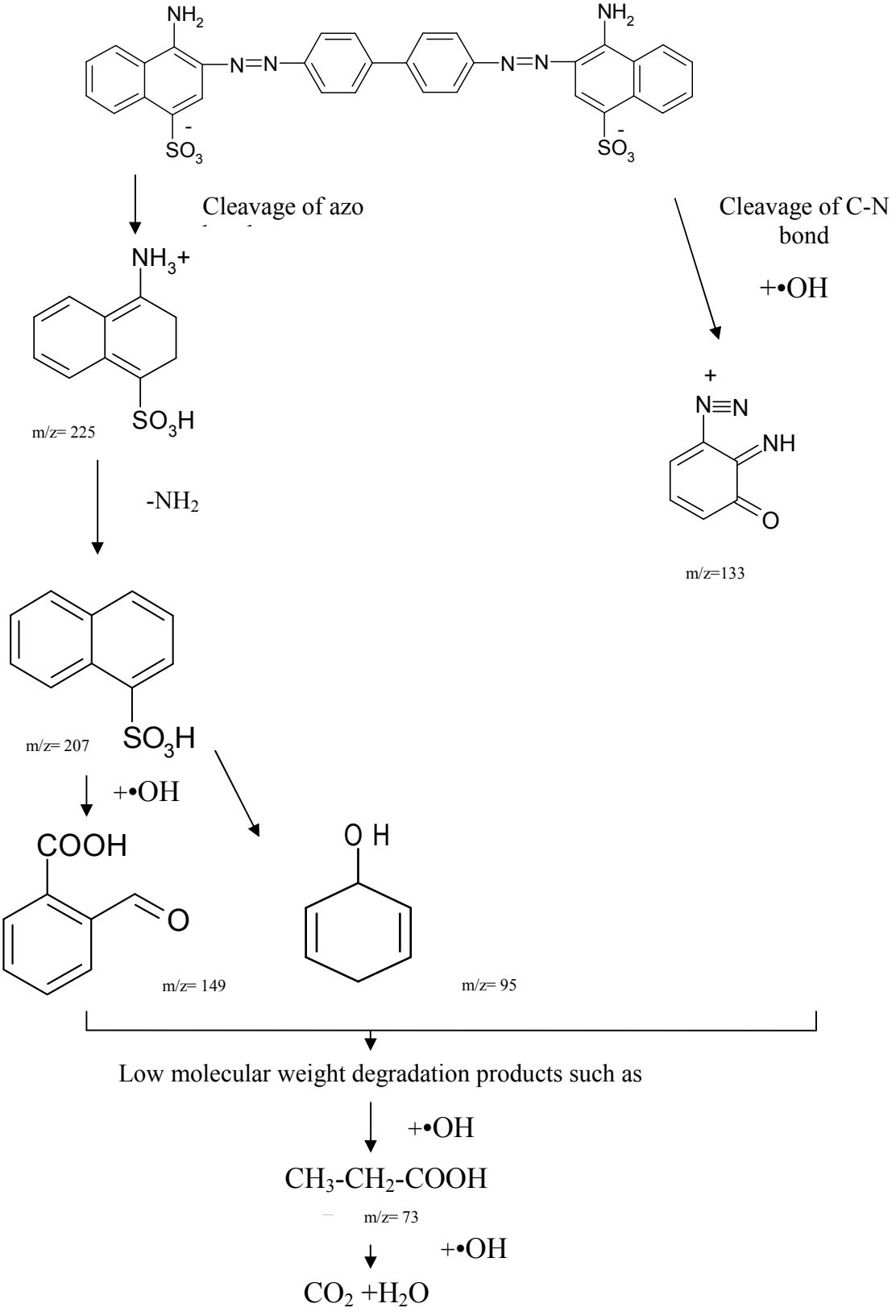

Figure 3-61: Proposed pathway for the photocatalytic degradation of CR

3.10 Comparison and evaluation of photocatalytic degradation of methyl orange and congo red azo dyes

Methyl orange and congo red showed high tendency to degrade at acidic pH depending on the principle that supposed to occur strong adsorption between titanium dioxide that carries positive charge at acidic medium and anionic azo dyes [177]. Congo red needed more irradiation time compared with that of methyl orange. This behavior mat be attributed to complicated structure of congo red [17]. The high value of activation energy of congo red compared with that of methyl orange means the degradation rate of CR is slow and it requires longer time to decompose relative to methyl orange. In other words there are large number of formed intermediates that result from CR photocatalytic degradation. This explanation is in an accordance with wheland principle [178, 179] of the stability of mechanism paths and intermediates. Furthermore, The faster decolorization of monoazo dye than diazo dye is another indication that, the number of azo and sulphonate groups in the dye molecule may be a determining factor for increasing the degradation rates [180]. Finally, although the final photo-mineralization products of organic dyes are CO_2, H_2O and mineral acids, but the photodegradation paths are not necessarily analogous as it is explictitly illustrated illustrated with CR and MO model dye pollutants.

3.11 General Conclusions

XRD analysis of the synthesized N-doped TiO_2 confirmed the neat anatase phase without rutile diffraction peaks. Images of SEM showed smooth and highly orderd surface. The excitation wavelength as determined from the integrated sphere UV-VIS spectrometer located at 410 nm. EDX

measurement revealed the atomic composition of all samples consist of nitrogen and titanium.

The impacts of many experimental parameters namely; initial solution pH, azo dye initial concentration, N-TiO_2 dosage and visible light intensity on the photodegradation of MO and CR dyes have been evaluated. The photocatalytic reaction is favored at relatively low photolysis solution pHs (2.5), a high visible light intensity, 40-50 mg/l N-TiO_2 dosages and 10-15 mg/l of initial dye concentrations.

Furthermore, the apparent quantum yield was also explicitly influenced by photolysis solution pH, TiO_2 dosage and initial dye concentration. Under optimum operational conditions, the solar photodecomposition of methyl orange attained better process rate and yield in comparison to the laboratory outcomes.

The kinetics and thermodynamics of the photocatalytic bleaching of both dyes employing N-TiO_2 nanocatalyst have also been investigated. The kinetics of the photocatalytic oxidation follows the well known Langmuir–Hinshelwood model which demonstrates the pseudo first order within the studied dye initial concentrations. The rate of the photocatalytic degradation was enhanced by the addition of H_2O_2 as well. Hydroxyl radicals played an appreciable role, other than O_2 gas, in the photobleaching process indicating the remarkable role of hydroxyl type chemistry mechanism in the process. On the other hand, an increase of the temperature has exhibited a positive impact on the kinetics of the process following the Arrhenius relation. The activation energies of the degradation for methyl orange and congo red azo dyes were found to be 25.8 and 33.7 kJ mol^{-1}, respectively.

Plausible pathways for the degradation of the concerned dyes were followed by HPLC, MS, NMR and FTIR. The photodegradation profile

houses several smaller aromatic and nitridated moieties as hydroxyl radical initiated primary oxidation intermediates which eventually renders into carbon dioxide and water.

3.12 Suggestions

In the light of the present research work, several suggestions for the future research activities can be reported:

1- Since the solar photocatalytic process has exhibited stimulating results, it would suggest employing immobilized nano TiO_2 units, for the photodetoxification of organic dyes under solar irradiation.

2- The study of the photocatalytic decontamination of the persisting organic pollutants in aqueous media together with computational authentication could be an interesting extension of this work.

3- The noble metal, Pt, Ag and Au, doping methodology of nano TiO_2 photocatalyst could also participate in the green chemistry strategy. Accordingly, we consolidate such line of research work to be adopted for the photomineralization of persisting organic moieties like poly aromatic hydrocarbons (PAH) and azo pollutants.

4-Adoption of semiconductor sensitization by means of dyes and coupling via other low band gap photocatalyst strategies could also be a good progressive pace for future work research.

References

[1] X. Qu, P. J. J. Alvarez, Q. Li, "Applications of nanotechnology in water and wastewater treatment", Water Res. 47 (2013) 3931-3946.

[2] S.Singh, K. C. Barick, D. Bahadur, "Functional oxide nanomaterials and nanocomposites for the removal of heavy metals and dyes", Nanomater. Nanotechnol. 3 (2013) 1-19.

[3] F. Kiriakidou, D. I. Kondarides, X.E. Verykios, "The effect of operational parameters and TiO_2-doping on the photocatalytic degradation of azo-dyes" Catal. Today 54 (1999) 119–130.

[4] W. H. Calze, J. W. Kang, D. H. Chapin, "The chemistry of water treatment processes involving ozone, hydrogen peroxide and ultraviolet radiation", Ozone Sci. Eng. 9 (1987) 355-352.

[5] M. Pelaeza, N. T. Nolan, S.C. Pillai, M. K. Seeryce, P. Falarasd, A. G. Kontosd, P. S. M.Dunlope, J. W. J. Hamilton, j. A. Byrnee, K. O'Sheaf, M. H. Entezaring, D. D. Dionysiou, "A review on the visible light active titanium dioxide photocatalysts for environmental applications" Appl. Catal. B: Environ. 125 (2012) 331-349.

[6] R. Toor, M. Mohseni, "UV-H_2O_2 based AOP and its integration with biological activated carbon treatment for DBP reduction in drinking water" Chemosphere 66 (2007) 2087-2095.

[7] B. Grote, "Application of advanced oxidation processes (AOP) in water treatment" 37th Annual Qld Water Industry Operations Workshop (2012) 17-23.

[8] A. Goi, "Advanced oxidation processes for water purification and soil remediation" Ph. D. thesis, Tallinn University Of Technology, 2005, pp. 15-16.

[9] U. I. Gaya, A. H. Abdullah, " Heterogeneous photocatalytic degradation of organic contaminants over titanium dioxide: A review of fundamentals, progress and problems" J. Photochem. Photobiol., C: Photochem Rev. 9 (2008) 1–12.

[10] M. I. Litter, " Heterogeneous photocatalysis Transition metal ions in photocatalytic systems" Appl. Catal., B: Environ. 23 (1999) 89–114.

[11] S. Malato , P. F. Ibanez, M.I. Maldonado, J. Blanco , W. Gernjak, " Decontamination and disinfection of water by solar photocatalysis: Recent overview and trends" Catal. Today 147 (2009) 1–59.

[12] A.R. Khataeea, M.B. Kasiri, " Photocatalytic degradation of organic dyes in the presence of nanostructured titanium dioxide: Influence of the chemical structure of dyes" J. Mol. Catal. A: Chem. 328 (2010) 8–26.

[13] A. Houas, H. Lachheb, M. Ksibi, E. Elaloui, C. Guillard, J. M. Herrmann, " Photocatalytic degradation pathway of methylene blue in water" Appl. Catal., B: Environ. 31 (2001) 145–157.

[14] V.K. Gupta, Suhas, " Application of low-cost adsorbents for dye removal A review" J. Environ. Manage. 90 (2009) 2313–2342.
[15] P. Bansal, D. Sud, " Photodegradation of commercial dye, Procion Blue HERD from real textile wastewater using nanocatalysts" Desalination 267 (2011) 244–249.
[16] B. J. Bruschweiler, S. Kung, D. Burgi, L. Muralt, E. Nyfeler, " Identification of non-regulated aromatic amines of toxicological concern which can be cleaved from azo dyes used in clothing textiles" Regul. Toxicol. Pharm. 69 (2014) 263–272.
[17] Z. Zainal, L. K. Hui, M. Z. Hussein, Y. H. Taufiq-Yap, A. H. Abdullah, I. Ramli, " Removal of dyes using immobilized titanium dioxide illuminated by fluorescent lamps" J. Hazard. Mater. B 125 (2005) 113–120.
[18] M.A. Rauf, M.A. Meetani, S. Hisaindee, " An overview on the photocatalytic degradation of azo dyes in the presence of TiO_2 doped with selective transition metals" Desalination 276 (2011) 13–27.
[19] M. Isik, D. T. Sponza, " Fate and toxicity of azo dye metabolites under batch long-term anaerobic incubations" Enzyme Microb. Technol. 40 (2007) 934–939.
[20] H. B. Mansour, D. Corroler, D. Barillier, K. G. L. Chekir, R. Mosrati, " Evaluation of genotoxicity and pro-oxidant effect of the azo dyes: Acids yellow17, violet 7 and orange 52, and of their degradation products by Pseudomonas putida mt-2" Food Chem. Toxicol. 45 (2007) 1670–1677.
[21] M. A. Rauf, S. S. Ashraf, " Fundamental principles and application of heterogeneous photocatalytic degradation of dyes in solution" Chem. Eng. J. 151 (2009) 10–18.
[22] J. Saien, A.R. Soleymani " Degradation and mineralization of Direct Blue 71 in a circulating upflow reactor by UV/TiO_2 process and employing a new method in kinetic study" J. Hazard. Mater. 144 (2007) 506–512.
[23] C. C. Hsueh, B. Y. Chen, "Exploring effects of chemical structure on azo dye decolorization characteristics by Pseudomonas luteola" J. Hazard. Mater. 154 (2008) 703–710.
[24] H. Lachheb, E. Puzenat, A. Houas, M. Ksibi, Elimame Elaloui, C. Guillard, J. M. Herrmann, "Photocatalytic degradation of various types of dyes (Alizarin S, Crocein Orange G, Methyl Red, Congo Red, Methylene Blue) in water by UV-irradiated titania" Appl. Catal., B: Environ. 39 (2002) 75–90.
[25] V. Augugliaro, C. Baiocchi, A. B. Prevot, E. G. Lopez, V. Loddo, S. Malato, G. Marci, L. Palmisano, M. Pazzi, E. Pramauro. "Azo-dyes photocatalytic degradation in aqueous suspension of TiO_2 under solar irradiation" Chemosphere 49 (2002) 1223–1230.
[26] S. M. Tsui, W. Chu "The reaction mechanisms and kinetics of removing azo reactive dye by indirect photolysis approaches" Water Environ. Res 74 (2002) 488-493.

[27] I. K. Konstantinou, T. A. Albanis, " TiO_2-assisted photocatalytic degradation of azo dyes in aqueous solution: kinetic and mechanistic investigations A review" Appl. Catal., B: Environ. 49 (2004) 1–14.
[28] M. A. Fox, M. T. Dulay, "Heterogeneous photocatalysis", Chem. Rev. 93 (1993) 341-357.
[29] K. S. Yu, J. Y. Shi, Z. l. Zhang, Y. M. Liang, W. Liu, " Synthesis, characterization, and photocatalysis of ZnO and Er-doped ZnO" J. Nanomater. Article ID 372951 (2013) 1-6.
[30] W. Yaoa, X. Songa, C. Huangb, Q. Xua, Q. Wu, " Enhancing solar hydrogen production via modified photochemical treatment of Pt/CdS photocatalyst" Catal. Today 199 (2013) 42– 47.
[31] B. Neppolian, H.C. Choi, S. Sakthive, B. Arabindoo, V. Murugesan, " Solar/UV-induced photocatalytic degradation of three commercial textile dyes" J. Hazard. Mater. B89 (2002) 303–317.
[32] G. C. Lakshmi1, S. Ananda, R. Somashekar, " Semiconductor-assisted photodegradation of dye and pesticide by ZnO: Ru and $ZnO/RuO_2/AgO$ nanocomposites, synthesised by electrolytic method" Int. J. Ad. Sci. Technol. 5 (2012) 40-53.
[33] B. Pant, H. R. Pant, M. Park, Y. Liu, J. W. Choi, " Electrospun $CdS–TiO_2$ doped carbon nanofibers for visible-light-induced photocatalytic hydrolysis of ammonia borane" Catal. Commun. 50 (2014) 63–68.
[34] L. Fass, " Imaging and cancer: A review" Mol. Onol. 2 (2008) 115–152.
[35] M. B. Radoicic, I. A. Jankovic, V. N. Despotovic, D. V. Sojic, Tatjana D. Savic, Zoran V. Saponjic, B. F. Abramovic, M. I. Comora, " The role of surface defect sites of titania nanoparticles in the photocatalysis: aging and modification" Appl. Catal., B: Environ.138– 139 (2013) 122– 127.
[36] S. Rehman, R. Ullah, A. M. Butt, N. D. Gohar, " Strategies of making TiO_2 and ZnO visible light active" J. Hazard. Mater. 170 (2009) 560–569.
[37] D. Chatterjee, S. Dasgupta, " Visible light induced photocatalytic degradation of organic pollutants" J. Photochem. Photobiol., C: Photochem. Rev. 6 (2005) 186–205.
[38] J. Zhao, C. Chen, W. Ma, " Photocatalytic degradation of organic pollutants under visible light irradiation" Top. Catal. 35 (2005) 269-278.
[39] H. Parka, Y. Parkb, W. Kimb, W. Choib, " Surface modification of TiO_2 photocatalyst for environmental applications" J. Photoch. Photobiol. C: Photochem. Rev. 15 (2013) 1– 20.
[40] B. Basheer, D. Mathew, B. K. George, C.P. R. Nair, " An overview on the spectrum of sensitizers: The heart of dye sensitized solar cells" Sol. Energy 108 (2014) 479–507.
[41] C. Y. Chien, B. D. Hsu, " Optimization of the dye-sensitized solar cell with anthocyanin as photosensitizer" Sol. Energy 98 (2013) 203–211.
[42] M. Tahir, N. S. Amin, " Advances in visible light responsive titanium oxide- based photocatalysts for CO_2 conversion to hydrocarbon fuels" Energy

Convers. Manage.76 (2013) 194–214.
[43] G. S. Mital, T. Manoj, " A review of TiO_2 nanoparticles" Chinese Sci. Bull. 56 (2010) 1639–1657.
[44] A. Matsuda, S. Sreekantan, W. Krengvirat, " Well-aligned TiO_2 nanotube arrays for energy-related applications under solar irradiation" J. Asian Ceramic Societies 1 (2013) 203–219.
[45] Y. Bessekhouad, D. Robert, J.V. Weber, " Bi_2S_3/TiO_2 and CdS/TiO_2 heterojunctions as an available configuration for photocatalytic degradation of organic pollutant" J. Photoch. Photobiol. A: Chem.163 (2004) 569–580.
[46] R.M. Mohamed, D.L. McKinney, W. M. Sigmund, "Enhanced nanocatalysts" Mater. Sci. Eng., R 73 (2012) 1-13.
[47] K. Nishijima, B. Ohtani, X. Yan, T. a. Kamai, T. Chiyoya, T. Tsubota, N. Murakami, T. Ohno, " Incident light dependence for photocatalytic degradation of acetaldehyde and acetic acid on S-doped and N-doped TiO_2 photocatalysts" Chem. Phys. 339 (2007) 64–72.
[48] R. Marschall, L. Wang, " Non-metal doping of transition metal oxides for visible-light photocatalysis" Catal. Today 225 (2014) 111– 135.
[49] D. W. Kwon, P. W. Seo, G. J. Kim, S. C. Hong, "Characteristics of the HCHO oxidation reaction over Pt/TiO_2 catalysts at room temperature: The effect of relative humidity on catalytic activity" Appl. Catal., B: Environ. 163 (2015) 436–443.
[50] Q. Huang, T. Gao, F. Niu, D. Chen, Z. Chen, L. Q, X. Sun, Y. Huang, K. Shu, "Preparation and enhanced visible-light driven photocatalytic properties of Au-loaded TiO_2 nanotube arrays" Superlattices Microstruct. 75 (2014) 890–900.
[51] M. Ni, M. K. H. Leung, D. Y. C. Leung, K. Sumathy, "A review and recent developments in photocatalytic water-splitting using TiO_2 for hydrogen production" Renewable and Sustainable Energy Reviews 11 (2007) 401–425.
[52] A. L. Linsebigler, G. Lu. J. T. Yastes, Jr, " Photocatalysis on TiO_2 surfaces: principles, mechanisms, and selected results" Chem. Rev. 95 (1995) 735-758.
[53] S. G. Kumar, L. G. Devi, " Review on modified TiO_2 photocatalysis under UV/Visible light: selected results and related mechanisms on interfacial charge carrier transfer dynamics" J. Phys. Chem. A 115 (2011) 13211–13241.
[54] E. J. Park, B. Jeong, M. G. Jeong, Y. D. Kim " Synergetic effects of hydrophilic surface modification and N-doping for visible light response on photocatalytic activity of TiO_2" Current Appl. Phys. 14 (2014) 300-305.
[55] A. Subrahmanyam, K. P. Biju, P. Rajesh, K. J. Kumar, M. R. Kiran, "Surface modification of sol-gel TiO_2 surface with sputtered metallic silver for Sun light photocatalytic activity: Initial studies" Sol. Energy Mater. Sol. Cells 101 (2012) 241–248.
[56] Y. K. Laia, J. Y. Huang, H. F. Zhanga, V. P. Subramaniam, Y. X. Tang, D. G. Gong, L. Sundar, L. Sun, Z. Chen, C. J. Lin, "Nitrogen-doped TiO_2 nanotube array films with enhanced photocatalytic activity under various

light sources" J. Hazard. Mater. 184 (2010) 855-863.
[57] W. X. Liu, P. Jiang, W. N. Shao, J. Zhang, W. B. Cao, "A novel approach for the synthesis of visible-light-active nanocrystalline N-doped TiO_2 photocatalytic hydrosol" Solid-State Sci. 33 (2014) 45-48.
[58] R. Asahi, T. Morikawa, T. Ohwaki, K. Aoki, Y. Taga, "Visible-light photocatalysis in nitrogen-doped titanium oxides" Sci 293 (2001) 269-271.
[59] D. Mitoraj, "Origin of visible light activity in urea modified titanium dioxide" Ph.D thesis, Alexander university (2009) pp. 18-19.
[60] C. M. Teh, A. R. Mohamed, "Roles of titanium dioxide and ion-doped titanium dioxide on photocatalytic degradation of organic pollutants (phenolic compounds and dyes) in aqueous solutions: A review" J. Alloys Compd. 509 (2011) 1648–1660.
[61] L. Jinlong, M. Xinxin, S. Mingren, X. Li, S. Zhenlun, "Fabrication of nitrogen-doped mesoporous TiO_2 layer with higher visible photocatalytic activity by plasma-based ion implantation" Thin Solid Films 519 (2010) 101–105.
[62] J. Xu, F. Wang, W. Liu, W. Cao, "Nanocrystalline N-doped TiO_2 Powders: mild hydrothermal synthesis and photocatalytic degradation of phenol under visible light irradiation" Int. J. Photoenergy (2013) Article ID 616139.
[63] M. Factorovich, L. Guz, R. Candal1, "N-TiO_2: Chemical Synthesis and Photocatalysis" Adv. Phys. Chem. (2011) Article ID 821204.
[64] J. Yuan, M. Chen, J. Shi,W. Shangguan, "Preparations and photocatalytic hydrogen evolution of N-doped TiO_2 from urea and titanium tetrachloride" Int. J. Hydrogen Energy 31 (2006) 1326 – 1331.
[65] A. Zaleska, "Doped-TiO_2: A Review" Recent Patents on Engineering 2 (2008) 157-164.
[66] M. J. Powell, C. W. Dunnill, I. P. Parkin, "N-doped TiO_2 visible light photocatalyst films via a sol–gel route using TMEDA as the nitrogen source" J. Photochem. Photobiol. A: Chem. 281 (2014) 27–34.
[67] F. Peng, L. Cai, H. Yu, H. Wang, J. Yang, "Synthesis and characterization of substitutional and interstitial nitrogen-doped titanium dioxides with visible light photocatalytic activity" J. Solid State Chem. 181 (2008) 130–136.
[68] C. Di Valentin, E. Finazzi, G. Pacchioni, A. Selloni, S. Livraghi, M. C. Paganini, E. Giamello, "N-doped TiO_2: Theory and experiment" Chem. Phys. 339 (2007) 44–56.
[69] Q. Wu, W. Li, D. Wang, S. Liu, "Preparation and characterization of N-doped visible-light-responsive mesoporous TiO_2 hollow spheres" Appl. Surf. Sci. 299 (2014) 35–40.
[70] G. Yang, Z. Jiang, H. Shi, T. Xiao, Z. Yan, "Preparation of highly visible-light active N-doped TiO_2 photocatalyst" J. Mater. Chem. 20 (2010) 5301–5309.
[71] N. T. Nolan, D. W. Synnott, M. K. Seery, S. J. Hinder, A. V. Wassenhoven, S. C. Pillai, "Effect of N-doping on the photocatalytic

activity of sol–gel TiO_2" J. Hazard. Mater. 211-212 (2012) 88– 94.
[72] Z. Zhang, J. Long, X. Xie, H. Zhuang, Y. Zhou, H. Lin, R. Yuan, W. Dai, Z. Ding, X. Wang, X. Fu, "Controlling the synergistic effect of oxygen vacancies and N dopants to enhance photocatalytic activity of N-doped TiO_2 by H_2 reduction" Appl. Catal., A: Gen. 425– 426 (2012) 117– 124.
[73] V. N. Kuznetsov, N. Serpone, "Visible light absorption by various titanium dioxide specimens" J. Phys. Chem. B 110 (2006) 25203-25209.
[74] N. Serpone, "Is the band gap of pristine TiO_2 narrowed by anion- and cation-doping of titanium dioxide in second-generation photocatalysts?" J. Phys. Chem. B 110 (2006) 24287-24293.
[75] D. A. Ward, E. I. KO, "Preparing catalytic materials by the sol-gel method" Ind. Eng. Chem. Res. 34 (1996) 421-433.
[76] O. J. d. Lima, A. T. Papacidero, L. A. Rocha, H. C. Sacco, E. J. Nassar, K. J. Ciuffi, L. A. Bueno, Y. Messaddeq, S. J. L. Ribeiro, "Sol–gel entrapped cobalt complex" Mater. Charact. 50 (2003) 101– 108.
[77] V. Lafond, P.H. Mutin, A. Vioux, "Non-hydrolytic sol–gel routes based on alkyl halide elimination: toward better mixed oxide catalysts and new supports application to the preparation of a SiO_2–TiO_2 epoxidation catalyst" J. Mol. Catal. A: Chem. 182–183 (2002) 81–88.
[78] O. Carp, C.L. Huisman, A. Reller, "Photoinduced reactivity of Titanium dioxide" Prog. Solid State Chem. 32 (2004) 33–177.
[79] F. Barbieri, D. Cauzzi, F. D. Smet, M. Devillers, P. Moggi, G. Predieri, P. Ruiz, "Mixed-oxide catalysts involving V, Nb and Si obtained by a non-hydrolytic sol–gel route: preparation and catalytic behaviour in oxidative dehydrogenation of propane" Catal. Today 61 (2000) 353–360.
[80] S. Rudiger, U. Grob, E. Kemnitz, "Non-aqueous sol–gel synthesis of nano-structured metal fluorides" J. Fluorine Chem. 128 (2007) 353–368.
[81] J. Livage, F. Beteille, C. Roux, M. Chatry, P. Davidson, "Sol-gel synthesis of oxide materials" Acta. mater. 46 (1998) 743-750.
[82] L. Bourget, R. J. P. Corriu, D. Leclercq, P. H. Mutin, A. Vioux, "Non-hydrolytic sol-gel routes to silica" J. Non-Cryst. Solids 242 (1998) 81-91
[83] A.B. Kashyout, M. Soliman, M. Fathy, "Effect of preparation parameters on the properties of TiO_2 nanoparticles for dye sensitized solar cells" Renewable Energy 35 (2010) 2914-2920.
[84] Damien P. Debecker, Vasile Hulea, P. Hubert Mutin, "Mesoporous mixed oxide catalysts via non-hydrolytic sol–gel: A review" Appl. Catal., A: Gen. 451 (2013) 192– 206.
[85] U.G. Akpan, B.H. Hameed, "The advancements in sol-gel method of doped-TiO_2 photocatalysts" Appl. Catal. A: General 375 (2010) 1–11.
[86] W. Bahnemann, M. Muneer, M.M. Haque, "Titanium dioxide-mediated photocatalysed degradation of few selected organic pollutants in aqueous suspensions" Catal. Today 124 (2007) 133–148.
[87] H. Kim, H. Y. Yoo, S. Hong, S. Lee, S. Lee, B. S. Park, H. Park, C. Lee, J.

Lee, "Effects of inorganic oxidants on kinetics and mechanisms of WO_3-mediated photocatalytic degradation" Appl. Catal., B: Environ. 162 (2015) 515–523.
[88] H. C Liang, X. Z. Li, Y. H. Yang, K. H. Sze, "Effects of dissolved oxygen, pH, and anions on the 2,3-dichlorophenol degradation by photocatalytic reaction with anodic TiO_2 nanotube films" Chemosphere 73 (2008) 805–812.
[89] U. G. Akpan, B. H. Hameed, "Parameters affecting the photocatalytic degradation of dyes using TiO_2-based photocatalysts: A review" J. Hazard. Mater. 170 (2009) 520–529.
[90] M. Y. Ghaly, J. Y. Farah, A. M. Fathy, "Enhancement of decolorization rate and COD removal from dyes containing wastewater by the addition of hydrogen peroxide under solar photocatalytic oxidation" Desalination 217 (2007) 74–84.
[91] X. R. Xu, X. Z. Li, "Degradation of azo dye Orange G in aqueous solutions by persulfate with ferrous ion" Sep. Purif. Technol. 72 (2010) 105–111.
[92] M. C. Yeber, L. Diaz, J. Fernindez, "Catalytic activity of the $SO_4^{\cdot-}$ radical for photodegradation of the azo dye Cibacron Brilliant Yellow 3 and 3,4-dichlorophenol: Optimization by application of response surface methodology" J. Photochem. PhotobiolA: Chem. 215 (2010) 90–95.
[93] J. B. Galvez, S. M. Rodraguez, "Solar detoxification" Published by the United Nations Educational, Scientific and Cultural Organization, India (2003) pp 86-88.
[94] C. G. Hatchard, C. A. Parker, "A new sensitive chemical actinometer. II. potassium ferrioxalate as a standard chemical actinometer" Math. Phys. Sci. 235 (1956) 518-536.
[95] A. A. Hussain, " Photocatalytic oxidation of phenol red on nanocrystalline TiO_2 particles" M.Sc. thesis, AL-Nahrain university (2014) pp.14 ,27, 78.
[96] A. H. Alwash, " Preparation and characterization of zeolite y – based catalyst for sonocatalytic degradation of organic dyes in water" Ph.D thesis, Sains Malaysia University (2013) pp. 65.
[97] S. K. Kansal, M. Singh, D. Sud, "Studies on photodegradation of two commercial dyes in aqueous phase using different photocatalysts" J. Hazard. Mater. 141 (2007) 581–590.
[98] A. A. M. Prabhu, G. Venkatesh, R. K. Sankaranarayanan, S.Siva, N. Rajendiran. "Azonium-ammonium tautomerism and inclusion complexation of 4-amino-2',3 dimethylazobenzene" Indian. J. Chem. (2010) 407-417.
[99] Sandeep Keshari Bhoi, "Adsorption charecterstics of congo red dye onto pac and gac based on S/N ratio: a taguchi approach" National Institute of Technology, Rourkela, Bachelor Project (2010) pp. 10-11.
[100] E. Pioorsch, A. Elhaddaou S. Turrixll, "Spectroscopic study of pH and sohrent effects on the structure of Congo red and its binding mechanism to amyloid-like proteins" Spectrochim. Acta., 50 (1994) 2145-2152.
[101] J. Ananpattarachai, P. Kajitvichyanukul, S. Seraphin, " Visible light

absorption ability and photocatalytic oxidation activity of various interstitial N-doped TiO_2 prepared from different nitrogen dopants" J. Hazard. Mater.168 (2009) 253–261.

[102] W. Guo, Y. Shen, G. Boschloo, A. Hagfeldt, T. Ma, " Influence of nitrogen dopants on N-doped TiO_2 electrodes and their applications in dye-sensitized solar cells" Electrochim. Acta 56 (2011) 4611–4617.

[103] L. Sun, J. Cai, Q. Wu, P. Huang, Y. Su, C. Lin, " N-doped TiO_2 nanotube array photoelectrode for visible-light-induced and photoelectrocatalytic activities" Electrochim. Acta 108 (2013) 525– 531.

[104] V. J. Babu, M. K. Kumar, A. S. Nair, T. L. Kheng, S. I. Allakhverdiev, S. Ramakrishna, "Visible light photocatalytic water splitting for hydrogen production from N-TiO_2 rice grain shaped electrospun nanostructures" Inter. J. hydrogen energy 37 (2012) 8897-8904.

[105] H. Sun, Y. Bai, W. Jin, N. Xu, "Visible-light-driven TiO_2 catalysts doped with low-concentration nitrogen species" Sol. Energy Mater. Sol. Cells 92 (2008) 76–83.

[106] K. M. Parida, S. Pany, B. Naik, "Green synthesis of fibrous hierarchical meso macroporous N doped TiO_2 nanophotocatalyst with enhanced photocatalytic H_2 production" Int. J. Hydrogen energy 38 (2013) 3545-3553.

[107] M. Xiaoqi, L. Lianqiang, Z. Kaishun, L. Juncheng, " The effect of SiO_2 on TiO_2 up-conversion photoluminescence film" Opt. Mater. 37 (2014) 367–370.

[108] J. Jayabharathi, C. Karunakaran, V. Thanikachalam, P. Ramanathan "Binding and fluorescence enhancing behaviour of phenanthrimidazole with different phases of TiO_2" New J. Chem. 38 (2014) 432-4335.

[109] S. G. Ghugal, S. S. Umare, R. Sasikala, " Enhanced photocatalytic activity of TiO_2 assisted by Nb, N and S multidopants" Mater. Res. Bull. 61 (2014) 298–305.

[110] J. Senthilnathan, Ligy Philip " Photocatalytic degradation of lindane under UV and visible light using N-doped TiO_2" Chem. Eng. J. 161 (2010) 83–92.

[111] A. I. Gusev, S.V. Rempel, "X-Ray diffraction study of the nanostructure resulting from decomposition of (ZrC) (NbC) solid solutions, Inorg. Mater. 39 (2003) 43-47.

[112] J. Fan, Z. Zhao, J. Wang, L. Zhu, " Synthesis of Cr, N-codoped titania nanotubes and their visible-light-driven photocatalytic properties" Appl. Surf. Sci.324 (2015) 691–697.

[113] S. Hu, A. Wang, X. Li , H. Lowe, " Hydrothermal synthesis of well-dispersed ultra fine N-doped TiO_2 nanoparticles with enhanced photocatalytic activity under visible light" J. Phys. Chem. Solids 71 (2010) 156–162.

[114] P. Guo, X. Wang, H. Guo , "TiO_2/Na-HZSM-5 nano-composite photocatalyst: Reversible adsorption by acid sites promotes photocatalytic decomposition of methyl orange" Appl. Catal. B: Environmental 90 (2009)

677–687.
[115] S. Parra ,J. Olivero, C. Pulgarin, "Relationships between physicochemical properties and photoreactivity of four biorecalcitrant phenylurea herbicides in aqueous TiO_2 suspension" Appl. Catal. B: Environmental 36 (2002) 75–85.
[116] H. X. Guo, K. L. Lin, Z. S. Zheng, F. B. Xiao, S. X. Li, " Sulfanilic acid-modified P25 TiO_2 nanoparticles with improved photocatalytic degradation on Congo red under visible light" Dyes and Pigments 92 (2012) 1278-1284.
[117] M. Movahedi, A. R. Mahjoub, S. J. Darzi "Photodegradation of congo red in aqueous solution on ZnO as an alternative catalyst to TiO_2" J. Iran. Chem. Soc.6 (2009) 570-577.
[118] J. Wanga, T. Ma, Z. Zhang, X. Zhang, Y. Jiang, Z. Pan, F. Wen, P. Kang, P. Zhang, "Investigation on the sonocatalytic degradation of methyl orange in the presence of nanometer anatase and rutile TiO_2 powders and comparison of their sonocatalytic activities" Desalination 195 (2006) 294–305.
[119] A. K. Mohammed, K. T. Mekenzie, "Photocatalytic degradation of Chicago Sky Blue 6B and Benzopurpurin 4B using titanium dioxide thin film" J. Environ. Sci. 17 (2005) 869-872.
[120] J. Mitrović, M. Radović, D. Bojić, T. Anđelković, M. Purenović, A. Bojić, " Decolorization of the textile azo dye Reactive Orange 16 by the UV/H_2O_2 process" J. Serb. Chem. Soc. 77 (4) (2012) 465–481.
[121] B. Neppolian, H.C. Choi, S. Sakthivel, B. Arabindoo, V. Murugesan, "Solar light induced and TiO_2 assisted degradation of textile dye reactive blue 4" Chemosphere 46 (2002) 1173–1181.
[122] M. Nikazar, K. Gholivand, K. Mahanpoor, " Photocatalytic degradation of azo dye Acid Red 114 in water with TiO_2 supported on clinoptilolite as a catalyst" Desalination 219 (2008) 293–300.
[123] N. Daneshvar, S. Aber, M. S. Seyed Dorraji, A. R. Khataee, and M. H. Rasoulifard, "Preparation and investigation of photocatalytic properties of ZnO nanocrystals: effect of operational parameters and kinetic study" Int. J. Chem. Nuclear, Metallurgical Mater. Eng.1 (2007) 1-6.
[124] N. A. Jamalluddin, A. Z. Abdullah, "Reactive dye degradation by combined Fe(III)/TiO_2 catalyst and ultrasonic irradiation: Effect of Fe(III) loading and calcination temperature" Ultrason. Sonochem. 18 (2) (2010) 669-678.
[125] J. Q Chen, D. Wang, M. X Zhu, C. J. Gao, "Photocatalytic degradation of dimethoate using nanosized TiO_2 powder" Desalination 207 (2007) 87–94.
[126] Z. Sun , Y. Chen, Q. Ke, Y. Yang, J. Yuan, "Photocatalytic degradation of cationic azo dye by TiO_2/bentonite nanocomposite" J. Photochem. Photobiol. A: Chem.149 (2002) 169–174.
[127] M. A. Quiroz, E. R. Bandala, C. A. Martinez-Huitle, "Advanced oxidation processes (AOPs) for removal of pesticides from aqueous media" Published

by Intech, China (2011) pp 692-694.
[128] M. A. Rauf, S. S. Ashraf, "Radiation induced degradation of dyes-An overview" J. Hazard. Mate.166 (2009) 6-16.
[129] M. R. Hoffmann, S. T. Martin, W. Choi, D. W. Bahnemann, "Environmental applications of semiconductor photocatalysis" Chem. Rev. 95 (1995) 69-96.
[130] L. Xu, J. Wang, "A heterogeneous Fenton-like system with nanoparticulate zero-valent iron for removal of 4-chloro-3-methyl phenol" J. Hazard. Mate. 186 (2011) 256-264.
[131] R. Chauhan , A. Kumar , R. P. Chaudhary, "Structural and photocatalytic studies of Mn doped TiO_2 nanoparticles" Spectrochimica Acta Part A: Molecular and Biomolecular Spectroscopy 98 (2012) 256–264.
[132] S. Yanga, P. Wang, X. Yang, L. Shan, W. Zhang, X. Shao, Rui Niu, "Degradation efficiencies of azo dye Acid Orange 7 by the interaction of heat, UV and anions with common oxidants: Persulfate, peroxymonosulfate and hydrogen peroxide" J. Hazard. Mater. 179 (2010) 552–558.
[133] V. Augugliaro, C. Baiocchi, A. B. Prevot, E. G. Lopez, V. Loddo, S. Malato, G. Marci, L. Palmisano, M. Pazzi, E. Pramauro, " Azo-dyes photocatalytic degradation in aqueous suspension of TiO_2 under solar irradiation" Chemosphere 49 (2002) 1223–1230.
[134] S. Irmak, E. Kusvuran, O. Erbatur, "Degradation of 4-chloro-2-methylphenol in aqueous solution by UV irradiation in the presence of titanium dioxide" Appl. Catal., B: Environ.54 (2004) 85–91.
[135] R. S.Thakur, R. Chaudhary, C. Singh, "Fundamentals and applications of the photocatalytic treatment for the removal of industrial organic pollutants and effects of operational parameters: A review" J. Renew Sustainable Energy 2 (2010) 1-37.
[136] Y. Bayat, F. Hajighasemali, M. Zarandi, " Novel approach trough TADB debenzylation by application of potassium bromate and cerium (IV) ammonium nitrate (CAN)" Am. J. Chem. Appl. 2 (2015) 28-31.
[137] Y. N. Tan, C. L. Wong, A. R. Mohamed, "An overview on the photocatalytic activity of nano-doped-TiO_2 in the degradation of organic pollutants" isrn mater. sci.(2011) 1-18.
[138] A. D. Paolaa, E. G. López,, G. Marcì, L. Palmisano, "A survey of photocatalytic materials for environmental remediation" J. Hazard Mater. 211– 212 (2012) 3– 29.
[139] Swati, Munesh, R. C. Meena, " Photocatalytic degradation of textile dye through an alternative photocatalyst methylene blue immobilized resin dowex 11 in presence of solar light " Archives Appl. Sci. Research, 4 (1): (2012) 472-479.
[140] R.C. Meena, R. B. Pachwarya, V. K. Meena, S. Arya, "Degradation of textile dyes ponceau-s and sudan iv using recently developed photocatalyst, immobilized resin dowex-11" Am. J. Environ. Sci. 5 (2009) 444-450.

[141] C. Mathivathana, V. Balasubramanian, K. Pandian, "The influence of the oxidizing agents on the rates of degradation of Rose bengal using titanium oxide nanoparticles" Elixir Dye Chem. 56 (2013) 13510-13518.
[142] E. M. Saggioro, A. S. Oliveira, T. Pavesi, C. G. Maia, L. F. V. Ferreira, J . C. Moreira "Use of titanium dioxide photocatalysis on the remediation of model textile wastewaters containing azo dyes" Molecules 16 (2011) 10370-10386.
[143] S. N. H. B. Yahya, "Solar photocatalytic degradation of textile dye direct blue 86 in ZnO suspension" Bachelor project University of Teknologi Petronas (2013) 1-57 p.23.
[144] S. Moziaa, A. W. Morawski, M. Toyoda, M. Inagaki, " Application of anatase-phase TiO_2 for decomposition of azo dye in a photocatalytic membrane reactor" Desalination 241 (2009) 97-105.
[145] J. C. Garcia, J. L. Oliveira, A.E.C. Silva, C.C. Oliveira, J. Nozaki , N.E. de Souza "Comparative study of the degradation of real textile effluents by photocatalytic reactions involving UV/TiO_2/H_2O_2 and UV/Fe^{+2}/H_2O_2 systems" J. Hazard. Mater. 147 (2007) 105–110.
[146] S. M. Ghoreishian, K. Badii, M. Norouzi, A. Rashidi, M. Montazer, M. Sadeghi, M. Vafaee, " Decolorization and mineralization of an azo reactive dye using loaded nano-photocatalysts on spacer fabric: Kinetic study and operational factors" J. Taiwan. Inst. Chem. Eng. 45 (2014) 2436–2446.
[147] K. hezrianjoo, H. Revanasiddappa "Langmuir-hinshelwood kinetic expression for the photocatalytic degradation of metanil yellow aqueous solutions by ZnO catalyst" Chem. Sci. J. Vol. 2012: CSJ-85.
[148] C. Oprea, P. Panait, J. Lungu, D.Stamate, A. Dumbravs, F. Cimpoesu, M. A. Gîruu, "DFT study of binding and electron transfer from a metal-free dye with carboxyl, hydroxyl, and sulfonic anchors to a titanium dioxide nanocluster" Int. J. Photoenergy Article ID 893850 (2013) 1-15.
[149] P. Atkins, J. D. Paula, "Atkins' Physical Chemistry" 8 edition (2006) PP. 877-880.
[150] A. L. Gupta, "Photochemistry" Published by Pragati Prakashan, India 5 edition (2011) pp. 63-66.
[151] N. Serpone, A. Salinaro, "Terminology, relative photonic efficiencies and quantum yields in heterogeneous photocatalysis. Part I: Suggested Protocol" Pure. Appl. Chem. 71 (1999) 303–320.
[152] F. Machuca, J. C. Márquez, M. Mueses, " Determination of quantum yield in a heterogeneous photocatalytic system using a fitting-parameters model" J. Adv. Oxid. Technol. 11 (2008) 1-8.
[153] A. Mills, S. L. Hunte, "An overview of semiconductor photocatalysis, " J. Photochem. Photobiol. A: Chem. 108 (1997) 1-35.
[154] D. M. Fouad, M. B. Mohamed " Comparative study of the photocatalytic activity of semiconductor nanostructures and their hybrid metal

nanocomposites on the photodegradation of malathion" J. Nanomater. Article ID 524123 (2012) 1-8.
[155] J. C. Colmenares, R. Luque , J. M. Campelo, F. Colmenares, Z. Karpiński, A. A. Romero, " Nanostructured photocatalysts and their applications in the photocatalytic transformation of lignocellulosic biomass: an overview" Mate. 2 (2009) 2228-2258.
[156] B. Tian, C. Li, F. Gu, H. Jiang, "Synergetic effects of nitrogen doping and Au loading on enhancing the visible-light photocatalytic activity of nano-TiO_2" Catal. Commun.10 (2009) 925–929.
[157] N. Barka, A. Assabbane, A. Nounahb, Y. A. Ichou, " Photocatalytic degradation of indigo carmine in aqueous solution by TiO_2-coated non-woven fibres" J. Hazard. Mater. 152 (2008) 1054–1059.
[158] R. Jain, S. Sikarwar "Photodestruction and COD removal of toxic dye erioglaucine by TiO_2-UV process: influence of operational parameters" Inter. J. Phys. Sci. 3 (2008) 299-305.
[159] L. B. Reutergradh, M. Iangphasuk "Photocatalytic decolourization of reactive azo dye: A compare between TiO_2 and CdS photocatalysis" Chemosphere 35 (1997) 585-596.
[160] L. O. B. Benetoli, B. M. Cadorin,a C. S. Postiglione, I. G. Souza, N. A. Debache " Effect of temperature on methylene blue decolorization in aqueous medium in electrical discharge plasma reactor" J. Braz. Chem. Soc., 22 (2011) 1669-1678.
[161] T. Lonhienne, C. Gerday, G.Feller, " Psychrophilic enzymes: revisiting the thermodynamic parameters of activation may explain local fexibility" Biochim. Biophys. Acta 1543 (2000) 1-10.
[162] Z. Shahryari, A. S. Goharrizi, M. Azadi, "Experimental study of methylene blue adsorption from aqueous solutions onto carbon nano tubes" Inter. J. Water Resour Environ. Eng. 2 (2010) 016-028.
[163] S. Zhu, X. Yang, W. Yang, L. Zhang, J. Wang, M. Huo, " Application of porous nickel-coated TiO_2 for the photocatalytic degradation of aqueous quinoline in an internal airlift loop reactor" Int. J. Environ. Res. Public Health 9 (2012) 548-563.
[164] A. F. Alkaim, T. A. Kandiel, F. H. Hussein, R. Dillert, D. W. Bahnemanna, " Solvent-free hydrothermal synthesis of anatase TiO_2 nanoparticles with enhanced photocatalytic hydrogen production activity" Appl. Catal. A: General 466 (2013) 32– 37.
[165] R. Ullah, J. Dutta " Photocatalytic degradation of organic dyes with manganese-doped ZnO nanoparticles" J. Hazard. Mater. 156 (2008) 194–200.
[166] T. Fotiou, T. M. Triantis, T. Kaloudis, A. Hiskia, " Evaluation of the photocatalytic activity of TiO_2 based catalysts for the degradation and mineralization of cyanobacterial toxins and water off-odor compounds under UV-A, solar and visible light" Chem. Eng. J. 261 (2015) 17–26.

[167] A. Khanna, V. K. Shetty, " Solar light induced photocatalytic degradation of Reactive Blue 220 (RB-220) dye with highly efficient Ag@TiO_2 core–shell nanoparticles: A comparison with UV photocatalysis" Solar Energy 99 (2014) 67–76.
[168] J. Lim, D. M. Satoca, J. S. Jang, S. Lee, W. Choi, " Visible light photocatalysis of fullerol-complexed TiO_2enhanced by Nb doping" Appl. Catal. B: Environ. 152–153 (2014) 233–240.
[169] J. Wang, Y. Jiang, Z. Zhang, G. Zhao, G. Zhang, T. Ma, W. Sun "Investigation on the sonocatalytic degradation of congo red catalyzed by nanometer rutile TiO_2 powder and various influencing factors" Desalination 216 (2007) 196–208.
[170] J. Sathiyabama, S. Rajendran, J. A. Selvi, A. J. Amalraj "Methyl orange as corrosion inhibitor for carbon steel in well water" Ind. J. Chem. 15 (2008) 462-466.
[171] H. Hou, R. Zhou, P. Wua, L. Wua "Removal of congo red dye from aqueous solution with hydroxyapatite/chitosan composite " Chem. Eng. J. 211–212 (2012) 336–342.
[172] M. Mina, G. S. Bang, H. Lee, B. C. Yu, " A photoswitchable methylene–spaced fluorinated aryl azobenzene monolayer grafted on silicon" Chem. Commun., 46 (2010) 5232-5234.
[173] D. L. Pavia, G. M. Lampman, G. S. Kriz "Introduction to spectroscopy" 3rd edition, Published by Thomas learning, USA (2001) pp.25-27.
[174] J. Kaur, S. Singhal, "Facile synthesis of ZnO and transition metal doped ZnO nanoparticles for the photocatalytic degradation of Methyl Orange" Ceram. Int. 40(2014)7417–7424.
[175] C. Baiocchi, M. C. Brussinoa, E. Pramauro, Al. B. Prevot, L. Palmisanob, G. Marc "Characterization of methyl orange and its photocatalytic degradation products by HPLC/UV–VIS diode array and atmospheric pressure ionization quadrupole ion trap mass spectrometry" Int. J. Mass Spectrom. 214 (2002) 247–256.
[176] M. Bhaumik, R. I. Mccrindle, A. Maity, " Enhanced adsorptive degradation of Congo red in aqueous solutions using polyaniline/Fe^o composite nanofibers" Chem. Eng. J. 260 (2015) 716–729.
[177] K.Tanaka, K. Padermpole, T. Hisanaga "Photocatalytic degradation of commercial azo dyes" Wat. Res. 34 (2000) 327-333.
[178] H. S. Wahab, "Molecular modeling of the adsorption and initial photocatalytic oxidation step for para-nitrophenol on nano-sized TiO_2 surface" Surf. Sci. 206 (2012) 624-633.
[179] H. S. Wahab, A. D. Koutselos "A computational study on the adsorption and $^{\cdot}OH$ initiated photochemical and photocatalytic primary oxidation of aniline" Chem. Phys. 238 (2009) 171-176.
[180] S. A. Abo-Farha "Photocatalytic degradation of monoazo and diazo dyes in wastewater on nanometer-sized TiO_2" Researcher 2 (2012) 1-20.

الملخص

أنجزت عملية التحطيم الضوئي في الوسط المائي لصبغتيّ المثيل البرتقالي والذي اختير كنموذج لأصباغ الأزوالأحادية و الكونكو الاحمر كنموذج لأصباغ الأزو الثنائية واللتان تعتبران من ملوثات المياه.

إن مساحيق ثنائي اوكسيد التيتانيوم المشوبة بكميات مختلفة من ذرات النتروجين (٢.٥% ، ٥% و ٧%) المحضرة مختبريا أظهرت فعالية ضوئية في المنطقة المرئية.

شُخصت مساحيق ثنائي أوكسيد التيتانيوم المشوبة بذرات النتروجين باستخدام العديد من التقنيات الطيفية والالكترونية. فقد استخدمت تقنية المجهر الالكتروني الماسح لدراسة شكل السطح والذي أظهر سطوحا سوية ومنتظمة. في حين ركّز فحصيّ الأشعة السينية ذو الطاقة المنتشرة ومنظومة (مطياف الكتلة- زمن التطاير للأيونات) على إثبات وجود النتروجين في المساحيق. كما أظهرت تقنية حيود الأشعة السينية وجود طور نقي من طور الانتيز في حين لم تظهر اي قمة حيود لطور الروتايل كما وجد ان الحجم الحبيبي ضمن المدى النانوي.

لأحتساب طاقات الفجوة للمساحيق فقد أستخدمت تقنية التحليل الطيفي في مجال الأشعة المرئية وفوق البنفسجية والتي ظهرت في المنطقة المرئية من الطيف الألكهرومغناطيسي.

تمت كذلك دراسة طيف التألق الضوئي لعينات ثنائي اوكسيد التيتانيوم المشوبة بذرات النتروجين حيث تبين ان النموذج الحاوي على ٢.٥% من ذرات النتروجين يُظهر اقل سرعة لعملية اعادة اتحاد الفجوة-الكترون. اخيراً تم اثبات ان جميع نماذج ثنائي اوكسيد التيتانيوم المشوبة بالنتروجين ذات مسامية متوسطة وذلك من خلال تقنية قياس المساحة السطحية.

تم دراسة المؤثرات التشغيلية الرئيسة على عملية القصر الضوئي لصبغتي الازو والتي تضمنت تأثير الدالة الحامضية، التركيز الابتدائي للصبغة، تركيز المحفز، شدة الضوء ودور بعض المؤكسدات.

عند الظروف التجريبية المثلى لعملية التفكك الضوئي للمثيل البرتقالي والتي كانت كالآتي: الدالة الحامضية مساوية الى ٢,٥ وكمية المحفز مساوية الى ٥٠ ملغم/لتر وبوجود $٣,٠٥ \times ١٠^{-٥}$ مول/لتر من الصبغة كانت قيمة ثابت السرعة ٠.٠٨٥ لكل دقيقة و ٠.٠٠١٤١ لكل ثانية وعمر نصف العملية مساوي الى ٠.١٣٣ ساعة بينما كانت الدالة الحامضية للكونكو الاحمر مساوية الى ٢.٥ ، ٤٠ ملغم/لتر من المحفز، $٢,١٥ \times ١٠^{-٥}$ مول/لتر من الصبغة وثابت السرعة مساوي

الى ٠.٠٠٠٣٠٥لكل ثانية و ٠.٠٣٤ لكل دقيقة وعمر نصف العملية ٠.٣٤٠ ساعة.
بينت دراسة الحركية لعملية القصر الضوئي لصبغتيّ المثيل البرتقالي والكونكو الأحمر إن العملية تتبع قانون المرتبة الأولى وبغض النظر عن ظروف التفاعل. علاوة على ذلك فأن منتوج الكم لعملية إلازالة الضوئية للون مساوي الى ٠,٠٧٧ و ٠,٠١٣٥ للمثيل البرتقالي والكونكو الأحمر على التوالي.
كشفت نتائج سرعة التفاعل ومنتوج الكم لعملية الأكسدة الضوئية ان كلا الصبغتين تتأثر بصورة كبيرة بأضافة بيروكسيد الهيدروجين والمؤكسدات الأخرى مثل البيرسلفات و الكلورات و البرومات والايودات.
وتم كذلك احتساب الدوال الثرموديناميكية الأساسية لعملية التفكك الضوئي للصبغتين المشار اليهما اعلاه مثل طاقة التنشيط وطاقة جبس والانثالبي والانتروبي.

بسم الله الرحمن الرحيم

Al-Nahrain University Journal
For Science
College of Science – Al-Nahrain University
Baghdad- Iraq

مجلة جامعة النهرين – العلوم
كلية العلوم – جامعة النهرين
بغداد - العراق

Ref :
Date :

العدد : ٨٠-٧٩
التأريخ : ٢٤/٨/٢٠١٥

قبول بحث للنشر

السيد / حسين محمد هادي .... المحترم
السيد / هلال شهاب وهاب .... المحترم

تدارست هيئة التحرير البحث المقدم من قبلكم والموسوم :

Visible Light Photocatalytic Decolourization of Methyl Orange Using N-Doped TiO_2 Nanoparticles

وبعد الاطلاع على أراء المقيمين ، فقد قررت هيئة التحرير في جلستها المرقمة (١٠) المنعقدة في ٢٨/٨/٢٠١٥، قبول البحث وسينشر في العدد القادم من المجلة والذي نتوقع صدوره قريباً .

د.ليث عبد العزيز العاني
رئيس هيئة التحرير
٢٨/٨/٢٠١٥

مجلة جامعة النهرين-العلوم

ميـ ٢/٢٣ ـادة

P.O.B : 64055 Jadriah - Baghdad - IRAQ
E–Mail: alnahrain_sci@hotmail.com Tel. : 7787024

لعنوان البريدي : جمهورية العراق - بغداد - الجادريه
ص.ب : ٦٤٠٥٥ هاتف : ٧٧٨٧٠٢٤

COLEG GWYDDORAU FFISEGOL A CHYMHWYSOL
COLLEGE OF PHYSICAL AND APPLIED SCIENCES

YSGOL CEMEG
SCHOOL OF CHEMISTRY

PRIFYSGOL
BANGOR
UNIVERSITY

Professor Igor F. Perepichka

Tel: +44 – (0)1248 38 2386
Fax: +44 – (0)1248 37 0528
E-mail: i.perepichka@bangor.ac.uk
http://www.chemistry.bangor.ac.uk/IP/index.php

Iraqi Cultural Attaché
14-15 Child's Place
Earls Court
London
SW5 9RX

01 December, 2014

Re: **Mr. Hussein Mohammed Hadi**
(MSc student from Department of Chemistry, College of Science, Al-Nahrain University, Baghdad, Iraq)

Dear Sir / Madam,

I am pleased to inform you that Mr. Hussein Mohammed Hadi has been visiting the School of Chemistry of Bangor University as a Guest MSc research student from Al-Nahrain University, Baghdad from 12 September to 9 December, 2014.

During his stay at Bangor University he was doing a research that included characterisation of doped titanium dioxide (TiO_2) nanoparticles and studies the mechanism of photocatalytic degradation of azo-dyes by these nanoparticles.

Yours sincerely,

Igor Perepichka
(*Professor of Chemistry*)

PRIFYSGOL BANGOR
BANGOR, GWYNEDD,
LL57 2UW, DU
FFÔN: +44 (0)1248 382375/7
FFACS: +44 (0)1248 370528
EBOST: chemistry@bangor.ac.uk

BANGOR UNIVERSITY
BANGOR, GWYNEDD,
LL57 2UW, UK
TEL: +44 (0)1248 382375/7
FAX: +44 (0)1248 370528
EMAIL: chemistry@bangor.ac.uk

www.bangor.ac.uk
www.chemistry.bangor.ac.uk

Ysgol Cemeg
School of Chemistry

جمهورية العراق

وزارة التعليم العالي والبحث العلمي

جامعة النهرين

كلية العلوم

قسم الكيمياء

التحفيز الضوئي لمركبات الآزو باستخدام ثنائي أوكسيد التيتانيوم المشوب

رسالة

مقدمة إلى كلية العلوم / جامعة النهرين

كجزء من متطلبات لنيل درجة الماجستير في علوم الكيمياء

من قبل

حسين محمد هادي

بكالوريوس 2009

إشراف

الأستاذ الدكتور

هلال شهاب وهاب

شعبان ١٤٣٦ه

حزيران ٢٠١٥ م